

DOT/FAA/TC-15/15

Federal Aviation Administration
William J. Hughes Technical Center
Aviation Research Division
Atlantic City International Airport
New Jersey 08405

Results of Health and Usage Monitoring System Fleet Data Analysis for Usage Credits

February 2016

Final Report

This document is available to the U.S. public
through the National Technical Information
Services (NTIS), Springfield, Virginia 22161.



U.S. Department of Transportation
Federal Aviation Administration

NOTICE

This document is disseminated under the sponsorship of the U.S. Department of Transportation in the interest of information exchange. The United States Government assumes no liability for the contents or use thereof. The United States Government does not endorse products or manufacturers. Trade or manufacturer's names appear herein solely because they are considered essential to the objective of this report. This document does not constitute FAA certification policy. Consult your local FAA aircraft certification office as to its use.

This report is available at the Federal Aviation Administration William J. Hughes Technical Center's Full-Text Technical Reports page: actlibrary.act.faa.gov in Adobe Acrobat portable document format (PDF).

1. Report No. DOT/FAA/TC-15/15		2. Government Accession No.		3. Recipient's Catalog No.	
4. Title and Subtitle RESULTS OF HEALTH AND USAGE MONITORING SYSTEM FLEET DATA ANALYSIS FOR USAGE CREDITS				5. Report Date February 2016	
				6. Performing Organization Code	
7. Author(s) Lewis Zion, Michael Chandler, David White				8. Performing Organization Report No.	
9. Performing Organization Name and Address U.S. Army-Aviation Engineering Directorate Redstone Arsenal, AL 35898				10. Work Unit No. (TRAIS)	
				11. Contract or Grant No. DTFACT-10-X-00005	
12. Sponsoring Agency Name and Address U.S. Department of Transportation Federal Aviation Administration FAA Southwest Regional Office 10101 Hillwood Parkway Fort Worth, TX 76177				13. Type of Report and Period Covered Final Report	
				14. Sponsoring Agency Code ASW-112	
15. Supplementary Notes The Federal Aviation Administration William J. Hughes Technical Center Aviation Research Division COR was Traci Stadtmueller.					
16. Abstract The purpose of this joint research effort between the Federal Aviation Administration (FAA) and Army Aviation Engineering Directorate was for the FAA to gain access to essential Army helicopter fleet Health and Usage Monitoring Systems (HUMS) data and the Army's knowledge of fleet data analyses and Condition Based Maintenance (CBM) implementation. Technical information generated from this effort can be used by the FAA to demonstrate applicable CBM and HUMS technologies, processes, and methodologies in support of the FAA's effort in establishing guidance and substantiation of the HUMS for life and/or maintenance credits. Such information can be used in the future HUMS for civil transport rotorcraft. Specifically, the joint FAA/Army HUMS research effort addresses the critical elements of the certification process as specified in Advisory Circular (AC) 29-2C, Section MG 15 (HUMS AC). This report documents a two-year effort that involved: 1) performing data analyses on an Army helicopter fleet HUMS equipped to generate technical information on the performance of a Structural Usage Monitoring System and associated sensors for determining CBM usage credits, 2) developing component health and usage indicators, algorithms, and validation methods used to determine structural, dynamic component, and life-limited parts' remaining useful life (RUL) based on HUMS data, 3) establishing processes and applicable evidence required for a validation method to show compliance, and 4) using HUMS data to demonstrate developed methods in accordance with the HUMS AC Credit Validation Process to substantiate proposed maintenance credits for component RUL.					
17. Key Words Regime recognition, Structural usage monitoring system, Structural usage credit, Health and usage monitoring system, Usage-based maintenance, Retirement-time adjustment, Life extension, Remaining useful life			18. Distribution Statement This document is available to the U.S. public through the National Technical Information Service (NTIS), Springfield, Virginia 22161.		
19. Security Classif. (of this report) Unclassified		20. Security Classif. (of this page) Unclassified		21. No. of Pages 115	22. Price

ACKNOWLEDGEMENTS

The authors would like to acknowledge the technical guidance and reviews provided by Terry Baker of the Army Aviation and Missiles Research, Development and Engineering Center Aviation Engineering Directorate Structures and Materials Division (SMD) and Jeff Finckenor, QinetiQ North America lead engineer of the SMD-QNA technology team.

TABLE OF CONTENTS

	Page
EXECUTIVE SUMMARY	xii
1. INTRODUCTION	1
1.1 PURPOSE	1
1.2 BACKGROUND	2
2. DISCUSSION	2
3. ANALYSIS	4
3.1 TASK 1 – PERFORM FLEET HUMS DATA ANALYSIS	4
3.1.1 Identify Airframe	4
3.1.2 Document Aircraft Selection Criteria	5
3.1.3 Acquire Data Files from Selected Aircraft	5
3.1.4 Compile Usage Database	5
3.1.5 Document Process for Mapping Regimes to CWC Usage	6
3.1.6 Document Statistical Analysis and Corrections	10
3.1.7 Compare New to Old Usage Spectrum	10
3.1.8 Identify Critical Flight Regimes for Credit Calculations	16
3.2 TASK 1 UPDATE – PERFORM HUMS FLEET DATA ANALYSIS	17
3.2.1 Expand and Refine UH-60M Usage Database	17
3.2.2 Expand and Refine Regime Recognition Algorithms	20
3.3 TASK 2 – DEVELOP USAGE CREDITS	22
3.3.1 Select Two Components	22
3.3.2 Review Fatigue Substantiation Document	22
3.3.3 Evaluate Reliability of OEM CRT	28
3.3.4 Develop Life Factor Method	49
3.3.5 Develop Usage Credits	55
3.4 TASK 2 UPDATE – USAGE CREDIT METHOD	59
3.4.1 Analyze UH-60M Operational Usage	59
3.4.2 Evaluate Damage Accumulation & Demonstrate Usage Credit Process	72
4. CONCLUSIONS	95
5. REFERENCES	95

APPENDICES

- A—Deterministic Evaluation of Inherent Composite Worst Case (CWC) Reliability
- B—Probabilistic Evaluation of Inherent Composite Worst Case (CWC) Reliability

LIST OF FIGURES

Figure		Page
1	Determination of CRT	4
2	Benefits of usage monitoring	4
3	UH-60M IVHMS flights and flight hours	13
4	UH-60M IVHMS flights and GAG cycles	13
5	CWC versus average regime usage (low-mid GW)	14
6	CWC versus average regime usage (mid-high GW)	14
7	CWC versus average regime usage (any GW)	15
8	CWC versus average regime usage (GAG and min-max)	15
9	Training aircraft flight hours	18
10	OCONUS 1 aircraft flight hours	19
11	OCONUS 2 aircraft flight hours	19
12	Snapshot of FlightViz animation	21
13	Selected components and failure modes	22
14	Component failure mode CWC damage by regime (low-mid GW)	26
15	Component failure mode CWC damage by regime (mid-high GW)	27
16	Component failure mode CWC damage by regime (any GW)	27
17	Schematic of CWC spectrum reliability generation	30
18	Effect of sample size when estimating true mean	32
19	Effect of sample size when estimating true standard deviation	33
20	Schematic of load severity (TOS bias + normal distribution) model	34
21	Sample fatigue test results with mean and reduced S-N curves	36
22	Example of 7050 forged aluminum small-scale coupon data [8]	36
23	Basic stress-strength interference model	38
24	Comparison of CSD versus CCV reduced S-N curves	39
25	Stress-strength joint probability portion of convolution integral	41
26	Dual process convolution matrix element	41
27	Numerical illustration of convolution	42
28	Graphical results from Table 8	44
29	Graphical results from Table 9	46
30	Comparison of inherent CWC reliability by method	46

31	Usage, stress, and ES damage rates of increase	47
32	Reliability versus fatigue life for component 1 failure modes	48
33	Reliability versus fatigue life for component 2 failure modes	49
34	Average usage versus CWC usage for grouped regimes	50
35	Average usage versus CWC damage—grouped regimes (component 1—mode A)	51
36	Average usage versus CWC damage—grouped regimes (component 1—mode B)	51
37	AVERAGE usage versus CWC damage—grouped regimes (component 2—mode A)	52
38	Average usage versus CWC usage—grouped regimes (component 2—mode B)	52
39	Component normalized damage versus flight hours	53
40	CWC, actual, and adjusted life in hours	54
41	CWC, actual, and adjusted life normalized to CWC life	54
42	DI build-up for component 1—mode A	56
43	DI build-up for component 1—mode B	56
44	DI build-up for component 2—mode A	57
45	DI build-up for component 2—mode B	57
46	DI extrapolation for component 2—mode B	58
47	Comparison of revised CONUS training usage with CWC usage	69
48	Comparison of revised OCONUS 1 usage with CWC usage	70
49	Comparison of revised OCONUS 2 usage with CWC usage	71
50	Selected components	72
51	Method to ensure that spectrum reliability meets or exceeds one 9	76
52	Effects of usage on MR rotating swashplate (CONUS training)	78
53	Usage data scatter for MR rotating swashplate (CONUS training)	78
54	Effects of usage on MR rotating swashplate (OCONUS 1)	79
55	Usage data scatter for MR rotating swashplate (OCONUS 1)	79
56	Effects of usage on MR rotating swashplate (OCONUS 2)	80
57	Usage data scatter for MR rotating swashplate (OCONUS 2)	80
58	Effects of usage on IDGB MR shaft (CONUS training)	81
59	Usage data scatter for IDGB MR shaft (CONUS training)	81
60	Effects of usage on IDGB MR shaft (OCONUS 1)	82
61	Usage data scatter for IDGB MR shaft (OCONUS 1)	82
62	Effects of usage on IDGB MR shaft (OCONUS 2)	83
63	Usage data scatter for IDGB MR shaft (OCONUS 2)	83

64	Effects of usage on left tie rod (CONUS training)	84
65	Usage data scatter for left tie rod (CONUS training)	84
66	Effects of usage on left tie rod (OCONUS 1)	85
67	Usage data scatter for left tie rod (OCONUS 1)	85
68	Effects of usage on left tie rod (OCONUS 2)	86
69	Usage data scatter for left tie rod (OCONUS 2)	86
70	SUMS comparison for MR rotating swashplate (CONUS training)	88
71	SUMS comparison for MR rotating swashplate (OCONUS 1)	88
72	SUMS comparison for MR rotating swashplate (OCONUS 2)	89
73	SUMS comparison for IDGB MR shaft (CONUS training)	89
74	SUMS comparison for IDGB MR shaft (OCONUS 1)	90
75	SUMS comparison for IDGB MR shaft (OCONUS 2)	90
76	SUMS comparison for left tie rod (CONUS training)	91
77	SUMS comparison for left tie rod (OCONUS 1)	91
78	SUMS comparison for left tie rod (OCONUS 2)	92
79	Example MR swashplate fatigue life expenditure	95

LIST OF TABLES

Table		Page
1	Regime mapping	7
2	Regime parameters and sample regime parameter values	12
3	Number of damaging regimes	16
4	Summary of selected aircraft	18
5	Selected component CWC damage fractions by regime (low-mid GW)	24
6	Selected component CWC damage fractions by regime (mid-high GW)	25
7	Selected component CWC damage fractions by regime (any GW)	26
8	Deterministic inherent CWC reliability by failure mode	44
9	Probabilistic inherent CWC reliability by failure mode	45
10	Revised CWC spectrum for CONUS training (low-mid GW)	60
11	Revised CWC spectrum for CONUS training (mid-high GW)	61
12	Revised CWC spectrum for CONUS training (any GW)	62
13	Revised CWC spectrum for OCONUS 1 (low-mid GW)	63
14	Revised CWC spectrum for OCONUS 1 (mid-high GW)	64
15	Revised CWC spectrum for OCONUS 1 (any GW)	65
16	Revised CWC spectrum for OCONUS 2 (low-mid GW)	66
17	Revised CWC spectrum for OCONUS 2 (mid-high GW)	67
18	Revised CWC spectrum for OCONUS 2 (any GW)	68
19	Component life and X-factor for operational environments	93
20	Component adjusted CRT for operational environments	94

LIST OF SYMBOLS AND ACRONYMS

α	Load severity factor or uncertainty level
β	Usage severity or constant term in damage equation
Δ_b	Load bias
$\varepsilon\%$	Percent error in Monte Carlo reliability prediction
γ	Exponent constant in damage equation or confidence level
μ	True mean of a normally distributed random variable
σ	True standard deviation of a normally distributed random variable, stress
Φ	Standard Normal Probability operator
i, j, k	Subscripts denoting the i^{th} , j^{th} and k^{th} occurrence of a random variable
n	Sample size or number of fatigue cycles
p	Binomial probability of success
q	Binomial probability of failure
tot	Subscript indicating total
\bar{x}	Sample mean of random variable X
E_∞	Endurance limit at infinity
AC	Advisory Circular
AED	Aviation Engineering Directorate
CBM	Condition-based maintenance
CONUS	Continental United States
CoV	Coefficient of variation
CRT	Component retirement time
CSD	Constant standard deviation
.csv	Comma-separated value
CWC	Composite worst case
DI	Damage index
EL	Endurance limit
ES	Endurance strength
FAA	Federal Aviation Administration
FSR	Fatigue substantiation report
GAG	Ground-air-ground
GW	Gross weight
HUMS	Health and usage monitoring system
I	Interference between load and strength; $I=S-L$
IDGB	Improved Durability Gearbox
IVHMS	Integrated Vehicle Health Management System
L	Load
MDS	Mission Design Series
N	Cycles to failure or number of trials
N_z	Vertical load factor (in a Cartesian coordinate system that is tied to the aircraft)
OCONUS	Outside the Continental United States
OEM	Original Equipment Manufacturer
Q	Unreliability or probability of failure; complement of reliability ($Q=1-R$)
R	Reliability or stress ratio

.rdf	Raw data files
RR	Regime recognition
RRA	Regime recognition algorithms
RUL	Remaining useful life
S	Strength or stress in damage equation
SS	Steady state
SUMS	Structural Usage Monitoring System
T	T-score of a random variable
TOS	Top-of-scatter
TR	Transient Z Standard normal score or number of standard deviations from the mean

EXECUTIVE SUMMARY

This report documents two research tasks that spanned 2 years. In year 1, task 1 was to perform fleet Health and Usage Monitoring System (HUMS) data analysis. An airframe was selected and the selection criteria documented. Data files from selected aircraft were acquired and compiled into a usage database. A process for mapping regimes to composite worst case (CWC) usage was developed. Statistical analysis and corrections were conducted to compare new to old usage spectra and identify critical flight regimes for credit calculations. This task was further expanded and refined in year 2 by identifying and selecting an aircraft with diverse usage, acquiring data files for the selected aircraft, and compiling a usage database for two operational environments. These results allowed for the expansion and refinement of regime recognition algorithms (RRA) to evaluate the accuracy of HUMS gross weight values. Additionally, a procedure was developed for validating RRA.

In year 1, task 2 focused on developing usage credits. Two components were selected and their fatigue substantiation documents reviewed. Additionally, the reliability of the original equipment manufacturer component retirement time was evaluated. Life factor methods and usage credits were developed.

In year 2, operational usage was analyzed by aircraft and operational environment. The CWC usage spectra were developed for operational environments. Additionally, operational CWC usage was compared to design CWC spectrum. A usage credit process was demonstrated on three selected components. A plan for usage credit implementation was also developed.

1. INTRODUCTION

1.1 PURPOSE

The purpose of this joint research effort between the Federal Aviation Administration (FAA) and the Army Aviation Engineering Directorate (AED) was for the FAA to gain access to essential Army helicopter fleet Health and Usage Monitoring System (HUMS) data and the Army's knowledge of fleet data analyses and Condition-based maintenance (CBM) implementation. Technical information generated from this effort can be used by the FAA to address the critical elements of the certification process for usage credits as specified in Advisory Circular (AC) 29-2C, Section MG 15[1]. Research areas included:

- Performing data analyses of Army helicopter fleets that are HUMS equipped to generate technical information on performance of Structural Usage Monitoring Systems (SUMS) and associated sensors for determining CBM usage credits.
- Developing component health and usage indicators, algorithms, and validation methods used to determine structural, dynamic-component, and life-limited parts' remaining useful life (RUL) based on HUMS data.
- Establishing processes and applicable evidence required for a validation method to show compliance.
- Using HUMS data; demonstrating developed methods in accordance with a HUMS AC credit validation process to substantiate proposed maintenance credits for component RUL.

The specific purpose of task 1 was for AED to provide documentation of fleet-wide HUMS data analyses to evaluate HUMS performance in reference to usage determinations on key dynamic components and to identify potential technical issues. The fleet-wide HUMS analyses were conducted for UH-60M rotorcraft with the current Integrated Vehicle Health Monitoring System (IVHMS). The purpose of these analyses was to identify potential technical issues using HUMS data for usage credit calculations; validate HUMS processes to be used for CBM purposes; determine essential dynamic components for CBM; identify critical flight load regimes for credit calculations; and generate technical information to support the FAA flight tests in validating HUMS regime recognition algorithms (RRA). These fleet-wide HUMS analyses can assist the FAA in understanding potential technical issues of broad HUMS applications for CBM for the civil fleet.

Task 2 focused on developing usage credits. Two components were selected and their fatigue substantiation documents reviewed. Additionally, the reliability of the original equipment manufacturer (OEM) component retirement time (CRT) was evaluated. Life factor methods and usage credits were developed.

Operational usage was then analyzed by aircraft and operational environment. Composite worst case (CWC) usage spectra were developed for operational environments. Additionally, operational CWC usage was compared to design CWC spectrum. A usage credit process was demonstrated on three selected components and a plan for usage credit implementation was also developed.

1.2 BACKGROUND

CBM has proven to be an effective process for monitoring the health of aircraft components, sub-systems, and systems by using HUMS. The system is designed for onboard diagnostics, prognostics, usage and structural monitoring, and data collection, which can be used to reduce aviation accidents and incidents, improve reliability, and adjust maintenance schedules and man-hours according to actual usage of rotorcraft operations.

The key objective of CBM is to reduce the unnecessary maintenance burden on field aircraft while potentially improving/ extending component useful life from one that is currently based on an assumed spectrum to one based predominately on actual usage while maintaining risk at an acceptable level. The ultimate goal of CBM is to know and understand the actual status of aircraft, which will potentially reduce unnecessary maintenance and reduce total (operation and sustainment) ownership costs. Sensor-based assessment of equipment condition therefore enables the refinement of scheduled maintenance requirements.

For CBM to be a success, aviation maintainers and logisticians—from the flight line to the Army Aviation and Missile Command Integrated Material Management Center to the depot—must have visibility on component usage, deterioration, failures, and availability. The Army will monitor critical maintenance data elements using platform-based processors to determine critical component and systems health by using algorithms jointly developed and validated by the Army and the OEM. These algorithms will support metrics that will use the physics of failure and or deterioration for each component and focus engineering efforts to merge traditional areas (such as system reliability, design, and controls) to rethink methods for the design, build, and support of future systems with new dynamic maintenance programs.

CBM processes and technologies, which are being fully developed and implemented on Army Aviation platforms, are available for application to the civil aviation domain for the same purposes (e.g., to enhance aircraft safety, minimize operating costs, and develop maintenance schedules based on actual usage information). Recognizing the transformation of CBM and HUMS technologies, the FAA published the AC 29-2C, MG-15 to address airworthiness approval of HUMS. The AC provides guidance for achieving airworthiness approval for installation, credit validation, and instructions for continued airworthiness for a full range of HUMS applications.

2. DISCUSSION

Army helicopter fatigue life-limited structural CRT is based on a composite worst case (CWC) usage spectrum that was derived for each Mission Design Series (MDS) to capture the most severe usage that helicopter model would ever be expected to experience.

Knowledge of actual operational usage can be used to identify unsafe usage, refine scheduled maintenance actions, and extend the operational flight hours of fatigue-life-limited components. The design regimes are assumed for helicopter usage as a part of the Army's desire to have at least "six-nines" of reliability for life-limited component structural fatigue [2]. The distribution

of the legacy six-nines method is roughly as follows: 1) one-nine of reliability is associated with the CWC usage spectrum that assumes a conservative amount of time is spent in damaging regimes, 2) two-nines of reliability are associated with the conservative enveloping of the range of strains experienced in each damaging regime, and 3) three-nines of reliability are associated with the application of a mean minus three sigma reduction in the fatigue test results. This process, illustrated in figure 1, has produced an excellent flight safety record. The Army has long recognized the potential for gaining significant cost and safety benefits by monitoring usage of individual life-limited structural components.

Aspects of flight that affect the fatigue of components (e.g., speed, altitude, bank angle, and gross weight [GW]) are categorized using regime recognition (RR). When Army MDS aircraft were initially designed, each damaging regime was assumed to be performed at a conservative rate that produces the design life for each fatigue-life-limited component. In figure 2, the CRT (①) is the point at which the component is retired. Most critical components experience a flight regime mix that is much less severe than the CWC usage and can fly well beyond the design flight hours (②) before accumulating 100% (④) of the design fatigue life. This is shown in the green shaded area (③) of figure 2. However, there are examples of parts that experience usage that is more severe than the design damage assumptions (⑤), as shown in the red shaded area (⑥) of figure 2. To protect safety, these parts should be removed and replaced prior to achieving the CRT (⑦). RRA are used to record the actual flight regime history for the aircraft and life-limited components and, depending upon the inherent reliability of the design CWC usage spectrum, the components have the potential to be retired at a revised time based upon operational usage.

Since the assumption of the OEMs is that the CWC usage provides approximately one of the six-nines of reliability, adjustments may have to be made to the operational usage results to ensure retention of the desired level of component reliability.

The purpose of the fleet usage monitoring is to gain insight into the accumulated damage that each helicopter experiences during operational usage and to use this information to evaluate overhaul and retirement times, increase safety and operational readiness, and reduce costs.

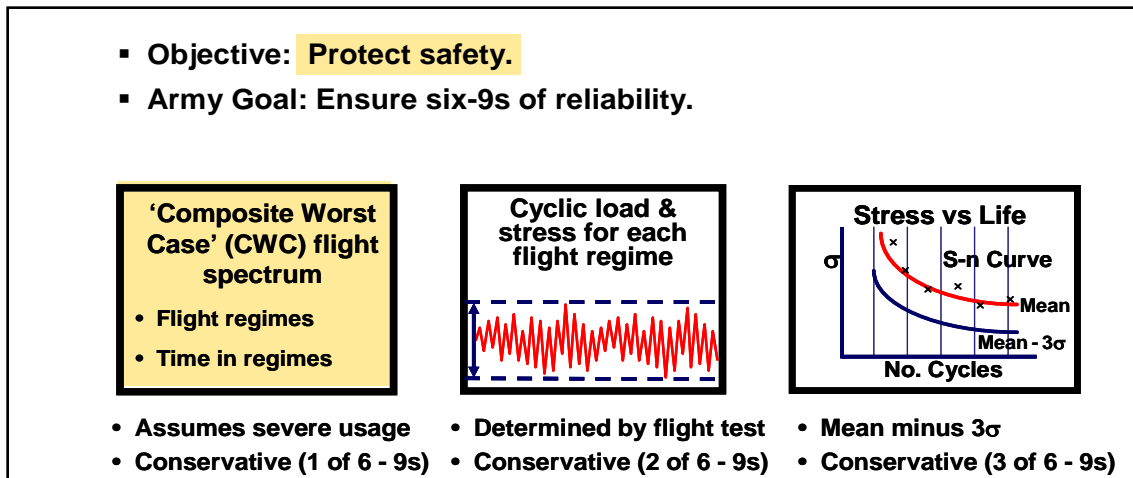


Figure 1. Determination of CRT

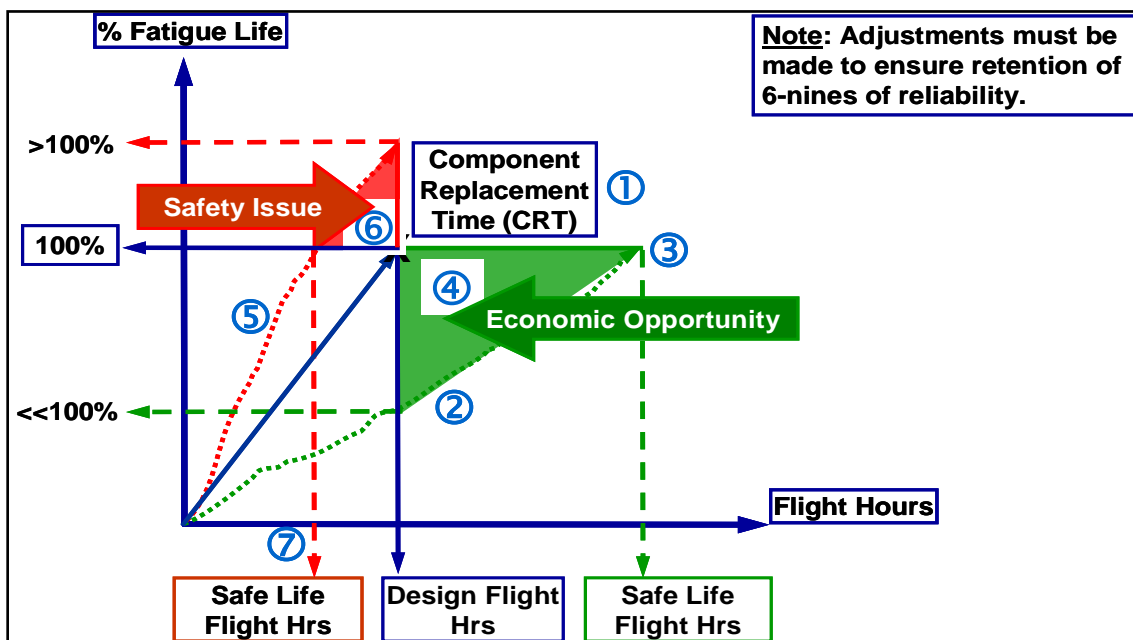


Figure 2. Benefits of usage monitoring

3. ANALYSIS

The results of tasks 1 and 2 are discussed below.

3.1 TASK 1—PERFORM FLEET HUMS DATA ANALYSIS

3.1.1 Identify Airframe

Army AED Structures provided a choice of either the UH-60L or UH-60M airframes to be considered as a basis for the fleet HUMS data analysis task. Both were assessed to be viable candidates, but for reasons discussed in the next section, the UH-60M was selected.

3.1.2 Document Aircraft Selection Criteria

The flight and ground recorded parameters of both the UH-60L HUMS and UH-60M IVHMS were assessed to determine which would be preferable in defining the damaging flight regimes required for the Fleet HUMS Data Analysis task. Both the UH-60L HUMS and UH-60M IVHMS databases contain all parameters required to identify damaging regimes [3 and 4].

The flight regimes of both the UH-60L HUMS and UH-60M IVHMS map very well into the damaging regimes defined in the respective Sikorsky UH-60L and UH-60M Fatigue Substantiation Reports (FSRs). The required quantity and quality of UH-60L and UH-60M usage parameters are available in the CBM data warehouse.

A comparison of the recorded parameters, defined regimes, and FSR damaging regimes of UH-60L and UH-60M resulted in the selection of the UH-60M for the following reasons:

- The UH-60M IVHMS is a later generation HUMS that records all of the parameters required to identify flight regimes, whereas some of the UH-60L parameters must be derived. For example, the UH-60L vertical load factor, N_z , is derived from vertical acceleration.
- The UH-60M IVHMS identifies control reversal and maneuver entry and recovery events (see the last two rows of table 2).

3.1.3 Acquire Data Files from Selected Aircraft

Reference 5 was reviewed to establish criteria for creating a UH-60M usage database. The criteria were necessary in order to accomplish the following activities associated with this task:

- Determine which of approximately 100 FSR regimes contribute damage to approximately 230 UH-60M component failure modes.
- Tabulate FSR regime/failure mode damage fractions to identify individual UH-60M operational flights that experience damaging regimes in major components.
- Verify CBM data warehouse UH-60M data quantity, quality, format, available parameters, and GW information.
- Coordinate with CBM data warehouse management to acquire UH-60M IVHMS data consisting of flight and ground parameters required to perform regime recognition.

Once these criteria were satisfied, UH-60M raw data files (.rdf) files were requested and acquired from the CBM data warehouse.

3.1.4 Compile Usage Database

The UH-60M operational usage data selected from the CBM data warehouse consisted of 839 hours recorded during 474 flights on 14 operational aircraft. All of the flight-recorded data were converted from the .rdf format into comma separated value (.csv) format using the Mechanical Diagnostic Analysis Toolset to facilitate the processing described below.

Parameters required for RR were selected and prepared for use:

- All parameters were converted to a common sample rate to facilitate RR.
- Some “noisy” parameters were filtered as required to provide time domain smoothing.

3.1.5 Document Process for Mapping Regimes to CWC Usage

Reference 4 was reviewed to further understand the UH-60M IVHMS. This report established and described IVHMS regimes, identified regime parameters, and defined a range of parameter values.

The dynamic component FSR for the UH-60M was also reviewed [5]. This report documented the fatigue substantiation for UH-60M dynamic components, presented UH-60M CWC usage spectrum, identified all of the regimes that the UH-60M aircraft are expected to experience, and presented the fatigue-life-limited component failure mode damage fractions for each regime.

IVHMS and FSR regimes were compared to assess regime nomenclature, definitions, and relationships and used one-to-one, one-to-many, and many-to-one cross-mappings to merge IVHMS regimes into FSR regimes. The mapped regimes were also compared and adjusted to be consistent with Sikorsky [6]. The regime mapping is documented in table 1. The regime numbers correspond to the original IVHMS and FSR regime numbers as indicated. The up and down arrows in the IVHMS regime tabulation indicate the necessity to insert an event before or after the adjacent IVHMS regime in order to map into the FSR regime damage.

Table 1. Regime mapping

IVHMS Regimes		FSR Regimes			
		Low-Mid GW	Mid-High GW	Any GW	No Stores
1	Power On Aircraft, Rotors Not Turning				
2	Power On Aircraft, Rotors Turning, Taxi Or Stationary	38	77		TAXI
3	Left taxi turn	39	78		TAXI TURN
4	Right taxi turn				
5	Takeoff	25	64		TAKE OFF
6	Landing			79	NML LAND
				80	RUN LAND
↓	Approach	37	76	37	HOV APP
7	IGE Hover	1	40		HOVER
8	OGE Hover				
9	Forward Flight to 0.3 VH	6	45		LF 0.1VH
↓	Entry			93	ENT R.S.
10	Right Sideward Flight	3	42		RT S FLT
↑	Recovery			94	REC R.S.
↓	Entry			91	ENT L.S.
11	Left Sideward Flight	2	41		LT S FLT
↑	Recovery			92	REC L.S.
↓	Entry			95	ENT RR
12	Rearward Flight	4	43		REAR FLT
↑	Recovery			96	REC RR
13	Left Hover Turn	26	65		L HOV TN
14	Right Hover Turn	27	66		R HOV TN
15	Rudder Reversal in Hover			81	HVRD REV
16	Longitudinal Reversal in Hover			83	HVLO REV
17	Lateral Reversal in Hover			85	HVLA REV
18	Level Flight up to 0.3 VH	7	46		LF 0.1VH
19	Level Flight between 0.3 VH and 0.4 VH	8	47		LF 0.4VH
20	Level Flight between 0.4 VH and 0.5 VH	9	48		LF 0.5VH
21	Level Flight between 0.5 VH and 0.6 VH	10	49		LF 0.6VH
22	Level Flight between 0.6 VH and 0.7 VH	11	50		LF 0.7VH
23	Level Flight between 0.7 VH and 0.8 VH	12	51		LF 0.8VH
24	Level Flight between 0.8 VH and 0.9 VH	13	52		LF 0.9VH
25	Level Flight between 0.9 VH and 1.0 VH	14	53		LF 1.0VH
26	Rudder Reversal in Level Flight to 1.0 VH			82	LFRD REV
27	Lateral Reversal in Level Flight to 1.0 VH			86	LFLA REV
28	Longitudinal Reversal in Level Flight to 1.0 VH			84	LFLO REV
29	Left Sideslip in Level Flight	15	54		SIDESLIP
30	Right Sideslip in Level Flight				
31	Best Rate of Climb	5	44		CLIMB
32	Intermediate Power Climb				CLIMB
33	Takeoff Power climb				CLIMB

Table 1. Regime mapping (continued)

IVHMS Regimes		FSR Regimes			
		Low-Mid GW	Mid-High GW	Any GW	No Stores
34	Left Sideslip in Climb	15	54		SIDESLIP
35	Right Sideslip in Climb				
36	Left Climbing Turn	5	44		CLIMB
37	Right Climbing Turn	5	44		CLIMB
38	Approach	38	39		HOV APP
39	Rough Approach				
↓	Entry			89	ENT AUTO
40	Autorotation	16	55		AUTO
↑	Recovery			90	REC AUTO
41	Autorotation with Left Sideslip	16	55		AUTO
42	Autorotation with Right Sideslip				
43	Rudder Reversal in Autorotation			82	LFRD REV
44	Longitudinal Reversal in Autorotation			84	LFLO REV
45	Lateral Reversal in Autorotation			86	LFLA REV
46	Collective Reversal in Autorotation	16	55		AUTO
47	Partial Power Descent	17	56		PART PWR
↑	Entry & Recovery	28	67		E&R PART PWR
48	Rudder Reversal in Partial Power Descent			82	LFRD REV
49	Longitudinal Reversal in Partial Power Descent			84	LFLO REV
50	Lateral Reversal in Partial Power Descent			86	LFLA REV
51	Dive	18	57		DIVE
52	Rudder Reversal in Dive			82	LFRD REV
53	Longitudinal Reversal in Dive			84	LFLO REV
54	Lateral Reversal in Dive			86	LFLA REV
55	Level Left Turns – 30° AOB Level Left Turn, 10° to 35° AOB	19	58		TURN 30L
56	Level Left Turns – 45° AOB Level Left Turn, 35° to 50° AOB	21	60		TURN 45L
57	Level Left Turns – 30° AOB Level Left Turn, 10° to 35° AOB	23	62		TURN 60L
58	Level Left Turns – > 60° AOB Level Left Turn, > 65° AOB				
59	Level Right Turns - 30° AOB Level Right Turn, 10° to 35° AOB	20	59		TURN 30R
60	Level Right Turns - 45° AOB Level Right Turn, 35° to 50° AOB	22	61		TURN 45R
61	Level Right Turns - 60° AOB Level Right Turn, 50° to 65° AOB	24	63		TURN 60R
62	Level Right Turns - > 60° AOB Level Right Turn, > 65° AOB				
63	Descending Left Turns – 30° AOB, 10° to 35° AOB	19	58		TURN 30L
64	Descending Left Turns – 45° AOB, 35° to 50° AOB	21	60		TURN 45L
65	Descending Left Turns – 60° AOB, 50° to 65° AOB	23	62		TURN 60L
66	Descending Left Turns – > 60° AOB, > 65° AOB				
67	Descending Right Turns – 30° AOB, 10° to 35° AOB	20	59		TURN 30R
68	Descending Right Turns – 45° AOB, 35° to 50° AOB	22	61		TURN 45R
69	Descending Right Turns – 60° AOB, 50° to 65° AOB	24	63		TURN 60R
70	Descending Right Turns – > 60° AOB, > 65° AOB				

Table 1. Regime mapping (continued)

IVHMS Regimes		FSR Regimes			
		Low-Mid GW	Mid-High GW	Any GW	No Stores
71	Autorotation Left Turns	35	74		AUT TN L
72	Autorotation Right Turns	36	75		AUT TN R
73	Symmetrical Pullouts – to 1.2 VH, Up to 1.8 G’s			87	MOD P.O.
74	Symmetrical Pullouts – to 1.2 VH, 1.9 to 3.0 G’s			88	SEV P.O.
75	Symmetrical Pullouts – to 1.2 VH, 3.1 to 4.0 G’s			99	PO 3.3G-SD
76	Left Rolling Pullouts – to 1.2 VH, Up to 1.8 G’s			87	MOD P.O.
77	Left Rolling Pullouts – to 1.2 VH, 1.9 to 3.0 G’s			88	SEV P.O.
78	Left Rolling Pullouts – to 1.2 VH, 3.1 to 4.0 G’s			99	PO 3.3G-SD
79	Right Rolling Pullouts – to 1.2 VH, Up to 1.8 G’s			87	MOD P.O.
80	Right Rolling Pullouts – to 1.2 VH, 1.9 to 3.0 G’s			88	SEV P.O.
81	Right Rolling Pullouts – to 1.2 VH, 3.1 to 4.0 G’s			99	PO 3.3G-SD
82	Pushovers – to 1.2 VH, 0.3 to 0.8 G’s	18	57		DIVE
83	Pushovers – to 1.2 VH, 0.0 to 0.3 G’s				
84	Pushovers – to 1.2 VH, -0.5 to -0.0 G’s				
85	Dynamic Yaw			98	EXTR MAN
86	Other Maneuver 1, Left Climbing Turn Exceeding AOB Limits			98	EXTR MAN
87	Other Maneuver 2, Right Climbing Turn Exceeding AOB Limits			98	EXTR MAN
88	Other Maneuver 3, Level Flight exceeding 1.0 VH	14	53		LF 1.0 VH
89	Other Maneuver 4, Dive exceeding 1.2 VH	18	57		DIVE
90	Other Maneuver 5, Symmetrical Pullout exceeding 1.2 VH			98	EXTR MAN
91	Right Turn Entry	30	69		E&R TURN 30R
		32	71		E&R TURN 45R
		34	73		E&R TURN 60R
92	Left Turn Entry	29	68		E&R TURN 30L
		31	70		E&R TURN 45L
		33	72		E&R TURN 60L
93	Right Turn Recovery	30	69		E&R TURN 30R
		32	71		E&R TURN 45R
		34	73		E&R TURN 60R
94	Left Turn Recovery	29	68		E&R TURN 30L
		31	70		E&R TURN 45L
		33	72		E&R TURN 60L
				97	DRP STOP
				102	GAG/FLT
				103	MIN-MAX

3.1.6 Document Statistical Analysis and Corrections

The majority of the statistical analysis revolves around the effort to maintain the Army's goal of maintaining six-nines of reliability. Since the results of RRA were needed to perform any reliability analysis, it was deemed appropriate to include the details of the reliability study in Task 2 (see section 3.3.3). A brief overview is given below.

The reliability can be evaluated deterministically or probabilistically; however, this report deals with ADS-79C [7], paragraphs A.6.4 and A.6.5, both of which are deterministic.

3.1.6.1 Deterministic Assessment

Using the raw RR (average) results, adjust the fatigue strength reduction until the calculated retirement life matches the OEM's component life.

The inherent CWC reliability is the difference between the adjusted fatigue strength reliability and 0.99865 (inherent reliability of $\mu-3\sigma$ strength reduction). In nines, this would be:

$$\text{Log}[1-\Phi(Z)] + \text{Log}[1-\Phi(3)], \text{ where } Z = \# \text{ of standard deviations of strength reduction.}$$

This process is illustrated in appendix A and explained in section 3.3.3.3.2.

3.1.6.2 Probabilistic Assessment

Although not a part of the current tasking, probabilistic modeling would recognize variability in fatigue strength and loads as follows:

- Once the model is created, run it first with the CWC spectrum and then adjust the reliability until fatigue life matches OEM-assigned life.
- When the RR average spectrum was run at the same level of reliability; the life was shown to increase.
- The RR average spectrum model reliability was then increased until the life decreased to OEM-assigned retirement life.
- The difference in reliability is the CWC's contribution to the component reliability.
- This process is illustrated in appendix B and explained in section 3.3.3.3.2.

3.1.7 Compare New to Old Usage Spectrum

3.1.7.1 RR

IVHMS regime parameters and regime definitions [4] were tabulated for a total of 93 flight regimes. A list of regime parameters and a sample of the regime definitions is shown in table 2.

RRA were developed and verified in Microsoft Excel. Algorithms were then programmed in an open-source language (Python). The RRA were developed based on Goodrich ground station regime definitions. The RRA were adjusted to obtain 100% recognition with no regime gaps or

overlaps. Any flight time that was found to be “Unrecognized” was assigned to the total regime time of a damaging regime that occurred either before or after the unrecognized flight time. Any regimes that had the potential to overlap had that time assigned to the most damaging regime to avoid double counting the time. Entry and recovery regimes, when not explicitly identified by IVHMS flags, were assumed to take place immediately before and after the associated steady state (SS) regime. The time for these entry and recovery regimes was added to the total time for the flight. The results of the RRA analysis were not compared to the Goodrich ground station output.

Operational UH-60M IVHMS data consisted of 839 flight hours and 2106 ground-air-ground (GAG) cycles recorded during 474 flights of 14 operational aircraft. The flights, flight hours, and GAG cycles for each of the 14 aircraft are shown in figures 3 and 4. It should be noted that not all .rdf “flights” are included in the RR database. By definition, a flight initiates when the rotor speed reaches 50%. To avoid biasing the RR results with non-flights (no takeoff) and very short flights (extremely short duration between takeoff and landing), these events were filtered from the database.

Low cycle maneuver-to-maneuver damage was neglected in this study. This is because the FSR only accounts for regime damage within each of the individually identified regimes and for GAG damage. Some OEMs address GAG damage by assuming a specified rate of takeoffs and landings. The takeoff rate should be higher than actual to address the undefined maneuver-to-maneuver (MTM) cycles. Others specify a rate of MTM pairings and calculate GAG damage by sorting and summing up the worst case load pairs with numbers of cycles defined by the spectrum. This activity addressed GAG by counting the number of takeoffs, per the definition of GAG, but did not explicitly account for MTM cycles.

A comparison of CWC usage with actual operational usage for each UH-60M regime is shown in figures 5–8. Note that very little of the operational usage occurred at GW values in the low-mid range ($\leq 17,000$ lb). Mid-high GW is defined as greater than 17,000 lb.

As shown in figure 8, there are two types of GAG events. If a landing has been identified, then one of the following two GAG events has occurred:

- Landing event without rotor shutdown = GAG
- Landing event with rotor shutdown = min-max

Table 2. Regime parameters and sample regime parameter values

Low-Mid GW	1		3	2	4	12	13	14	15	19	21	23	
Mid-High GW	40		42	41	43	51	52	53	54	58	60	62	
FSR Regimes	HOVER		RTS FLT	LTS FLT	REAR FLT	LF 0.8VH	LF 0.9VH	FL 1.0VH	SIDESLIP (Left)	TURN 30L	TURN 45L	TURN 60L	
IVHMS Regimes →	7	8	10	11	12	23	24	25	29	55	56	57	58
	Low Speed Maneuvers					Forward Flight Maneuvers							
	Hover		Sideward Flight		Rear Flight	Level Flight			Sideslip	Level Flight Turns			
	IGE	OGE	Right	Left		0.7 Vh – 0.8 Vh	0.8 Vh – 0.9 Vh	0.9 Vh – 0.1.0 Vh	Left	Left			
									30° AOB (10° - 35°)	45° AOB (35° - 50°)	60° AOB (50° - 65°)	>60° AOB (>65°)	
WOW Delayed	0	0	0	0	0	0	0	0	0	0	0	0	0
Landing Flag	0	0	0	0	0	0	0	0	0	0	0	0	0
Takeoff Flag	0	0	0	0	0	0	0	0	0	0	0	0	0
Main Rotor Speed													
Radar Altitude	<=80	>80											
Calibrated Airspeed	<=43	<=43	<=43	<=43	<=43	>43	>43	>43	>43	>43	>43	>43	>43
Roll Attitude	>=-6.0 <=0.0	>=-6.0 <=0.0	>0.0	<-6.0	>=-6.0 <=0.0	>=-10 <=+10	>=-10 <=+10	>=-10 <=+10	>=-10 <=+10	<-10 >-35	<-35 >-50	<-60 >-65	<-65
Pitch Attitude	>=+1.0 <=+7.0	>=-6.0 <=0.0	>=0.0 <=+7.0	>=1.0 <=+7.0	>+7.0								
Altitude Rate						>=-600 <=+600	>=-600 <=+600	>=-600 <=+600	>=-600 <=+600	>=-600 <=+600	>=-600 <=+600	>=-600 <=+600	>=-600 <=+600
Lateral Acceleration, Filtered						>=-0.08 <=+0.08	>=-0.08 <=+0.08	>=-0.08 <=+0.08	>+0.08				
Yaw Rate	>=-2.5 <=+2.5	>=-2.5 <=+2.5				>=-5 <=+5	>=-5 <=+5	>=-5 <=+5	>=-5 <=+5				
Corrected Nz						>=0.8 <=1.2	>=0.8 <=1.2	>=0.8 <=1.2	>=0.8 <=1.2	<=1.2	<=1.2	<=1.2	<=1.2
RMS Nz													
Vh Fraction						>0.7 <=0.8	>0.8 <=0.9	>0.9 <=1.05	<=1.05				
Derived TGT													
Eng 1 Torque													
Eng 2 Torque													
Total Eng Torque													
Control Reversal Flag	0	0				0	0	0	0				
Turn Entry Recovery ID						0	0	0	0	0	0	0	0

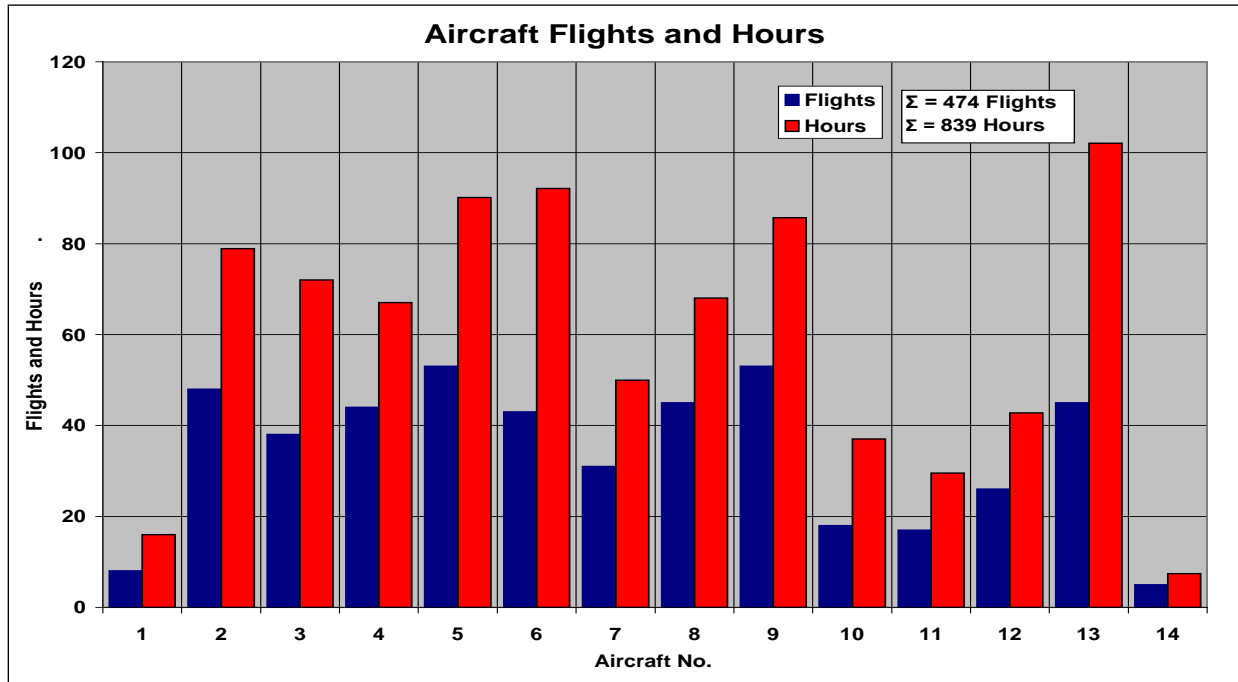


Figure 3. UH-60M IVHMS flights and flight hours

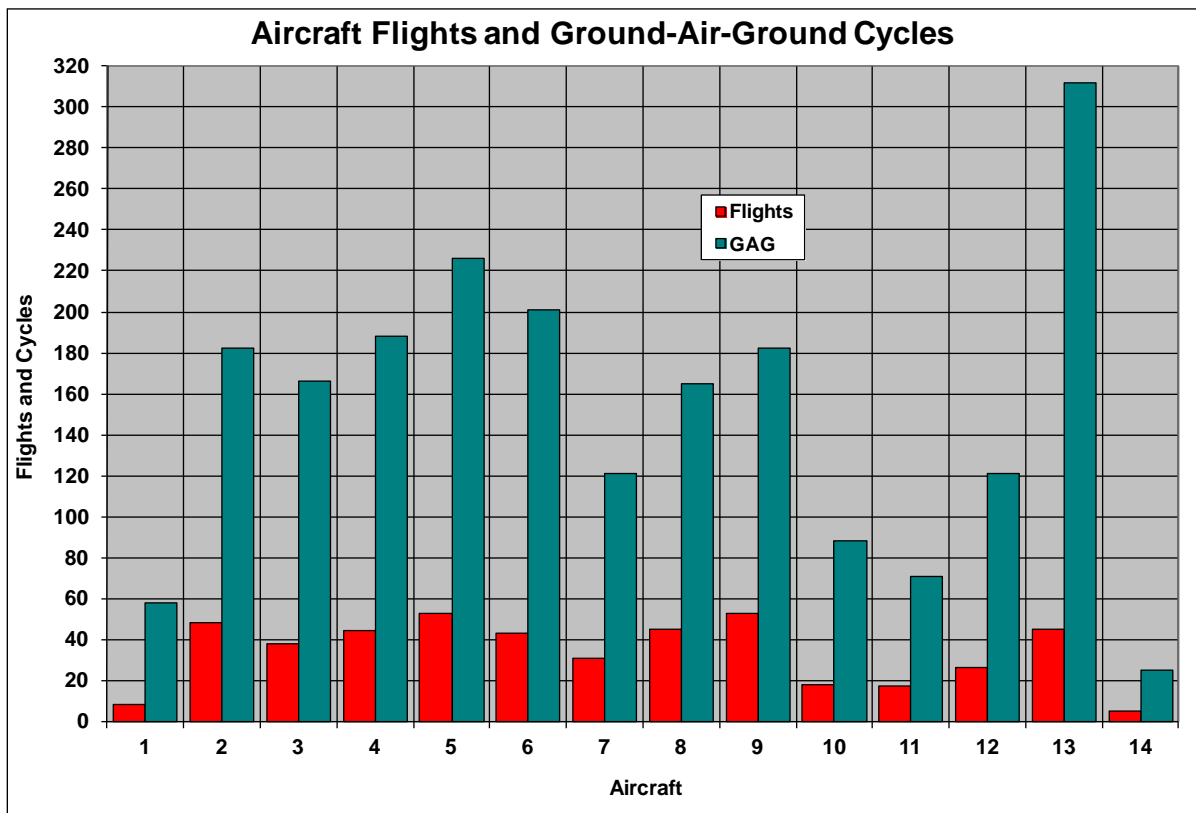


Figure 4. UH-60M IVHMS flights and GAG cycles

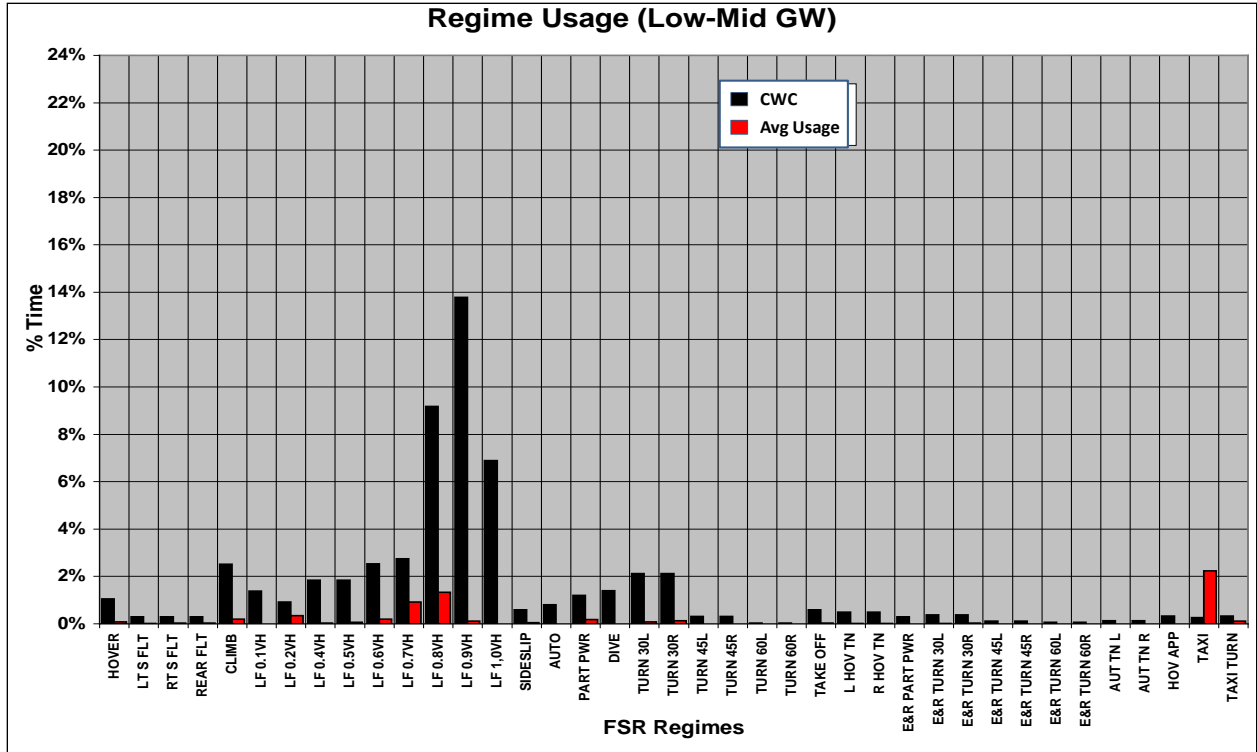


Figure 5. CWC versus average regime usage (low-mid GW)

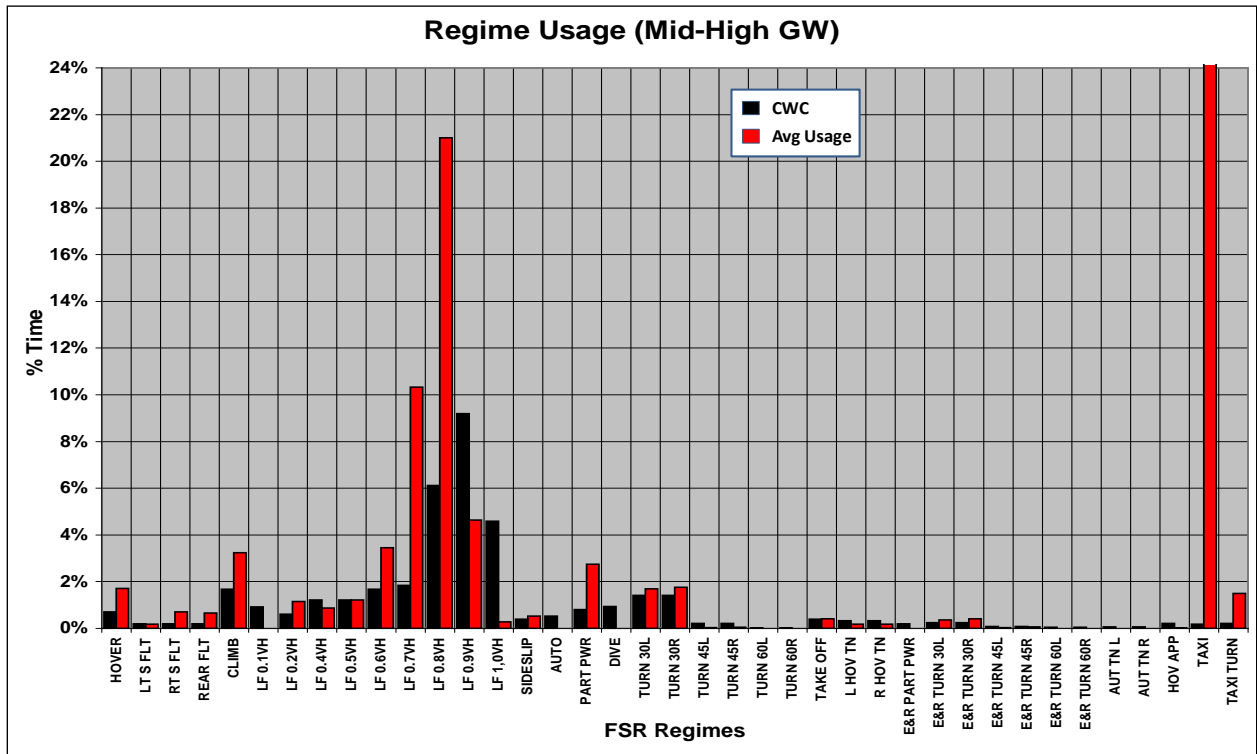


Figure 6. CWC versus average regime usage (mid-high GW)

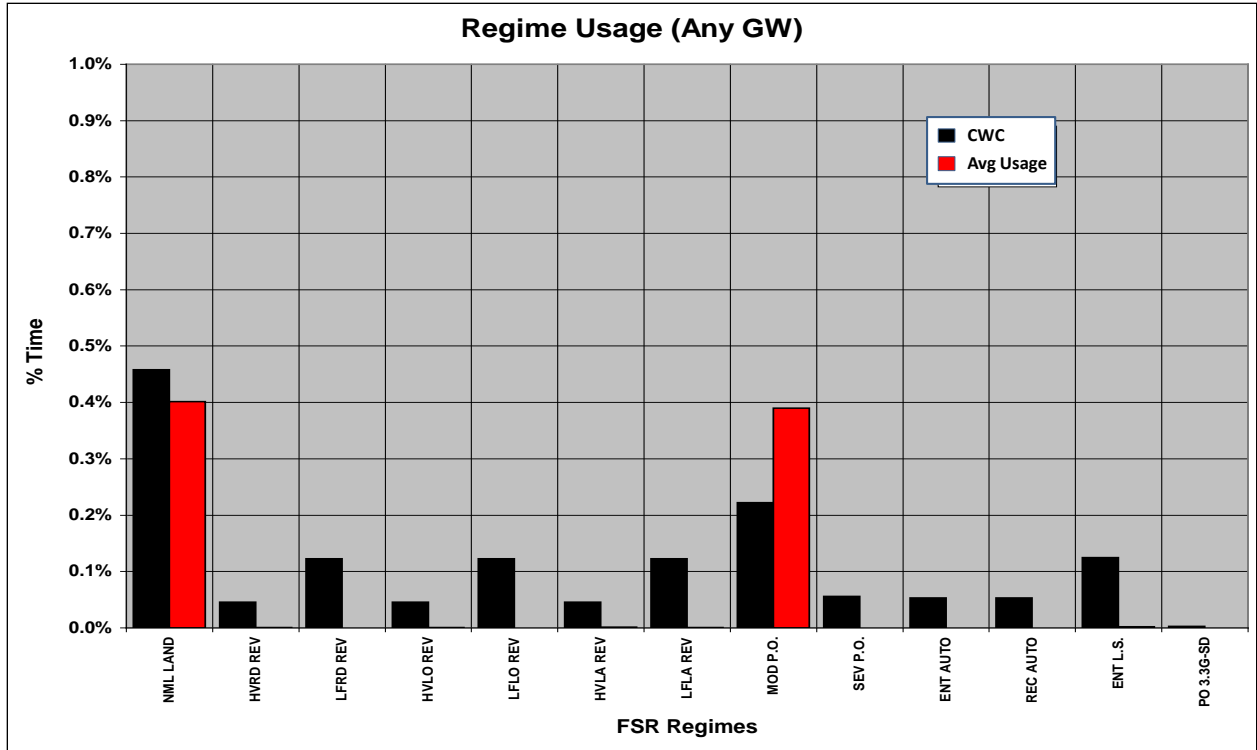


Figure 7. CWC versus average regime usage (any GW)

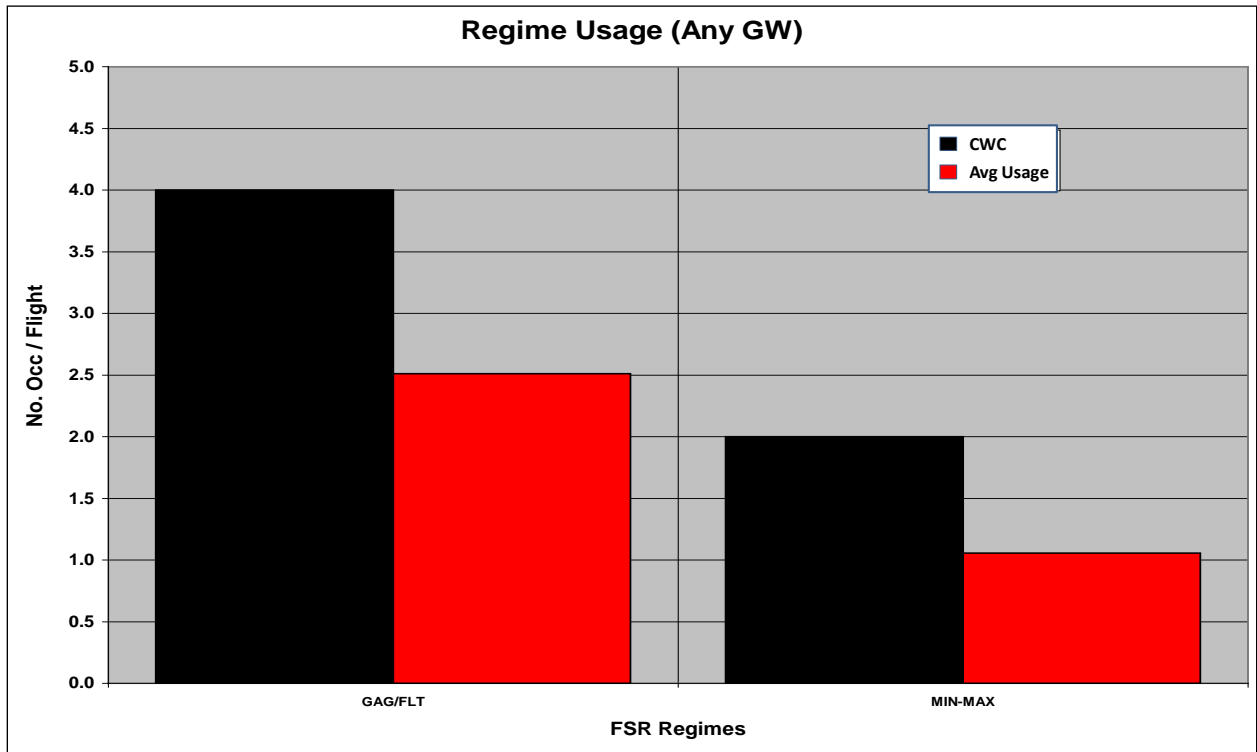


Figure 8. CWC versus average regime usage (GAG and min-max)

3.1.8 Identify Critical Flight Regimes for Credit Calculations

A review of the UH-60M FSR reveals that many regimes produce damage in one or more of the UH-60M fatigue-life-limited dynamic component failure modes.

UH-60M flight regimes selected for credit calculations depend upon the dynamic components selected for usage credit consideration.

It is recommended that all regimes that produce measurable damage in any fatigue-life-limited dynamic component be selected for the process.

Table 3 shows the percentage of damaging regimes for all 230 UH-60M failure modes. The percentage of those damaging regimes that produce damage in the four components and failure modes selected for developing usage credits will be discussed in section 3.3.

Table 3. Number of damaging regimes

Total No. Regimes	230 FSP Failure Modes		4 Selected Failure Modes	
	No. Damaging Regimes	% All Regimes	No. Damaging Regimes	% Damaging Regimes
93	64	68.8%	43	63.2%

3.2 TASK 1 UPDATE—PERFORM HUMS FLEET DATA ANALYSIS

The purpose of the Task 1 update was to expand and refine the original Task 1 effort:

Expand and refine UH-60M usage database:

- Identify and select UH-60M with diverse usage
- Acquire data files for selected aircraft
- Compile usage database for two operational environments

Expand and refine RRA:

- Evaluate accuracy of HUMS GW values
- Develop procedure for validating RRA

3.2.1 Expand and Refine UH-60M Usage Database

The UH-60M usage database was expanded and refined as described in sections 3.2.1.1–3.2.1.3.

3.2.1.1 Identify and Select UH-60M with Diverse Usage

UH-60M usage environments were evaluated with the objective of identifying diverse operational usage. Selections were based upon mission requirements, operations tempo, and operating environment, and included training and deployed environments. The objectives for selecting the aircraft follow.

Training aircraft selection objectives:

- A minimum of 20 aircraft (preferably 25) stationed at Fort Rucker
- A minimum of 1000 flight hours over a period of a year

Deployed aircraft selection objectives:

- A minimum of 20 aircraft (preferably 25) each from outside the Continental United States (OCONUS) 1 and OCONUS 2 (from several units) for a total of 40 aircraft
- A minimum of 500 flight hours each from OCONUS 1 and OCONUS 2 over a period of a year for a minimum of 1000 flight hours

The results of the selection process are summarized in table 4.

Table 4. Summary of selected aircraft

Operational Environment	Number of Aircraft	Number of Flights	Number of Flight Hours
CONUS Training	32	475	741
OCONUS 1	30	1107	3367
OCONUS 2	29	1308	1923
Total	91	2890	6031

*CONUS=Continental United States

The flight hours for each of the individual aircraft in each of the three operational environments are shown in figures 9–11.

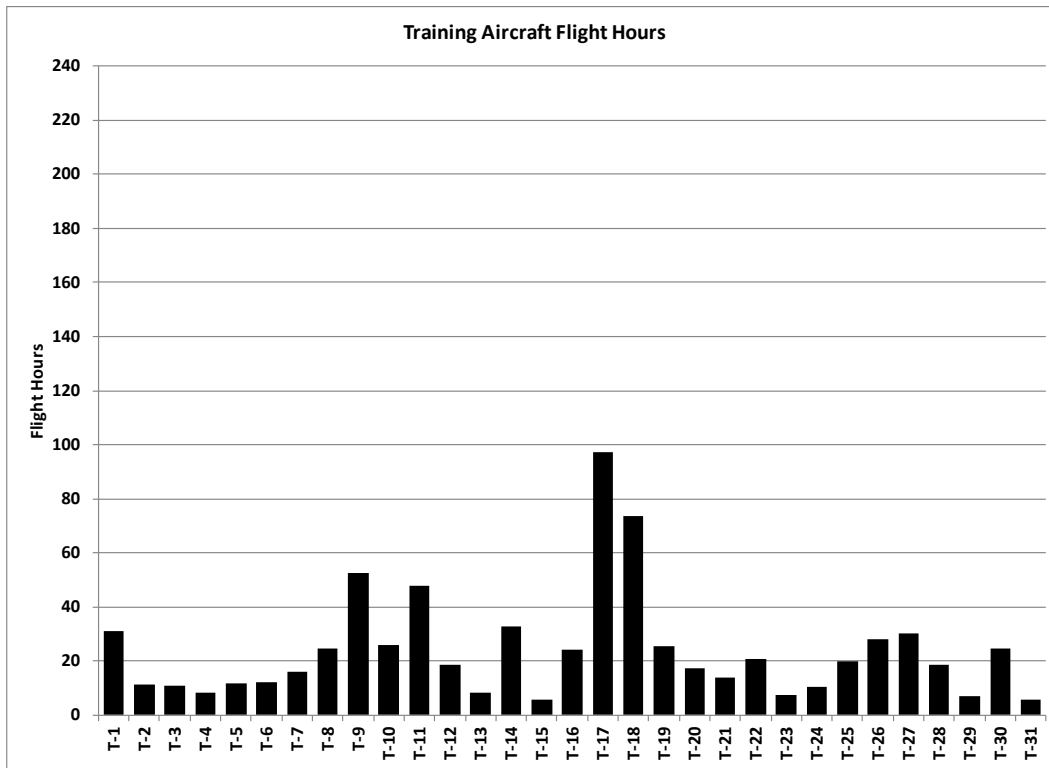


Figure 9. Training aircraft flight hours

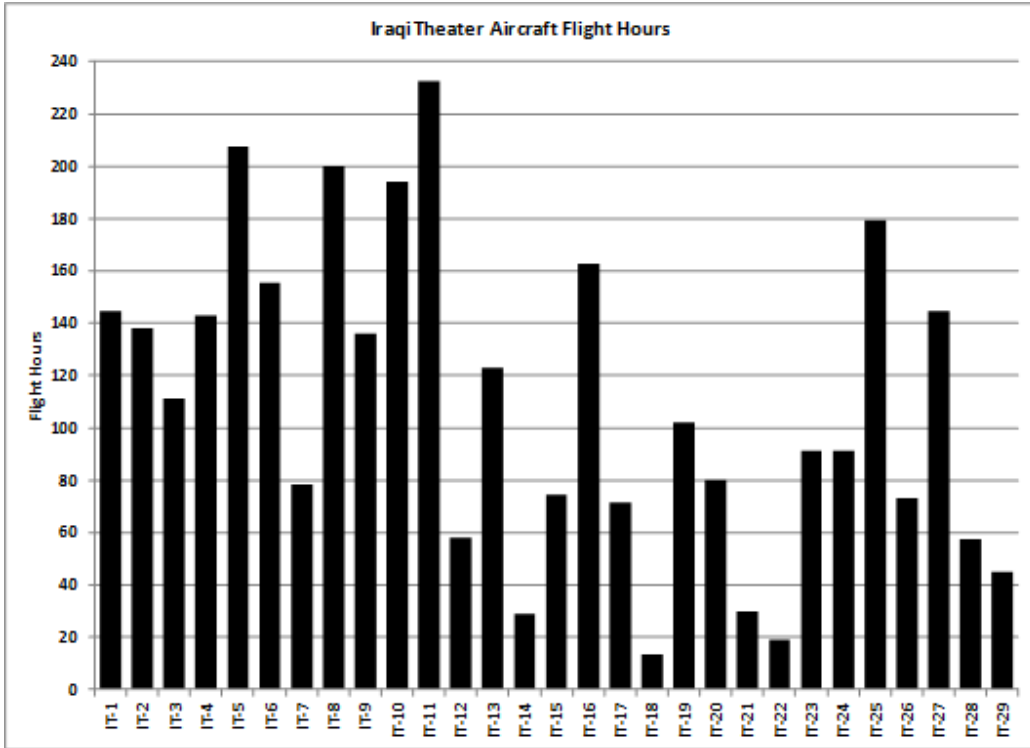


Figure 10. OCONUS 1 aircraft flight hours

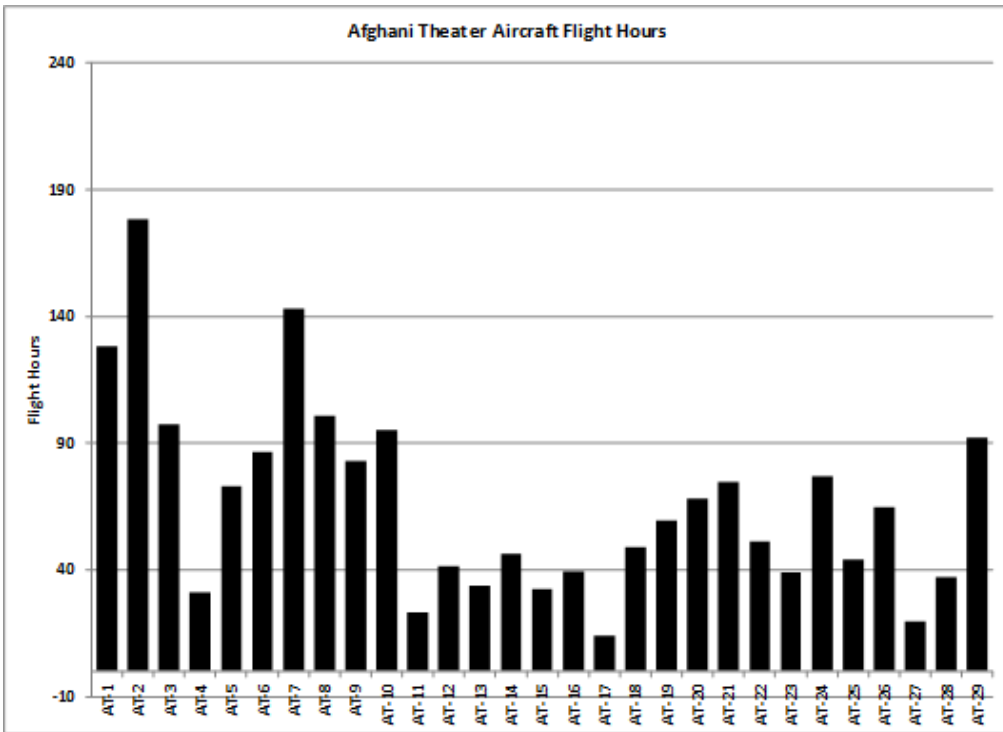


Figure 11. OCONUS 2 aircraft flight hours

3.2.1.2 Acquire Data Files for Selected Aircraft

The process and criteria for identifying and acquiring the data for the selected aircraft are described in sections 3.1.2 and 3.1.3. Once these criteria were satisfied, UH-60M data files were requested and acquired from the AED Aeromechanics Division.

3.2.1.3 Compile Usage Database for Selected Environments

The UH-60M operational usage data requested and obtained from Aeromechanics consisted of 6031 hours recorded during 2,890 flights on 91 operational aircraft. All flight-recorded data were converted from .rdf format into .csv format to facilitate the processing described below.

Parameters required for RR, as shown in table 2, were selected and prepared for use:

- All parameters were converted to a common sample rate to facilitate RR.
- Some noisy parameters were filtered, as required, to provide time domain smoothing.

3.2.2 Expand and Refine RR Algorithms

The RRA that were developed as described in section 3.1.7.1 were reviewed and refined as required to ensure that there would be no gaps or overlaps in regimes recognized. A sample of the IVHMS parameter values used for RR is shown in table 2.

3.2.2.1 Evaluate Accuracy of HUMS GW Values

The accuracy of HUMS GW values was not evaluated because GW prediction algorithms were not available.

3.2.2.2 Develop Procedure for Validating RR Algorithms

The recommended procedure for validating the RRA consists of three steps. Scripted flights with three repeats of damaging maneuvers/regimes by three different pilots will be flown. The scripted flights will be processed using the RR software and compared to the flight plan. The RR results should match 97% of the maneuvers on the flight script to pass this step of the validation, per the guidelines of ADS-79C [7]. This means that the maneuver and duration should be accurately recorded so that 97% of the flight time is properly identified.

The RR results from fielded aircraft will be compared to pilot surveys that consist of questionnaires and interviews used to determine the flight maneuvers flown by each pilot. The pilot surveys will be used to provide a picture of the general usage of the monitored aircraft. This step of the validation will be a success if no significant discrepancies between the RR results and pilot surveys are found.

Flight visualization software will be used to animate selected flight segments and display the aircraft attitude, flight path, cockpit instrument images, and aircraft state parameter time history plots and digital values for the flight maneuvers. The animation of the flight will be compared to

the RR results to determine if any maneuvers are misidentified. For any time categorized as “Unrecognized Time” by the RR software, the flight visualization software will be utilized to determine the severity of the unidentified maneuvers. A snapshot of the information available from FlightViz is shown in figure 12.

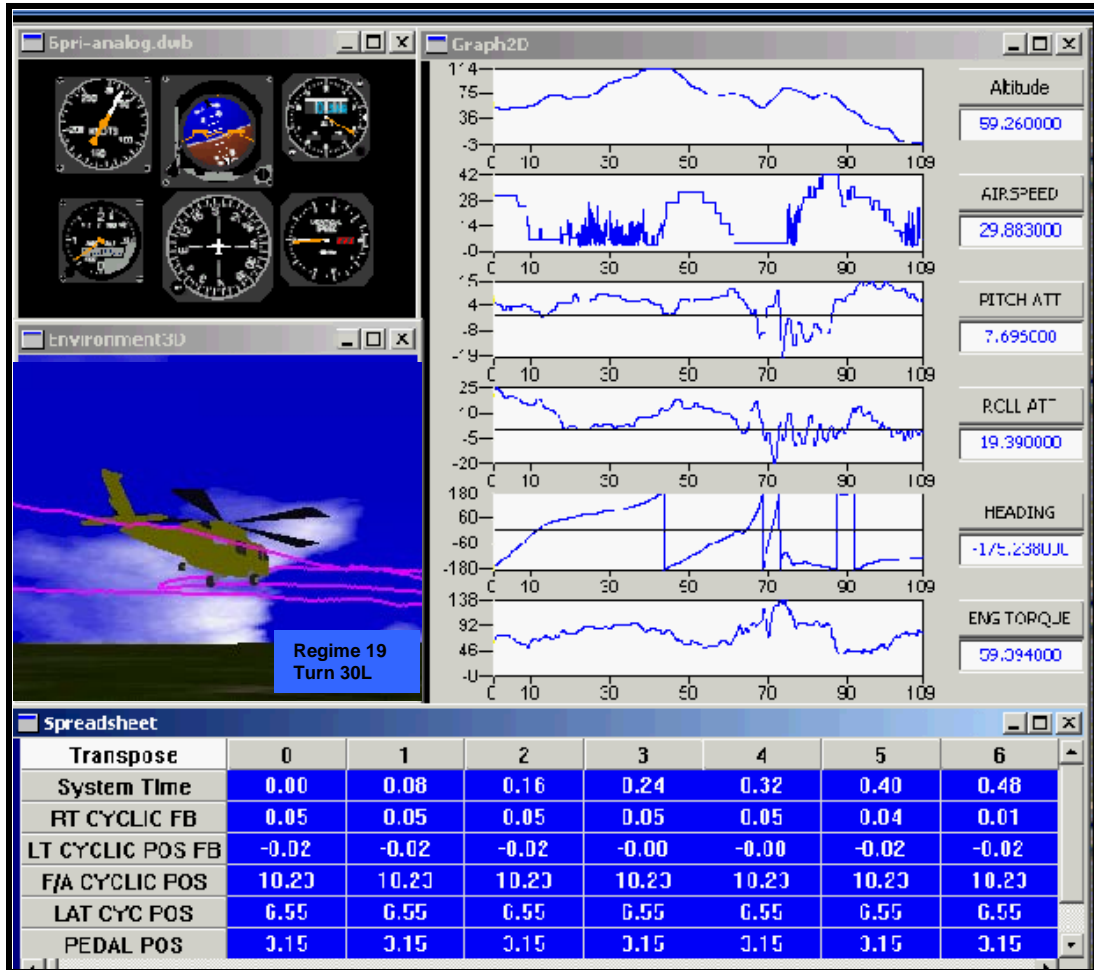


Figure 12. Snapshot of FlightViz animation

3.3 TASK 2—DEVELOP USAGE CREDITS

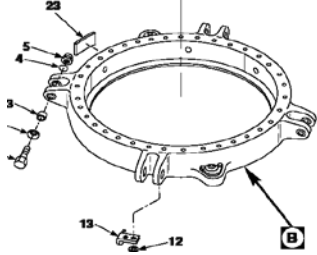
3.3.1 Select Two Components

Criteria were developed for selecting UH-60M components to be used for demonstrating the process and benefits of usage monitoring. The criteria specified that each selected component should:

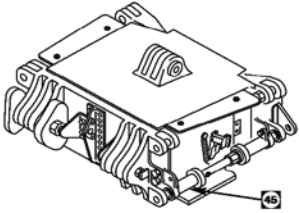
- Be a major, high-value component.
- Have relatively short CRTs.
- Be sensitive to multiple damaging regimes.

The two components selected met these criteria and each had two failure modes. The selected components are identified and described in figure 13.

Component		Part No.	Failure Mode		CRT	
1	Main Rotor Rotating Swashplate Assembly	70104-08001-044,-045,-050	A	Pushrod Attachment Mode	Chafing	5,000
			B		Non-Chafing	7,400
2	Composite Stabilator Center Box Assembly	702000-27000-049	A	Aft Fitting	Chafing	1,000
			B		Non-Chafing	2,400



70104-08001-044
Main Rotor Rotating Swashplate Assy
Fracture Mode: Pushrod Attachment
SER-70114



702000-27000-049
Composite Stabilator Center Box Assembly
Fracture Mode: Aft Fitting
SER-520203

Figure 13. Selected components and failure modes

3.3.2 Review Fatigue Substantiation Document

Sikorsky's UH-60M FSR was reviewed for the two selected components and the CWC damage fractions were summarized for each damaging regime in tables 5–7 for each of the three GW ranges. The blank cells indicate there is no damage produced by that regime. The black cells contain the FSR damage fraction produced for 100 hours of CWC usage. As shown at the bottom of table 7, the red shaded numbers are the summation of all damage for each of the component failure modes, and the blue shaded number is the calculated CRT. The calculated CRT is

determined by dividing the damage fraction sum into 100. The percentage of CWC damage that is produced by each of the regimes is shown in figures 14–16. The sum of the bar charts for each component failure mode in figures 14–16 is 100%.

Table 5. Selected component CWC damage fractions by regime (low-mid GW)

FSR Regime		Design %Time	Design Occ per 100 Hrs	MR ROTATING SWASHPLATE ASSEMBLY, PUSHROD ATTACHMENT MODE		COMPOSITE STABILATOR CENTER BOX ASSEMBLY, CUMULATIVE'	
				Chafing	Non-Chafing	Chafing	Non-Chafing
				70104-08001-044,-045,-050		702000-27000-049	
LOW-MID GW							
1	HOVER	1.058%					
2	LT S FLT	0.300%					
3	RT S FLT	0.300%					
4	REAR FLT	0.300%					
5	CLIMB	2.520%					
6	LF 0.1VH	1.376%					
7	LF 0.2VH	0.920%					
8	LF 0.4VH	1.836%					
9	LF 0.5VH	1.836%					
10	LF 0.6VH	2.526%					
11	LF 0.7VH	2.755%					
12	LF 0.8VH	9.187%					
13	LF 0.9VH	13.782%					
14	LF 1,0VH	6.891%				0.0226	
15	SIDESLIP	0.600%				0.0039	0.0005
16	AUTO	0.801%					
17	PART PWR	1.200%				0.0031	
18	DIVE	1.394%		0.0058	0.0019	0.0282	0.0217
19	TURN 30L	2.125%				0.0018	
20	TURN 30R	2.125%					
21	TURN 45L	0.312%				0.0003	
22	TURN 45R	0.312%					
23	TURN 60L	0.025%			0.0001	0.0000	
24	TURN 60R	0.025%		0.0002	0.0001	0.0000	
25	TAKE OFF	0.600%	360	0.0002			
26	L HOV TN	0.500%	150				
27	R HOV TN	0.500%	150				
28	E&R PART PV	0.300%	720			0.0008	
29	E&R TURN 30L	0.375%	900			0.0018	0.0004
30	E&R TURN 30R	0.375%	900			0.0008	0.0002
31	E&R TURN 45L	0.113%	204			0.0006	0.0002
32	E&R TURN 45R	0.113%	204			0.0003	0.0001
33	E&R TURN 60L	0.064%	92	0.0001	0.0000	0.0003	0.0002
34	E&R TURN 60R	0.064%	92	0.0002	0.0001	0.0006	0.0003
35	AUT TN L	0.138%	33				
36	AUT TN R	0.138%	33				
37	HOV APP	0.333%	300				
38	TAXI	0.270%					
39	TAXI TURN	0.333%	480				

Table 6. Selected component CWC damage fractions by regime (mid-high GW)

FSR Regime		Design %Time	Design Occ per 100 Hrs	MR ROTATING SWASHPLATE ASSEMBLY, PUSHROD ATTACHMENT MODE		COMPOSITE STABILATOR CENTER BOX ASSEMBLY, CUMULATIVE'	
				Chafing	Non-Chafing	Chafing	Non-Chafing
				70104-08001-044,-045,-050		702000-27000-049	
MID-HIGH GW							
40	HOVER	0.705%					
41	LT S FLT	0.200%					
42	RT S FLT	0.200%					
43	REAR FLT	0.200%					
44	CLIMB	1.680%		0.0016	0.0004		
45	LF 0.1VH	0.918%					
46	LF 0.2VH	0.613%					
47	LF 0.4VH	1.224%					
48	LF 0.5VH	1.224%					
49	LF 0.6VH	1.684%					
50	LF 0.7VH	1.837%					
51	LF 0.8VH	6.125%					
52	LF 0.9VH	9.188%					
53	LF 1,0VH	4.594%				0.0028	
54	SIDESLIP	0.400%				0.0011	
55	AUTO	0.534%					
56	PART PWR	0.800%				0.0025	
57	DIVE	0.930%				0.0076	0.0025
58	TURN 30L	1.417%				0.0015	
59	TURN 30R	1.417%				0.0010	
60	TURN 45L	0.207%		0.0014	0.0006		
61	TURN 45R	0.207%		0.0012	0.0005		
62	TURN 60L	0.017%		0.0004	0.0004		
63	TURN 60R	0.017%		0.0004	0.0005		
64	TAKE OFF	0.400%	240				
65	L HOV TN	0.333%	100				
66	R HOV TN	0.333%	100				
67	E&R PART PV	0.200%	480			0.0008	
68	E&R TURN 30L	0.250%	600			0.0012	0.0003
69	E&R TURN 30R	0.250%	600			0.0009	0.0002
70	E&R TURN 45L	0.076%	136	0.0001	0.0000	0.0008	0.0001
71	E&R TURN 45R	0.076%	136	0.0003	0.0000	0.0008	0.0000
72	E&R TURN 60L	0.043%	62	0.0008	0.0009	0.0009	0.0000
73	E&R TURN 60R	0.043%	62	0.0013	0.0016	0.0001	0.0000
74	AUT TN L	0.061%	22				
75	AUT TN R	0.061%	22				
76	HOV APP	0.222%	200				
77	TAXI	0.180%					
78	TAXI TURN	0.222%	320				

Table 7. Selected component CWC damage fractions by regime (any GW)

FSR Regime		Design %Time	Design Occ per 100 Hrs	MR ROTATING SWASHPLATE ASSEMBLY, PUSHROD ATTACHMENT MODE		COMPOSITE STABILATOR CENTER BOX ASSEMBLY, CUMULATIVE'	
				Chafing	Non-Chafing	Chafing	Non-Chafing
ANY GW							
79	NML LAND	0.458%	550				
81	HVRD REV	0.046%	110				
82	LFRD REV	0.123%	294			0.0003	0.0002
83	HVLO REV	0.046%	110				
84	LFLO REV	0.123%	294			0.0011	0.0005
85	HVLA REV	0.046%	110				
86	LFLA REV	0.123%	294			0.0008	0.0002
87	MOD P.O.	0.222%	80	0.0010	0.0010	0.0002	0.0001
88	SEV P.O.	0.056%	40	0.0020	0.0025	0.0004	0.0002
89	ENT AUTO	0.053%	95			0.0002	
90	REC AUTO	0.053%	95	0.0001	0.0000	0.0002	
91	ENT L.S.	0.125%	180				
99	PO 3.3G-SD	0.003%	2	0.0001	0.0002		
102	GAG/FLT		400	0.0020	0.0026	0.0080	0.0136
103	MIN-MAX		200				
Σ Damage				0.0192	0.0136	0.0984	0.0417
				5208	7355	1016	2399

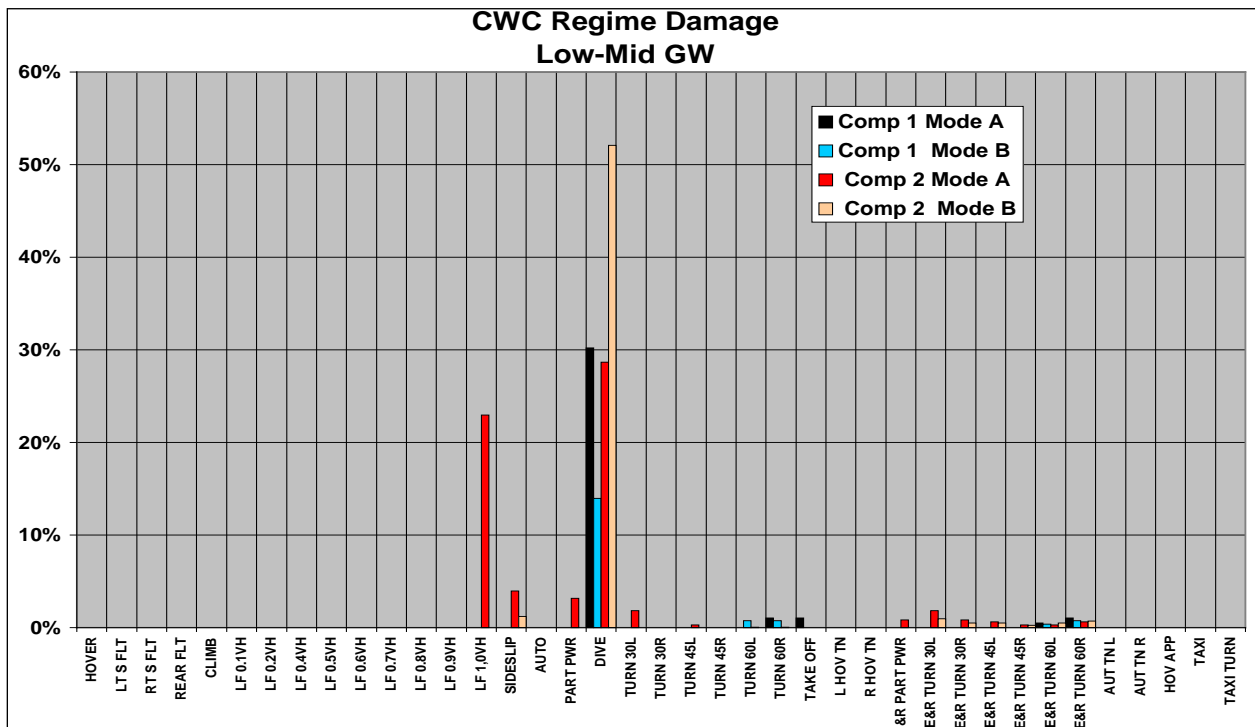


Figure 14. Component failure mode CWC damage by regime (low-mid GW)

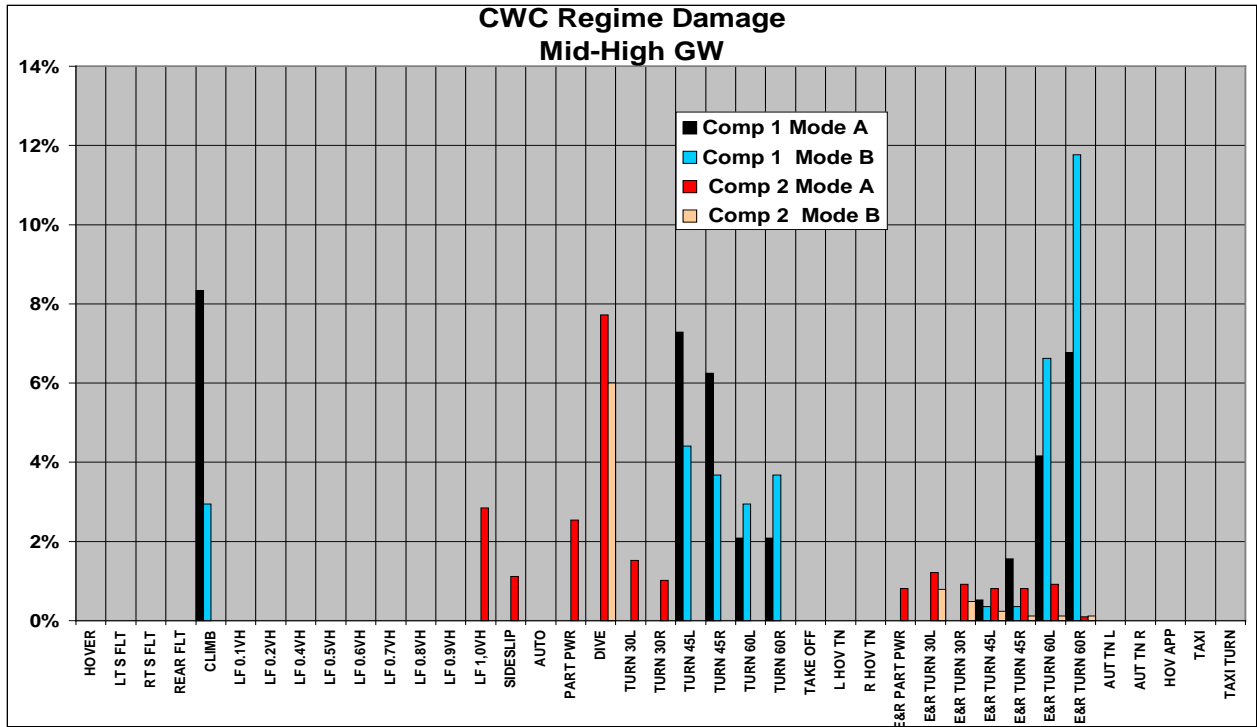


Figure 15. Component failure mode CWC damage by regime(mid-high GW)

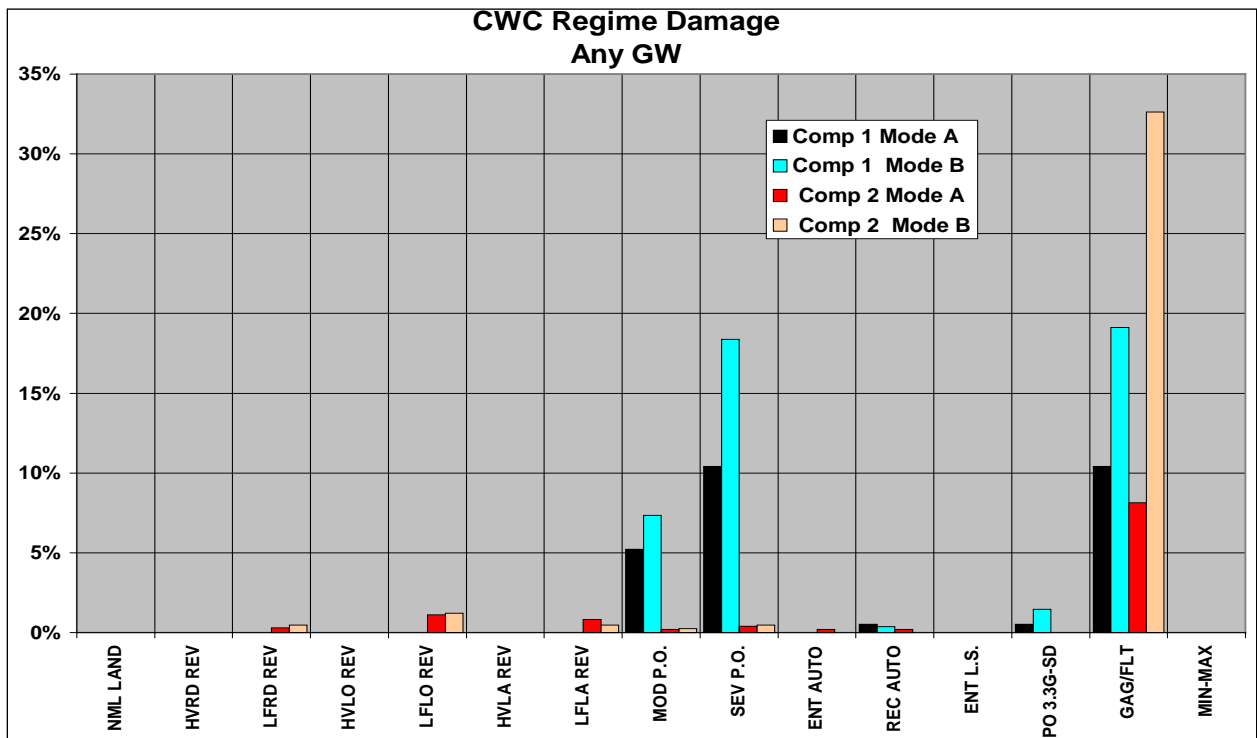


Figure 16. Component failure mode CWC damage by regime (any GW)

3.3.3 Evaluate Reliability of OEM CRT

SUMS represent a technology that has been steadily evolving within the rotorcraft community for more than 20 years. Improvements in both data processing and storage capabilities have brought the cost of this technology down to the point where an entire fleet can be outfitted with SUMS relatively easily and inexpensively. The benefit realized from increases in component fatigue lives due to measured, rather than postulated, usage is obvious when the conservative bias associated with a CWC usage spectrum is removed. However, replacing the conservative CWC with a SUMS-based usage spectrum causes a reduction in component reliability. At the component level, reliability is traditionally calculated based on three random variables: fatigue strength, flight loads, and aircraft usage, the last taking the form of a so-called loading spectrum comprised of a sequence of both SS and transient flight regimes that sum to a standardized block of 1 hour of flight time. The analysis in this sub-task determined how component fatigue life reliability changes when SUMS data are used as the basis for the usage spectrum.

The first part of this sub-task discusses how the SUMS-based spectrum alters the historical approach to calculating fatigue life. In all, 474 flights encompassing 839 hours of flight time from 14 different aircraft were processed for this investigation. It was no surprise that many of the severe regimes contained in the CWC spectrum were not flown during the SUMS data acquisition. The second part of the sub-task looked at fatigue life versus reliability for two structural components, each having two modes of failure. Both the deterministic methodology that is generally followed by OEMs as well as a probabilistic methodology will be used in evaluating the four failure modes.

3.3.3.1 Background

Historically, fatigue life has been calculated deterministically by assuming conservatively biased values for the three random variables that are responsible for fatigue damage—namely usage, flight loads, and fatigue strength. Usage takes the form of the CWC spectrum. The flight regimes contained in CWC may be thought of as an array in which SS and transient (TR) flight conditions are represented by rows and the aircraft states or prorates are represented by columns. The SS flight conditions (e.g., level flight, climb, sideslip) generally contain harmonic time histories and, as such, are time-based, whereas TR flight conditions are characterized by a large aperiodic cycle that can be attributed to control input/output upon which a harmonic signal rides because of the periodicity of the rotor. Because the aperiodic signal is responsible for most, if not all, of the damage in a transient event, it is generally considered on an occurrence (not time) basis when computing fatigue life. Prorate variables are generally takeoff GW, center of gravity, density altitude, and possibly cargo configuration (e.g., internal payload, slung load). The CWC spectrum is deliberately made severe enough to cover the worst-case scenario of regimes from a fatigue damage standpoint and intrinsically intended to cover the most severely flown aircraft contained in the fleet.

Traditionally, flight loads have been deliberately biased to the so-called top-of-scatter (TOS) condition measured during the flight test for the given maneuver. In the case of SS regimes, TOS is the highest peak oscillatory load measured during the flight test. Because of the harmonic character of the time history and the significant amount of time the aircraft spends in SS regimes,

the sample size from which the TOS load is drawn is large. However, in general, there tends to be very little damage done in SS regimes. In the case of TR regimes, where the power input/output signal typically occurs only once during the regime, the TOS event is usually the one with the highest damage rate or event that contains the highest oscillatory load, although very often these two criteria lead to the same result. The TR regimes are generally responsible for most of the fatigue damage that a component incurs, yet they are often flown only once or, in some instances, replicated one or two times during a flight strain survey (FSS). Thus, TR regimes represent a statistically small sample size or, in the case of a single sample, there is no statistical significance.

Fatigue strength is deliberately biased by reducing the mean endurance limit (EL) and associated S-N curve to an estimated $\mu-3\sigma$ working curve. The reduction in EL is based on a small sample, usually six or fewer, of laboratory fatigue tests of full-scale specimens. The S-N curve is generally, but not necessarily, characterized statistically by a large sample of small-scale coupons made from the same material, subject to the same or similar processing steps (heat treatment, surface finish, etc.), and exhibiting the same mode of failure. The coupon testing may have been carried out by the OEM or available from a source such as the one described in “Metallic Materials Properties Development and Standardization” [8]. The stochastic nature of the coupon testing is generally not addressed, but, rather, once an S-N curve shape is established, it is non-dimensionalized and used whenever suitable.

In the late 1980s, during the light helicopter experimental competition (which later led to the Comanche program), the Army issued a reliability requirement of six-nines (mathematically 0.999999 or 0.9_6 in shorthand) for all dynamic components being qualified for that program as well as future programs. The complementary risk to six-nines is one in a million failures. Because the large fleet of helicopters the Army might be flying at any given time would be about 8000 and they would each contain 100 fatigue critical component failure modes, the original thought process was that a risk level of roughly one in a million ($.000001$ or $.0_51$ in shorthand) could be tolerated [9].

The rotorcraft industry responded to the requirement by demonstrating that their deterministic method, as described implicitly, contained six-nines of reliability or more because of all the deliberate conservatism put into it (e.g., [10] and [11]) and, as such, no major changes were necessary on the part of the OEMs. The advent of SUMS has now made it possible to determine actual usage. When updating the CWC spectrum with SUMS data, use of the average usages would lose a measure of reliability, which would have to be made up in loads or strength. Therefore, ADS-79C [7], paragraph A.6.5, suggests a statistical biasing and calls the use of a mean spectrum inappropriate. It states that when using individual flight usage monitoring with the legacy approach to loads and strength, the usage is biased to maintain reliability by doubling the accrued damage. For a more fully statistical approach with individual aircraft-monitored loads, all six-nines of reliability must come from loads and strength. With a direct monitoring of loads, the only remaining statistical value (and source of reliability) is strength.

3.3.3.2 Quantifying Reliability Inherent in Traditional Lifting Method

In the previous section, the essentials of the traditional deterministic fatigue life methodology were discussed. It was also noted that the rotorcraft industry’s position is that the method meets or exceeds six-nines of reliability. In this section, the reliability contribution of each of the three key ingredients that go into the analysis—namely CWC usage, TOS loads, and a $\mu-3\sigma$ working curve—will be assessed.

3.3.3.2.1 Quantifying the Inherent Reliability in CWC

As mentioned in the previous section, the CWC spectrum is intended to be very conservative and, as such, severe enough to cover the most severely operated aircraft in the fleet. There is a question as to how one goes about quantifying its inherent reliability. The answer is that it must be compared to the average usage for the aircraft or fleet being investigated; the former would apply to an “individual aircraft tracking program” (IATP), the latter to a revised spectrum for a fleet of aircraft. The inherent reliability of CWC is notionally displayed in figure 17, where it can be seen that the red dashed line’s relationship to the green solid line, which is the RR average, is where the reliability comes from. The CWC dashed red line has been drawn at a standard normal Z-score of 1.282, which corresponds to the 90th percentile of a normal distribution. The solid green RR average line lies at the median or 50th percentile of the distribution (mean, median, and mode are coincident if it is a normal distribution). In terms of reliability, the CWC dashed line appears to have one-nine of reliability, while the RR average solid line at the median has a reliability that is equal to its unreliability (i.e., success or failure have the same probability). However, because an incremental change in usage does not have the same effect as an incremental change in load severity or fatigue strength, the actual inherent reliability in CWC will be less. In section 3.3.3.2.2, it will be demonstrated how the CWC reliability contribution is situation-dependent.

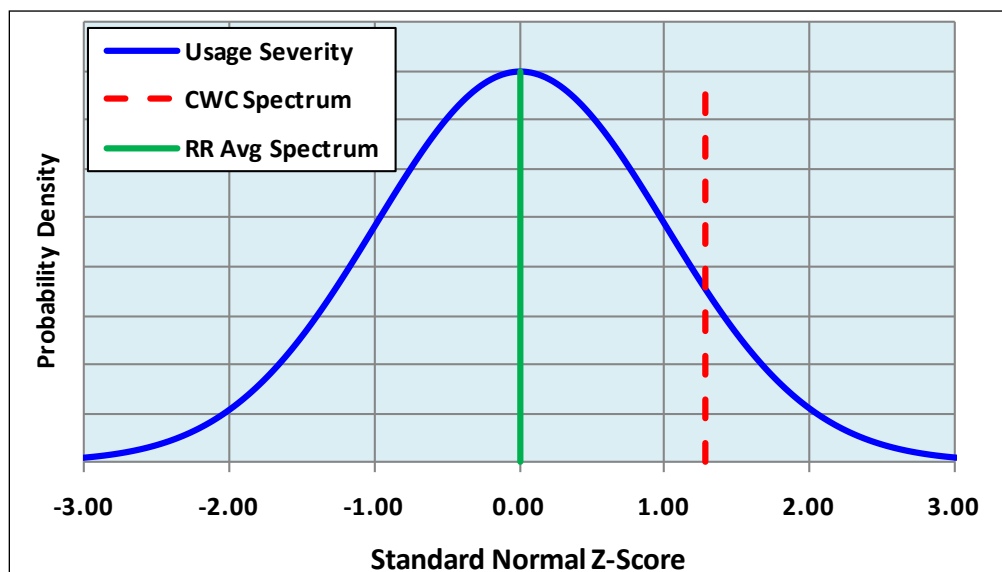


Figure 17. Schematic of CWC spectrum reliability generation

3.3.3.2.2 Quantifying the Inherent Reliability of TOS Loading

The TOS aspect of the traditional fatigue life methodology was described in section 3.3.3.1. It was pointed out that quantifying the inherent reliability of TR, where most of the fatigue damage is done, is greatly hindered by the fact that the sample size of applicable events is often limited to between one and three and, in certain cases (e.g., telemetry dropout for a rotating component), is zero. The zero cases are handled through substitution, which further clouds the issue depending on what substituted event is available. Unless steps are taken to fly enough replicate events to constitute a reasonable sample size of, for instance 10, given the time and expense of flight testing, the analyst cannot place a high level of confidence in obtaining an extreme value for the requisite event. The inherent reliability of the so-called TOS event notionally comes from the same type of situation as illustrated in figure 17, if one simply adopts the label of TOS damage rate for the dashed red line and average damage rate for the solid green line.

To understand how the lack of confidence manifests itself, it is helpful to see what effect sample size has on predicting the true mean, μ , of a normally distributed random variable. The confidence interval relating the sample mean to the true mean is student t -distributed according to the following relationship:

$$\bar{x} - \frac{\sigma}{\sqrt{n}} t_{\alpha/2, v} \leq \mu \leq \bar{x} + \frac{\sigma}{\sqrt{n}} t_{\alpha/2, v} \quad (1)$$

Equation (1) can be represented visually as is done for the case of a 90% confidence interval when estimating a true standard normal variate (i.e., $\mu=0$ and $\sigma=1$) in figure 18. The fact that standard normal variate is the basis of figure 18 makes it generally applicable to all normal random variables. It can clearly be seen that the upper and lower confidence levels funnel inward as the sample size increases from $n=2$ to 60. Figure 18 begins at a sample size of $n=2$ because that is the minimum requirement to make a statistical estimate. This means that the case of a single record, which is often the case when acquiring transient records, cannot be addressed statistically. Notice that the upper 95% confidence bound moves to $\leq 5\%$ when the number of samples is approximately six or more, but two samples means one may be more than 11% in error.

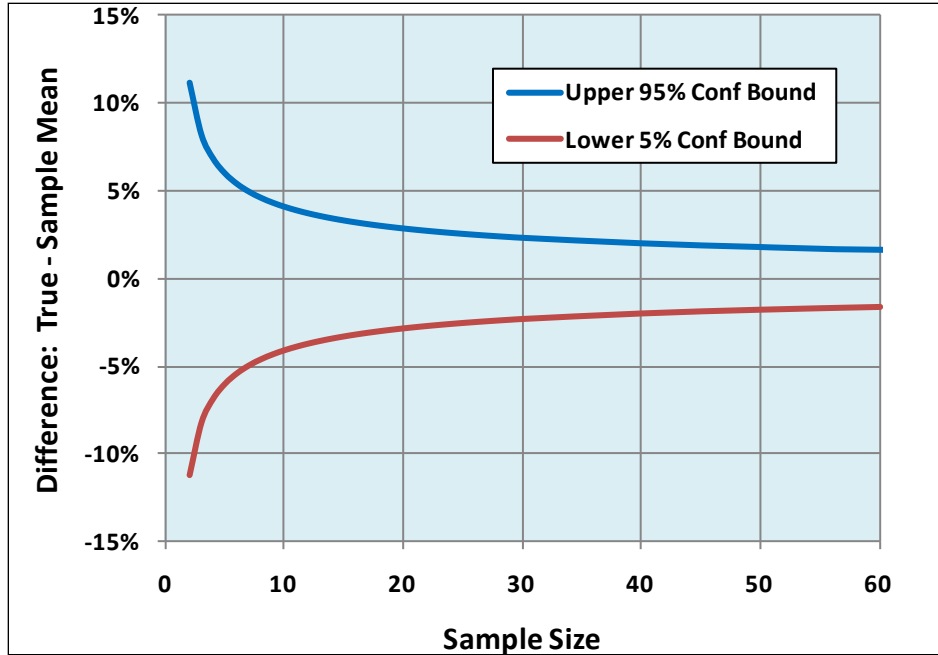


Figure 18. Effect of sample size when estimating true mean

The relationship between the upper 95% confidence bound and the true standard deviation, σ , is much more sensitive to small sample size, as can be seen for the upper and lower confidence bounds as follows:

$$\sqrt{\frac{v s^2}{\chi_{\alpha, v}^2}} \leq \sigma \leq \sqrt{\frac{v s^2}{\chi_{1-\alpha, v}^2}} \quad (2)$$

The above statement is shown for a 90% confidence interval in figure 19. The figure begins at a sample size, $n=3$, to provide good resolution because, even though a sample size of 2 is valid, the upper 95% is inflated to almost 1,600% of the sample, rendering it all but impractical. It is important to note that, unlike figure 18, which plots the difference between the sample and true means (on the ordinate), figure 19 plots the ratio of the true to the sample standard deviation. Figure 19 clearly shows that it takes a much larger sample size to estimate the true standard deviation. In fact, even though the confidence bounds are nearly asymptotic at a sample size of $n=30$, the true-to-sample standard deviation ratio is still about 128%. Obviously, given the potential for error when estimating the true regime parameters, the small number of samples involved in flight testing will not provide the necessary confidence with which to estimate the inherent reliability in TOS.

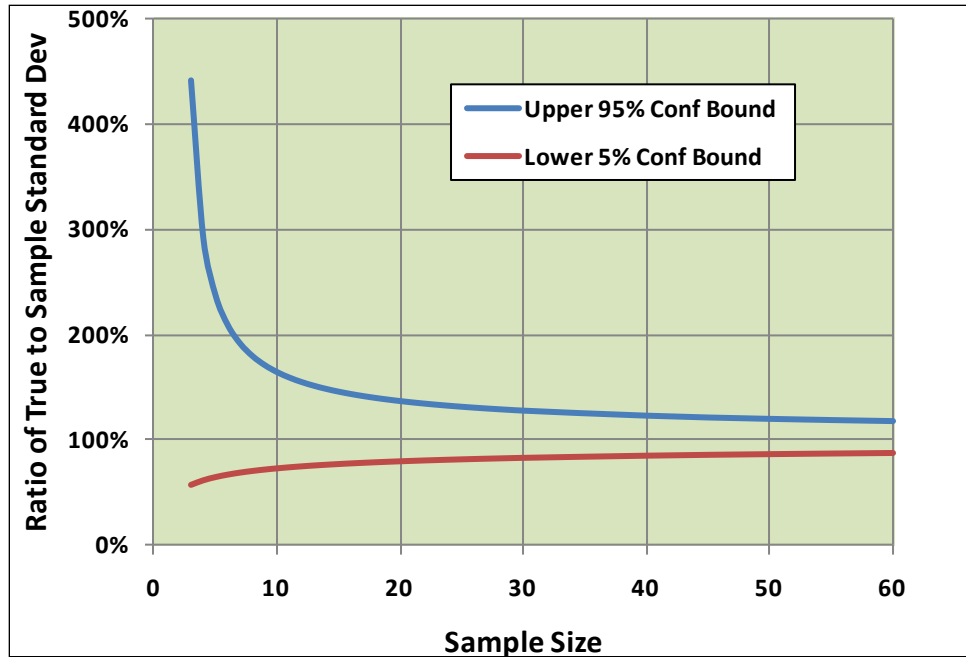


Figure 19. Effect of sample size when estimating true standard deviation

For this investigation, the only flight loads data available were in the FSR, which contained the results of the TOS method but no possible way of determining the sample size involved, although, as already stated, the number of flight event samples for a given regime is generally 1–3. This necessitated that some engineering judgment be used to construct a reasonable probabilistic model. Such a model, while postulated, could be improved in the Bayesian sense as additional loads become available.

The essence of the model is the assumption that there is deliberate bias put into the acquisition process. For this reason, a deterministic bias value, $\Delta_b=80\%$, is assumed to exist, on average, for the entire collection of acquired load records. Thus far, the confidence (or lack thereof) discussion has considered only TR regimes, which, as stated earlier, constitute most of the damage. However, there are SS regimes that also cause measurable amounts of damage. Most, but not all, of these damaging SS regimes do indeed utilize the TOS oscillatory load (some are necessarily prorated or cycle counted because they are somewhat unsteady), which comes from a large sample. The reason for mentioning this is to further substantiate the overall load bias of 80%.

Superimposed on top of the deterministic bias is a probabilistic load severity (α) model characterized by a normal distribution. The parameters of the severity distribution are a mean of 80% to be consistent with the bias and a coefficient of variation (CoV) of 8%, which together put the $\mu+3\sigma$ load severity at roughly 100%, as illustrated schematically with a standard normal distribution in figure 20. It is worth mentioning that the CoV observed in previous work of this type was 8%–10%. That CoV range was obtained from a variety of damaging regimes that were non-dimensionalized to create a significant sample size ($n=30$).

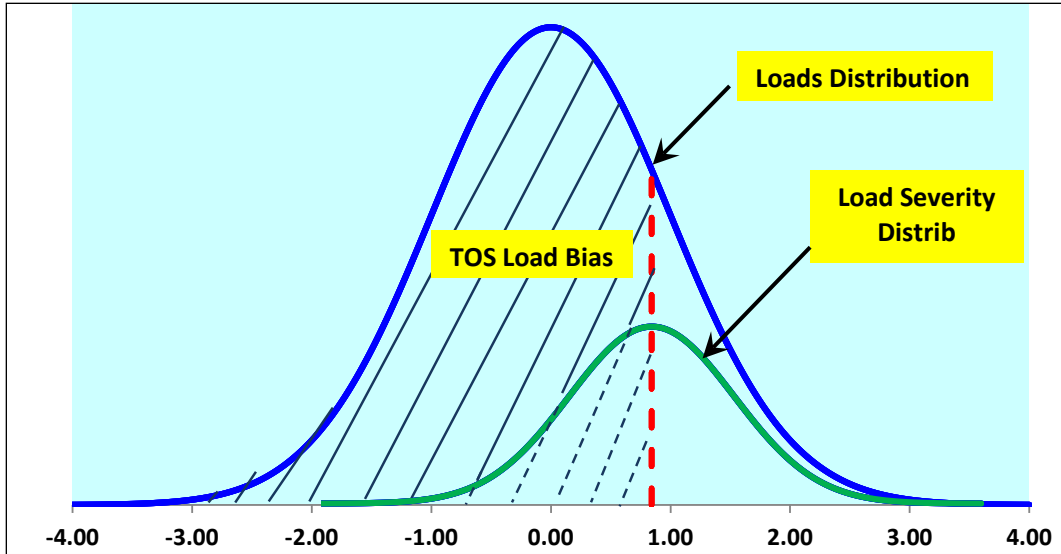


Figure 20. Schematic of load severity (TOS bias + normal distribution) model

The model described in the preceding paragraphs was necessary because of the inadequacy of the loads data available in the FSR, although it is unlikely that having access to all the flight strain survey data would have been adequate enough to confidently characterize loads statistically. Because of the paucity of data, it seemed reasonable to take an engineering approach to loads characterization by assuming that TOS is 80% as severe as the capability of the aircraft would allow and that a $\mu+3\sigma$ extreme in load severity would indeed capture the true maximum oscillatory load.

3.3.3.2.3 Quantifying Inherent Reliability of “ $\mu-3\sigma$ ” Reduced S-N Curve

Recall that the traditional approach to fatigue strength, at its core, depends on fatigue test results from six full-scale specimens [12]. While six are typical, it is often reduced for large and/or expensive components and increased for small and/or inexpensive components. In any event, the sample size is small in comparison to what is needed to generate a high degree of confidence in the true standard deviation, σ , estimate as figure 19 clearly shows. The sample size would seem to be adequate for estimating the true mean, μ , within 5% at a lower one-sided confidence level of $\gamma=95\%$. However, because of some of the possible outcomes that develop when conducting fatigue testing, this might not necessarily be the case.

Consider the fatigue test data sample depicted in figure 21, in which it is immediately noticed that not all of the six specimens tested did in fact fail. The mean procedure followed in such situations is to include any run outs (specimens that did not fail) that would inflate the mean of the failures while discarding those run outs that fall below the mean. In the case of figure 21, none of the run outs is usable. If the standard deviation is calculated from the test data, only failures can be considered. If the CoV is estimated from the sample, only failures should be considered to calculate both the sample mean and standard deviation. In many instances, the analyst will apply an additional knockdown if less than approximately five of the test data points are usable; however, such procedures do not need to be considered to develop the probabilistic

model. If the effect of a small sample size needs to be quantified, the statistical confidence in the fatigue life result can be examined.

The normal distribution shown in figure 21 represents the distribution of endurance strength (ES) and, as such, is tailor-made for probabilistic analysis without any further development. Absent confidence considerations, a $\mu-3\sigma$ estimate from a normal distribution deterministically provides 0.99865 of inherent reliability. This level can be found in a standard normal table or using the NORMSDIST function in Microsoft Excel.

As mentioned earlier, the shape of the S-N curve usually comes from a statistically significant sample of small-scale coupon test results, as illustrated in figure 22. Note that there are three different stress ratios and that a non-linear regression package is used to come up with the best fit to all the data so there is variance; however, it is not customary to address this variation in a probabilistic analysis. Instead, the S-N curve shapes are considered as a material and processing/failure mode invariant property. However, to be conservative, in some cases the worst case curve shape (i.e., the flattest one possible) within the scatter band is chosen. In some cases, a better fit can be obtained by considering only data for the stress ratio of interest.

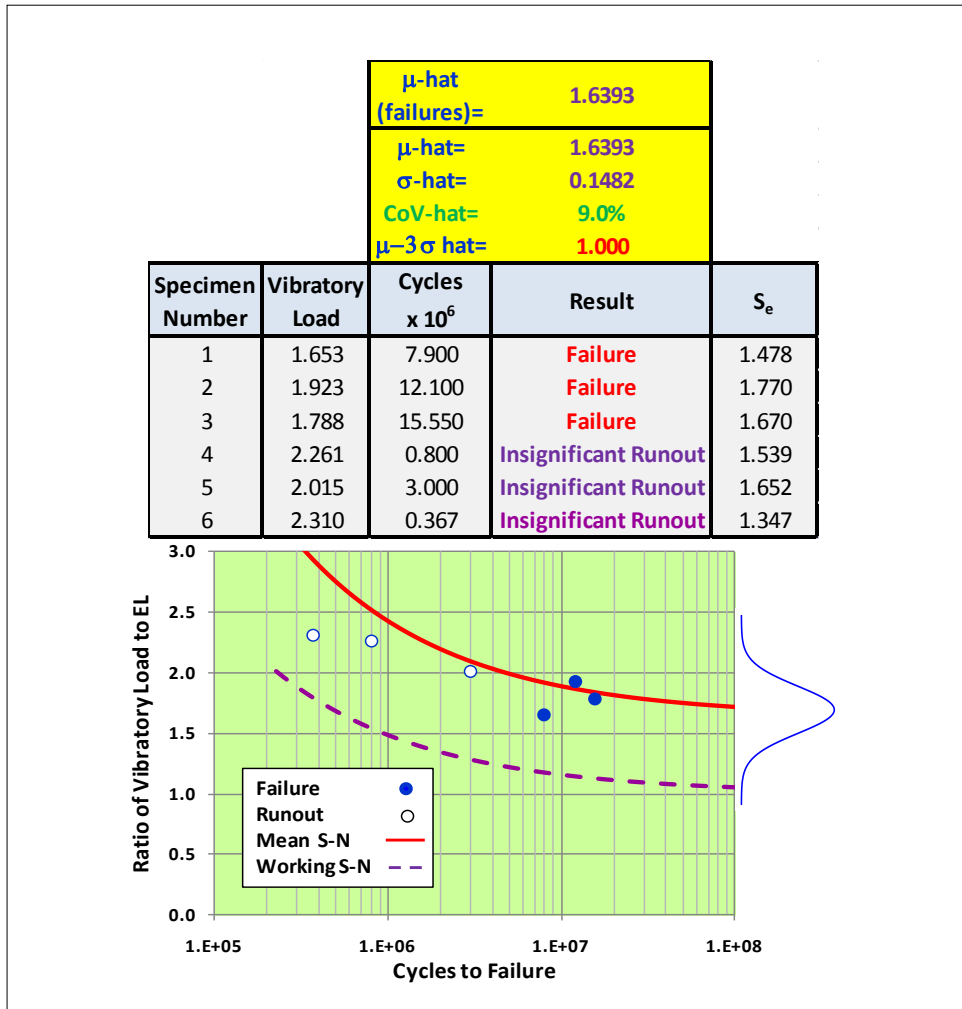


Figure 21. Sample fatigue test results with mean and reduced S-N curves

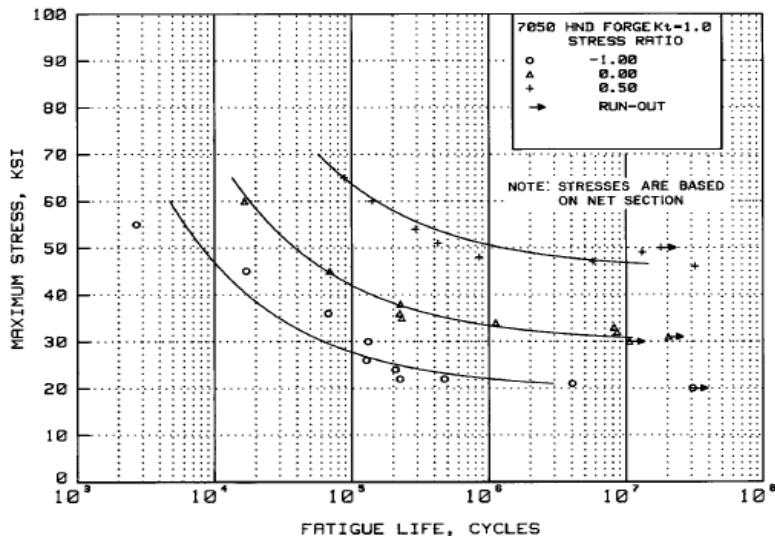


Figure 22. Example of 7050 forged aluminum small-scale coupon data [8]

3.3.3.3 Reliability Computation

This section provides an in-depth discussion of the various methods that could be used to compute fatigue life reliability. The advantages and disadvantages of each method are then summarized and the method of choice identified. It begins with a brief examination of the available methods and justifies the choice of convolution integration as the method of choice. Finally, that discussion is followed by methodology implementation details and the section concludes with the general findings and specific results that emerged.

3.3.3.3.1 Comparison of Available Methods

There are several acceptable methods for computing reliability. The list includes, but is not limited to: (1) Monte Carlo simulation, (2) enhanced Monte Carlo simulation with importance or other stratified sampling, (3) closed-form solutions that have limited application depending on the distributions involved, (4) convolution integration, and (5) other techniques generally referred to as second-moment methods.

3.3.3.3.1.1 Monte Carlo Simulation

Monte Carlo simulation is a technique that can be used in any application involving random variables. The essence of the method is that by drawing many times from the underlying probability distributions of each variable, the inherent reliability of a process can be determined. Unfortunately, an extremely large number of trials must be conducted when a high level of reliability is being sought, as is the case with six-nines (0.999999). It can be shown that the accuracy of the reliability prediction can be determined using the following relationship from [13], which is based on a binomial distribution (i.e., each trial results in either success or failure):

$$\varepsilon\% = 200 \times \sqrt{\frac{p}{Nq}} \quad (3)$$

where p is the probability of success, q is the complementary probability of failure, and N is the number of Monte Carlo trials.

If a 10% error in reliability is acceptable, 400 million trials will be needed. If a 50% error is acceptable, the number of trials drops to 16 million. The salient point is that a great number of trials is going to be necessary when the reliability is this high. The accompanying error in fatigue life will depend on how it varies with reliability.

3.3.3.3.1.2 Enhanced Monte Carlo Simulation

In reference [14], methods of greatly reducing the number of trials without introducing significant error are discussed. They include the incorporation of importance sampling and stratified sampling to work in tandem with the Monte Carlo simulation. These techniques essentially bias the sampling to be much greater in the tail region, thereby greatly reducing the number of trials and also reducing the variance (i.e., the square of the standard deviation). When

attempting to simulate a process that has $Q \leq 1 \times 10^{-6}$, techniques such as these are seen as essential to make Monte Carlo simulation viable.

3.3.3.3.1.3 Closed-Form Solution

Closed-form solution methods can be used to assess the reliability in certain situations. One such class of problems is generically referred to as stress-strength (or load-capacity) interference analysis, which is illustrated schematically in figure 23 below. Fortunately, many different issues with which aero-structural engineers are concerned (e.g., static strength, buckling, fatigue life, and crack propagation life) can be probabilistically posed as stress-strength interference problems.

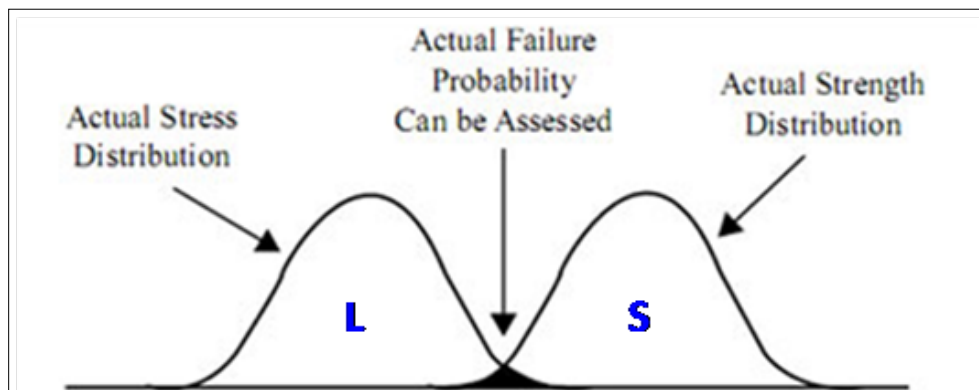


Figure 23. Basic stress-strength interference model

A major drawback of the closed-form solution methods is that they are restricted to certain probability distribution combinations of stress (or load) and strength (or capacity):

1. Load and strength are both normally distributed.
2. Load and strength are both lognormally distributed.
3. Load and strength are both exponentially distributed.
4. Load is exponentially distributed with strength normally distributed or vice versa.
5. The trivial case of both load and strength is uniformly distributed.

Fortunately, many problems can be posed within these constraints. Detailed solutions to items 1–4 above can be found in comprehensive reliability text books, such as [15]. One important caveat to using this method to assess fatigue life reliability is that it intrinsically reduces the mean S-N curve using a constant standard deviation (CSD), whereas the traditional method uses a constant coefficient of variation (CCV) approach. The difference in the two methods is displayed in figure 24 below.

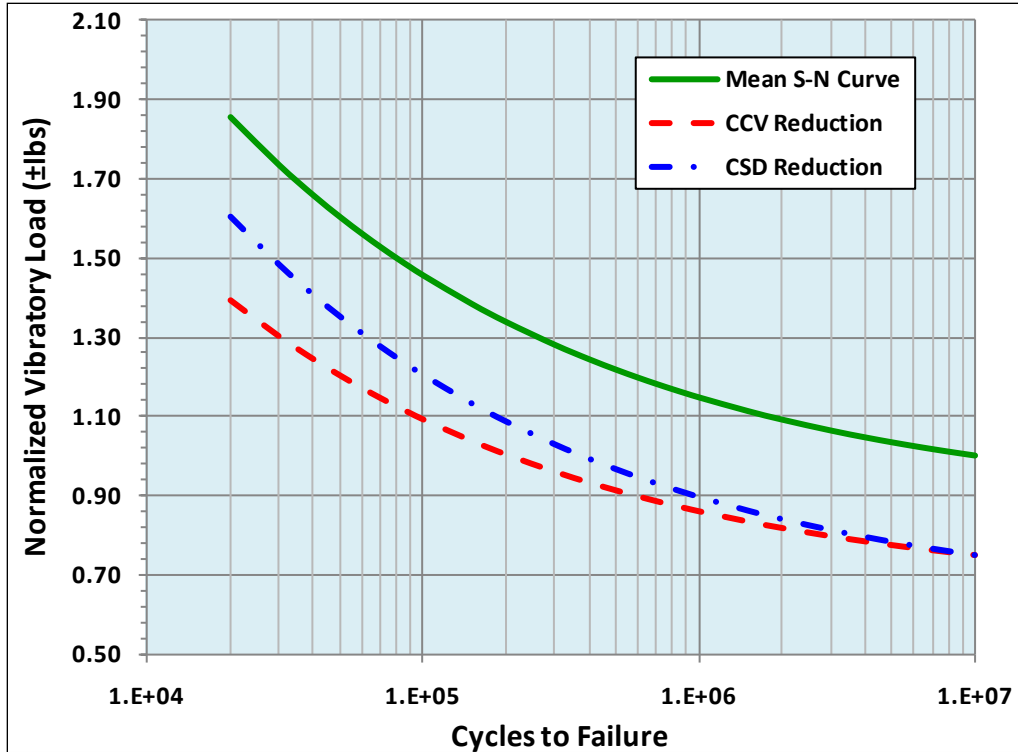


Figure 24. Comparison of CSD versus CCV reduced S-N curves

3.3.3.3.1.4 Convolution

Convolution is a form of ordered integration that is well-suited to the stress-strength interference problems and particularly so for assessing fatigue life reliability. It is a nonparametric method in the sense that stress and strength can be represented by any probability distributions (two in the case of stress-strength interference). The method can also be extended to three or four dimensions (random variables); however, doing so will greatly slow the computation if Microsoft[®] Excel[®] is the chosen analytical tool and may, in fact, suffer the same outcome if a dedicated program is being used depending on the resolution (i.e., integration increments) of the problem.

To understand how convolution works, it is helpful to understand the basic mathematics of the stress-strength interference model, which comes from [16], but this model can also be found in any comprehensive reliability textbook. It is also important to go into some depth here because it was the method of choice for this investigation. In this discussion, the load, L , is synonymous with stress in the figure. As long as L is greater than the strength, S , then the so-called limit state has been exceeded. Conversely, as long as the strength, S , exceeds the load, L , there is no limit state violation and, therefore, the operation is reliable, which in mathematical terms is expressed as:

$$R = P[S > L] \quad (4)$$

As long as S and L are independent from one another, the reliability, R , can also be expressed as an integration process as follows:

$$R = \int_0^{\infty} f_L(L) \left[\int_L^{\infty} f_S(S) dS \right] dL \quad (5)$$

The order of integration does not matter, so without any loss of generality, equation (5) can be rewritten as:

$$R = \int_0^{\infty} f_S(S) \left[\int_0^S f_L(L) dL \right] dS \quad (6)$$

In addition to the obvious change in the order of integration, there is also a subtle difference between equations (5) and (6) in the integration limits of the inner (inside the brackets) integral. Specifically, when strength is the inner integral, L is the lower limit—whereas, when load is the inner integral, S is the upper limit. The limits are obvious in light of figure 23 and equation (4). However, if a new random variable, $I=S-L$, is introduced, the reliability can be simplified to:

$$R = S - L > 0 = P[I > 0] \quad (7)$$

$$R = \int_0^{\infty} \int_0^{\infty} f_S(I+L) f_L(L) dL dY \quad (8)$$

The form presented in equation (8) is generically referred to as a convolution integral.

Employing either equation, (6) or (8), in the context of probabilistic fatigue life analysis requires that the reliability be evaluated numerically. When evaluating high levels of reliability, R , it is much easier to evaluate the unreliability, Q . To carry this out, the load, L , and strength, S , probability density functions must be discretized; however, because the goal is to calculate Q , the discretization can usually be confined to values above the mean of the load distribution and values below the mean of the strength distribution.

A joint probability distribution of the two independent random variables of interest to this investigation can then be generated by forming a matrix from the discrete probability density function values of the load severity and ES distributions, which are illustrated schematically in figure 25.

The overall unreliability, Q , can be calculated by a summation of certain of these blocks. To understand how this takes place, it is important to know what each of these blocks actually represents. Figure 26 illustrates what is actually transpiring within the discrete convolution process vis-à-vis a summation of matrix elements of the type shown. Specifically, in the evaluation of fatigue life reliability, each element is bounded on the corners by the ES and load severity (α) cumulative density function values according to the chosen level of discretization. As such, the cell joint probability density is the product of the delta marginal probability densities of the two random variables.

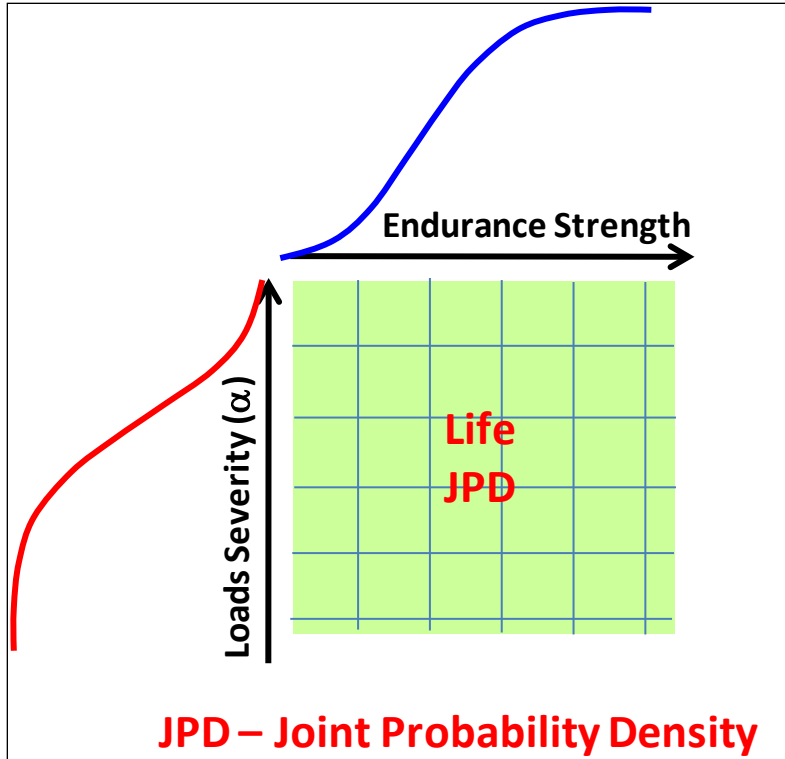


Figure 25. Stress-strength joint probability portion of convolution integral

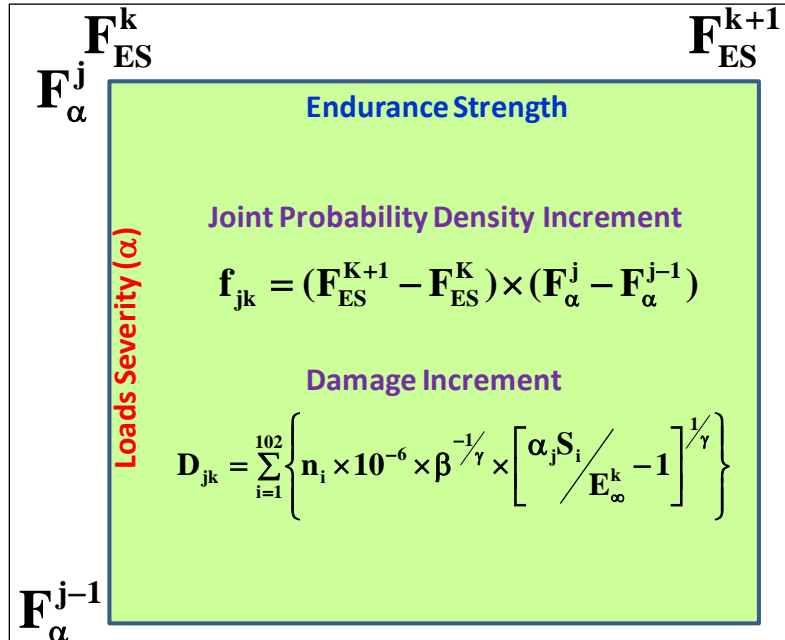


Figure 26. Dual process convolution matrix element

Figure 26 also contains the damage increment that follows from the k^{th} average ES (i.e., average of k and $k+1$ value) and j^{th} average load severity (α) value. The i -index denotes the elements in the deterministic usage spectrum (i.e., CWC or RR average). These include the i^{th} oscillatory

stress level, S_i ; applied load cycles, n_i ; and corresponding cycles to failure, N_i . It is worth noting that any particular i -index element can be expanded into a fourth dimension to accommodate cycle counting. In order to evaluate fatigue life reliability, the matrix of these elements are converted to a vector and sorted in ascending order of life (i.e., reciprocal of damage) while the associative joint probability is carried along. If the reliability, R , required is six-nines (0.9_6), the unreliability, Q , is 0.000001 (0.0_51). Therefore, the joint (failure) probability density is accumulated up to that level and the corresponding life obtained. Because the technique is discrete, interpolation is usually involved. Figure 27 below provides a numerical illustration of convolution.

It should be readily apparent that convolution is ideally suited to evaluating fatigue life reliability. What might not be apparent is that it is extremely easy to program and the answers come back quickly. The details of the method will become more evident when the results of the investigation are discussed in detail in section 3.3.3.3.1.6.

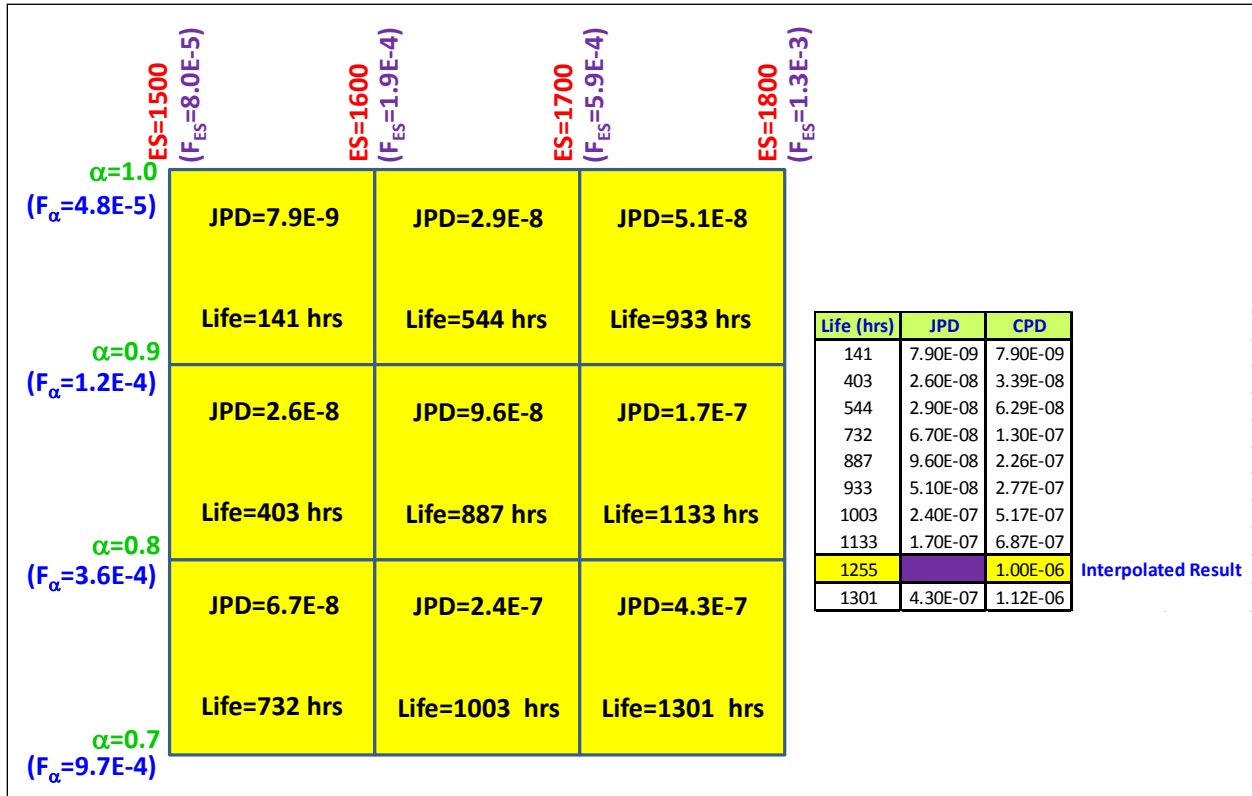


Figure 27. Numerical illustration of convolution

3.3.3.3.1.5 Second Moment Methods

Reliability analysts are often asked to solve more difficult problems than stress-strength interference. In such cases, there are generally three or more random variables involved and often one or more of them has a probability distribution other than normal. Solutions to such problems are not easily obtainable and the problem may, in fact, not be solvable without applying simplifying assumptions. In such cases, second moment methods represent each

distribution by its first and second moments that respectively represent its mean and variance (whose square root is the standard deviation). Thus, each random variable is being represented by a normal distribution. There may not be a unique solution, but there will be an optimum answer. The optimum solution involves finding the maximum likelihood of the limit state function. Finding the solution involves transformation and, in some cases, cannot be solved without resorting to numerical methods. Second moment methods have many applications in reliability engineering but are not warranted for the fatigue life reliability problem posed herein because they will involve significantly more computational rigor than the other methods discussed in section 3.3.3.3. The intricacies of these methods can be found in textbooks, such as [17].

3.3.3.3.1.6 Summary of Reliability Methods

The previous paragraphs in section 3.3.3.3 provided insight into some of the potential methods that could be used to address fatigue life reliability. From the discussion of Monte Carlo simulation, it is obvious that too many trials would be required when the reliability is 0.96, but enhanced Monte Carlo simulation could be used to greatly reduce the number of trials. To utilize enhanced Monte Carlo simulation, one must identify a biased probability distribution that is compatible with the sampling distribution. This is usually done through trial and error. Closed-form solution is, as was pointed out, limited to certain combinations of distributions and also contains an inherent CSD knockdown, which is unconservative. Second moment methods would be overkill for this type of problem. Thus, convolution is seen as the simplest and most versatile method and was the method chosen for this investigation.

3.3.3.3.2. Evaluating the Reliability of the CWC Spectrum

In this section, the reliability associated with CWC will be evaluated both deterministically and probabilistically.

3.3.3.3.2.1 Deterministic Inherent CWC Reliability

The deterministic method uses the traditional fatigue life calculation process, as described in section 3.3.3.1, and evaluates the CWC reliability contribution using the following steps:

- Using a spreadsheet, reproduce the component life listed in the FSR using the CWC spectrum, TOS loads, and estimated $\mu-3\sigma$ S-N curve.
- Copy the spreadsheet and replace the RR average for the CWC spectrum. This will usually result in a significantly higher fatigue life. The RR average was based on RRAs developed by the Army, not Goodrich.
- Reduce the working S-N curve and its EL until the fatigue life matches the one listed in the FSR. Note the new Z-score (number of standard deviations of reduction).
- Subtract the reliability associated with the $\mu-3\sigma$ EL in step 1 from the reliability associated with the Z-score in step 3. Mathematically stated as:

$$\mathbf{9's\ of\ CWC\ Reliability} = -\mathbf{Log[1-\Phi(Z_{step\ 3})]} + \mathbf{Log[1-\Phi(3)]} \quad (9)$$

Note that the plus sign is the result of the negative of a negative. Also, the greater the difference between the Z score in step 3 and Z=3 standard deviations, the greater the error in the reliability estimate in terms of 9s; however, the error is conservative.

Because of the size and breadth of the spreadsheets involved, it would be difficult to present any calculations here. As such, the important aspects of the spreadsheets used to evaluate the first component are provided in appendix A. The results for the 14 aircraft considered in the investigation along with the (time-weighted) average are provided in table 8 and figure 28. This four-step evaluation addresses the reliability of CWC under the scenario discussed in [5].

Table 8. Deterministic inherent CWC reliability by failure mode

Failure Mode Description	1	2	3	4	5	6	7	8	9	10	11	12	13	14	Avg
	Deterministic Composite Worst-Case (CWC) Inherent Nines of Reliability														
Component 1, Failure Mode A	1.43	1.60	1.40	1.71	1.67	1.58	1.58	1.75	1.71	1.43	1.56	1.43	1.48	1.38	1.58
Component 1, Failure Mode B	1.05	0.89	0.74	0.95	1.09	0.88	0.88	1.00	0.89	0.79	0.75	0.93	1.11	1.14	0.98
Component 2, Failure Mode A	1.12	1.24	1.22	1.35	1.26	1.32	1.32	1.25	1.39	0.99	1.23	1.14	1.12	1.05	1.19
Component 2, Failure Mode B	1.14	1.13	1.11	1.15	1.14	1.16	1.16	1.17	1.18	1.09	1.07	1.05	1.04	1.10	0.96

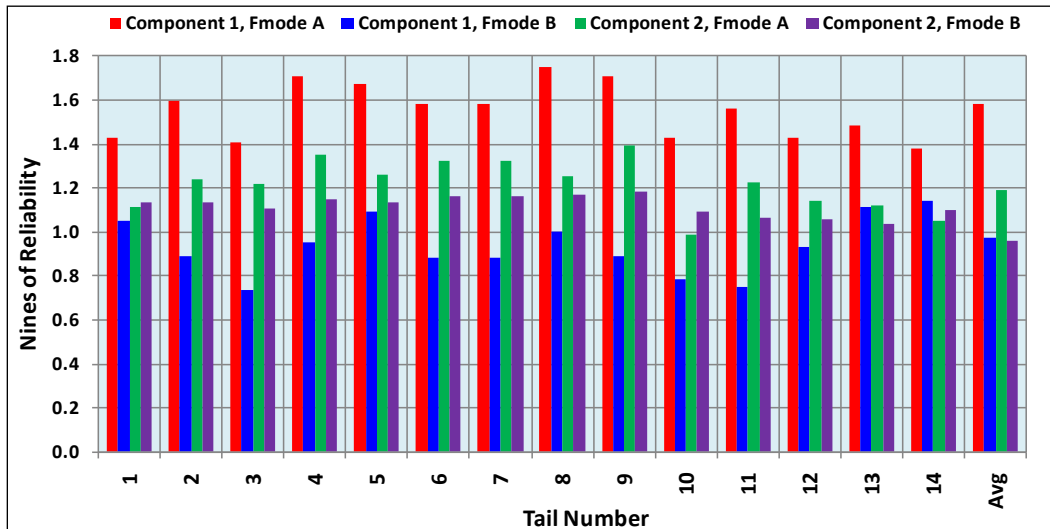


Figure 28. Graphical results from Table 8

3.3.3.3.2.2 Probabilistic Inherent CWC Reliability

The probabilistic method for evaluating the inherent reliability in the CWC spectrum bears some semblance to the deterministic technique. In the latter, the TOS loads are invariant while in the former, the same load severity distribution and 80% bias are present throughout. In the

deterministic method, the loss of reliability that occurs when the RR average is substituted for the CWC spectrum is offset by a reduction in the working EL to return the fatigue life to that of the FSR. In a somewhat analogous manner, when the CWC is replaced by the RR average in the probabilistic method, the overall reliability is increased to get back to the FSR life. The step-by-step procedure follows:

- Reproduce the component life listed in the FSR using the CWC spectrum, along with the convolution spreadsheet, by reading the reliability level from the sum of the JPD vector at the FSR Life once the life-JPD vector has been sorted by life-altering the input reliability level (see example in figure 27).
- Copy the spreadsheet and replace the RR average for the CWC spectrum. This will result in a significantly higher fatigue life at the reliability level of the previous step.
- Increase the input reliability level until the fatigue life matches the one in the FSR.
- Subtract the step 1 reliability from the step 3 reliability. Mathematically stated as:

$$\mathbf{9's\ of\ CWC\ Reliability} = -\mathbf{Log[1-R_{step\ 3}]} + \mathbf{Log[1-R_{step\ 1}]} \quad (10)$$

Again, note that the plus sign is the result of the negative of a negative.

As in the previous section, the size and breadth of the spreadsheets involved make it difficult to present any calculations here. As such, the important aspects of the spreadsheets used to evaluate the first component are provided in appendix B. The results for the 14 aircraft considered in the investigation along with the (time-weighted) average are provided in table 9 and figure 29. These results are generally slightly lower than their deterministic counterparts. In fact, the correlation between the deterministic and probabilistic averages is 92% (coefficient of determination, $R^2 \approx 85\%$).

Table 9. Probabilistic inherent CWC reliability by failure mode

	1	2	3	4	5	6	7	8	9	10	11	12	13	14	Avg
Failure Mode Description	Deterministic Composite Worst-Case (CWC) Inherent Nines of Reliability														
Component 1, Failure Mode A	1.33	1.46	1.32	1.59	1.59	1.46	1.60	1.61	1.59	1.33	1.46	1.34	1.36	1.30	1.46
Component 1, Failure Mode B	0.96	0.80	0.65	0.86	1.00	0.80	1.01	0.91	0.80	0.69	0.66	0.83	1.01	1.01	0.85
Component 2, Failure Mode A	1.21	1.22	1.22	1.33	1.33	1.33	1.11	1.22	1.37	1.00	1.22	1.22	1.22	1.09	1.22
Component 2, Failure Mode B	0.57	0.58	0.59	0.59	0.59	0.59	0.59	0.59	0.59	0.49	0.49	0.49	0.49	0.49	0.59

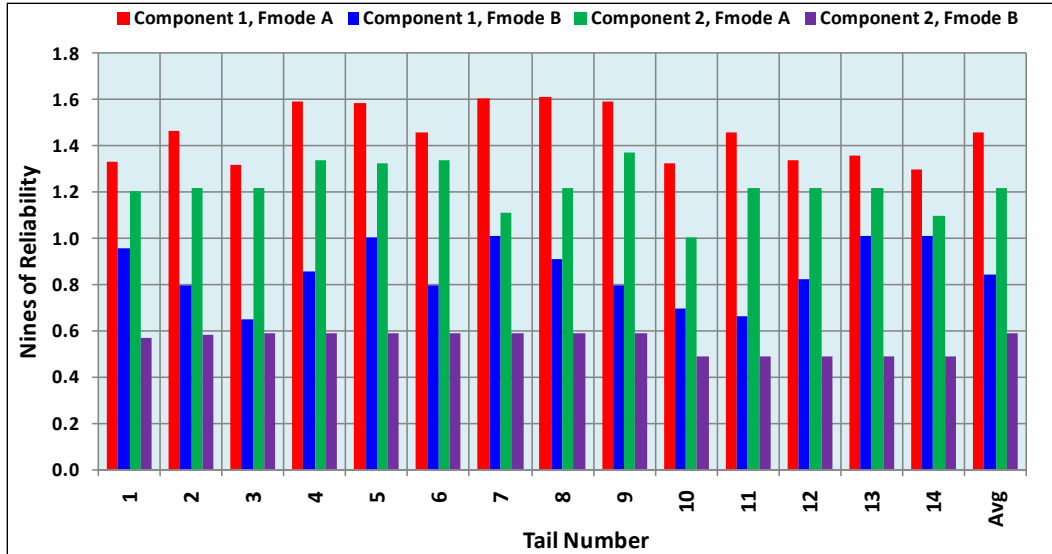


Figure 29. Graphical results from Table 9

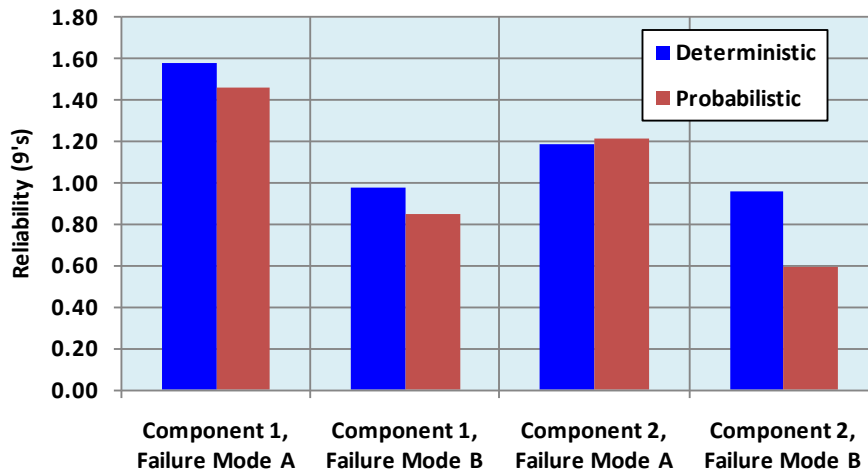


Figure 30. Comparison of inherent CWC reliability by method

3.3.3.3.2.3 Incremental Damage Comparison and its Effect on Reliability

In many cases, the non-dimensional S-N curve shape mentioned earlier can be represented by the following equation:

$$\frac{S}{E_{\infty}} = 1 + \beta \times N^{-\gamma} \quad (11)$$

where N is expressed in millions of cycles, β and γ are shape constants, and E_{∞} is the EL at an infinite number of cycles. Since Miner's rule of linear cumulative damage is being used (i.e., increment of damage, $D_i = n_i / N_i$), the following damage equation emerges:

$$D_i = n_i \times 10^{-6} \times \beta^{-1/\gamma} \times \left[\frac{S}{E_\infty} - 1 \right]^{1/\gamma} \quad (12)$$

By varying the independent variables (n , S or E_∞) individually, the delta effect on damage can be measured. Suppose that $\beta=0.056$, $\gamma=0.587$, $E_\infty=14,70$ lb. (deterministic $\mu-3\sigma$ EL estimate projected to an infinite number of cycles) and that all the damage for the component of interest can be balanced at $S/E_\infty=1.6$ at $n_{tot}=10$ cycles/hour; using these parameters leads to the damage relationships depicted in figure 31. It can readily be seen that, while usage damage increases linearly, damage from stress (or load) as well as a reduction in ES increases geometrically. Though these observations are interesting, the rates of increase of both stress and ES are situation-dependent—that is, they depend on β , γ , E_∞ , and S/E_∞ —and the rate of increase of usage damage will always be linear. The line of equivalency in figure 31 provides a means of putting usage on the same level with ES. Fortunately, when RR average usage is in the model, it does not make a significant contribution to the overall reliability, so the differences in rate of damage increase need not be considered. Moreover, the reliability contribution of CWC has already been determined in subsections 3.3.3.8.1 and 3.3.3.8.2 and is invariant with respect to a particular aircraft or fleet average.

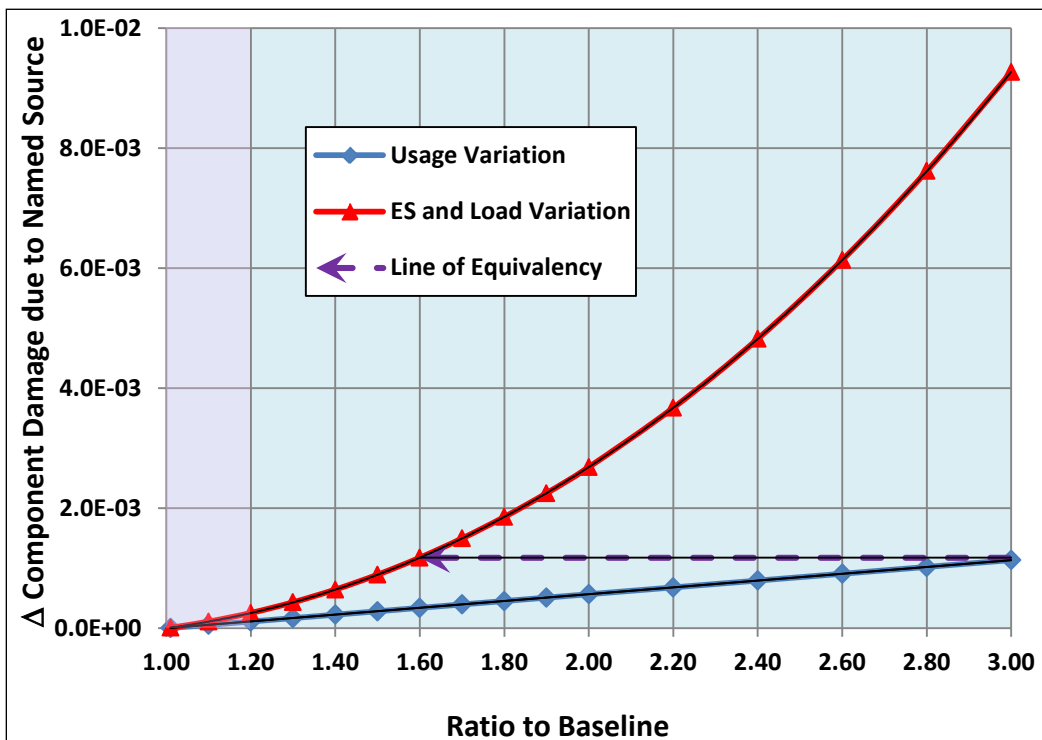


Figure 31. Usage, stress, and ES damage rates of increase

3.3.3.3.3 Reliability Versus Fatigue Life for Four Component Failure Modes

The four components investigated were evaluated to see how much overall reliability the FSR contained and how the fatigue life varies with reliability or its complementary risk. Both of these

questions can be answered for component 1 using figure 32. The solid blue line with the diamond symbols and the pink line with the square symbols depict how reliability decreases as life is increased (upper) and how the complementary risk increases. The dashed green and red lines represent the fatigue lives listed in the FSR for modes A and B, respectively. Notice that, given the load variability assumptions, both components fall between five and six 9s of reliability, but much closer to six as would be consistent with what the industry claims—particularly when one examines the lower logarithmic risk axis where the goal is 1.E-06, the complement of six 9s. Yet, neither of these failure modes would be good candidates for usage credits because, in order to claim such a credit, the reliability must surpass six 9s by a fairly significant margin.

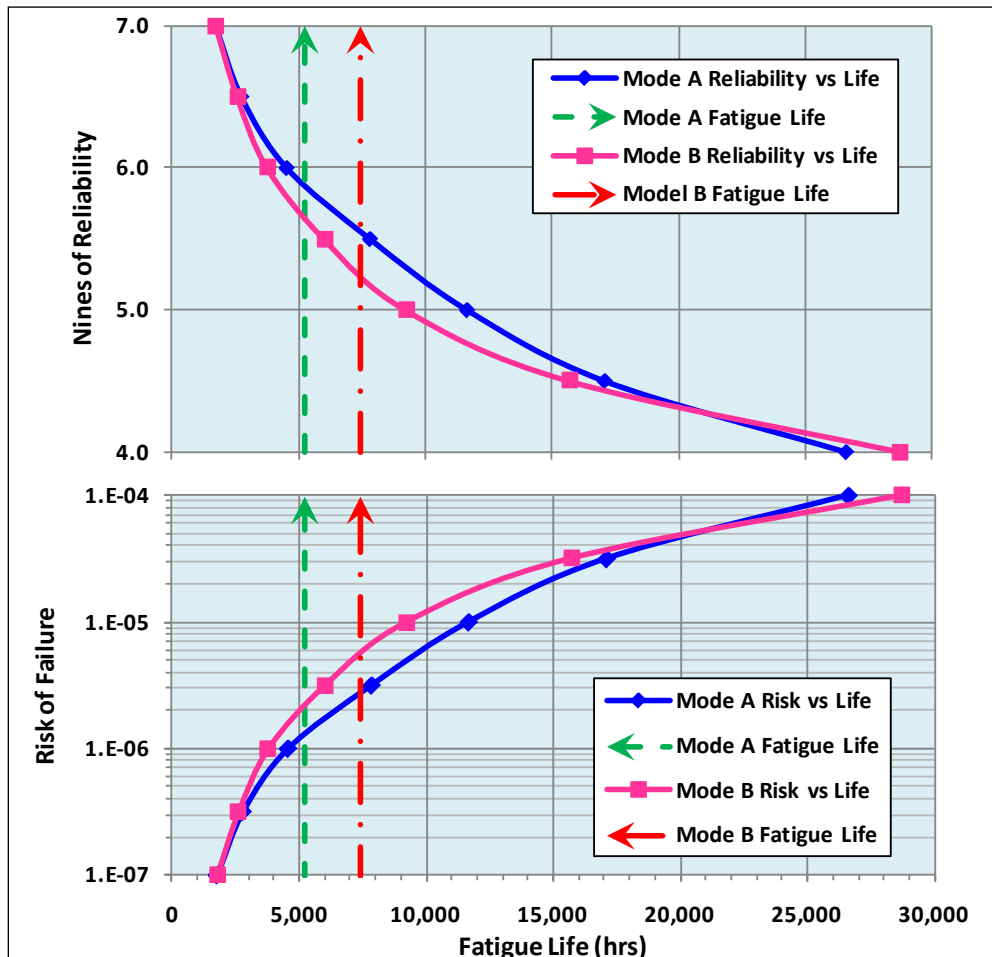


Figure 32. Reliability versus fatigue life for component 1 failure modes

In similar fashion to component 1, both component 2 failure modes fall between five and six 9s but closer to six. However, unlike figure 32, mode A in figure 33 shows a fairly precipitous drop in reliability. This is somewhat worrisome because the analysis contains assumptions, and if the relationship between reliability and life is off slightly, a significantly different picture might emerge. Fortunately, this component comes from the airframe, so some conservative assumptions were put into the analysis from the outset. In all likelihood, the component is actually significantly stronger than the analysis assumes.

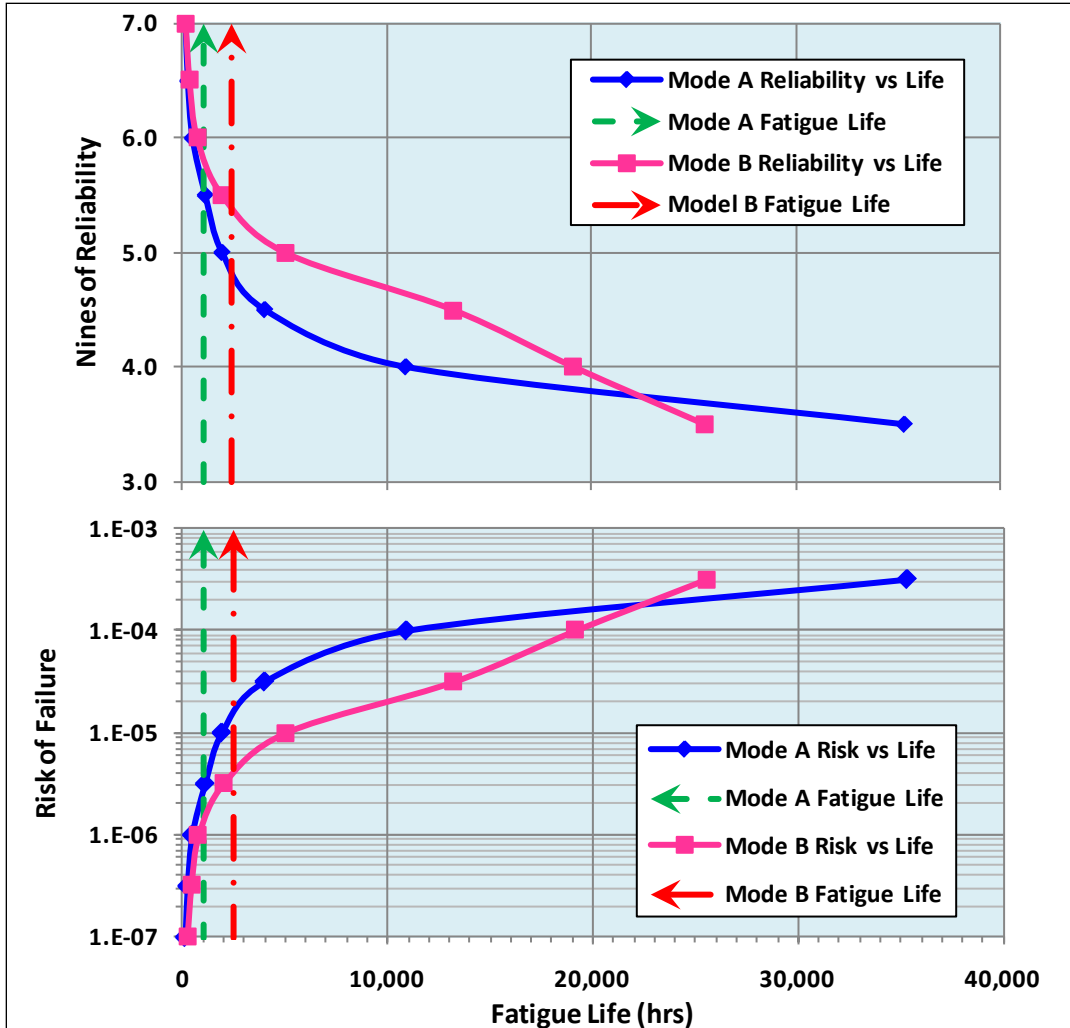


Figure 33. Reliability versus fatigue life for component 2 failure modes

3.3.4 Develop Life Factor Method

The life factor method described in this section is for tracking individual aircraft and individual components by serial number. The method is based on RR of operational usage and calculating the resulting accumulated fatigue damage. In the demonstrated application, the results are adjusted to ensure that the desired reliability is maintained. This was accomplished by applying the approach provided in paragraph A.6.4 of ADS-79C [7], which states, “If a detailed probabilistic analysis is not available, maximum accumulated damage should be tracked to no more than 0.5.”

Figure 34 shows the average regime usage as compared with CWC usage for grouped regimes. In both cases, the sum of the bar charts is 100%. This figure is interesting in that it shows a comparison of actual and CWC usage but does not provide useful information related to the resulting component failure mode damage accumulation.

Figures 35–38 show the average damage produced for the grouped regimes, as compared to the CWC damage, for each of the component failure modes. In each figure, the sum of the CWC bar charts is 100% and the sum of the component failure mode actual usage bar charts is as follows:

- Component 1 – Mode A: 37.0%
- Component 1 – Mode B: 34.1%
- Component 2 – Mode A: 24.3%
- Component 2 – Mode B: 23.3%

It should be noted that there is no direct correlation between time in a basic regime and the resulting damage for that regime. For example, figure 34 shows that the average percentage of time spent in Climb is very similar for both the CWC and average usage. However, the resulting component 1 mode A damage for Climb is quite different, as shown in figure 35. This can be explained by the fact that CWC usage occurs primarily in the low-mid GW range, whereas the average usage occurs in the mid-high GW range (see figures 5 and 6, respectively). Also, note that component 1 mode A experiences no damage during low-mid GW Climb (see regime 5 in table 5), whereas it does experience damage in mid-high GW Climb (see regime 44 in table 6).

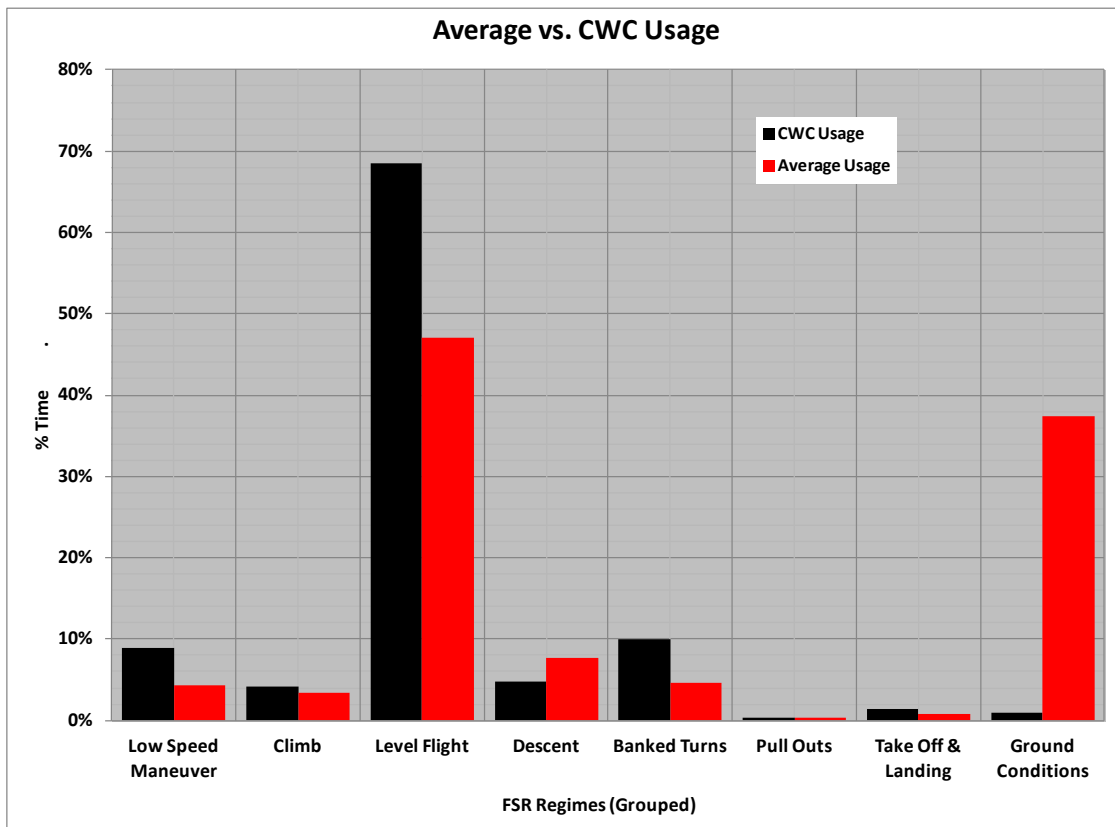


Figure 34. Average usage versus CWC usage for grouped regimes

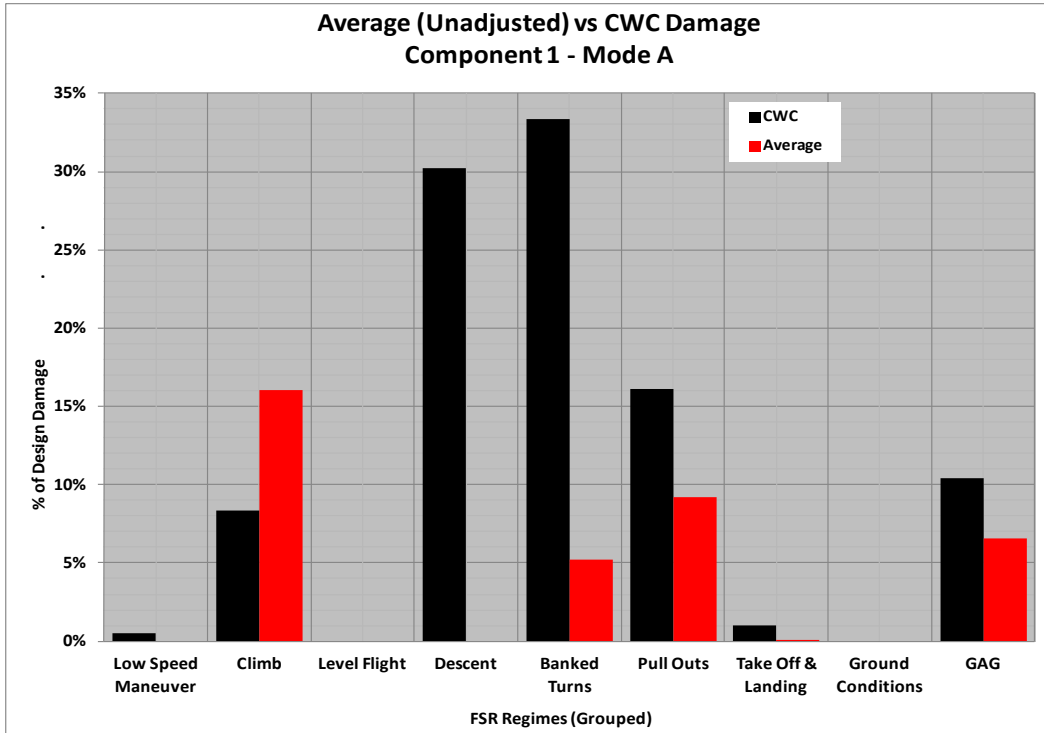


Figure 35. Average usage versus CWC damage—grouped regimes (component 1–mode A)

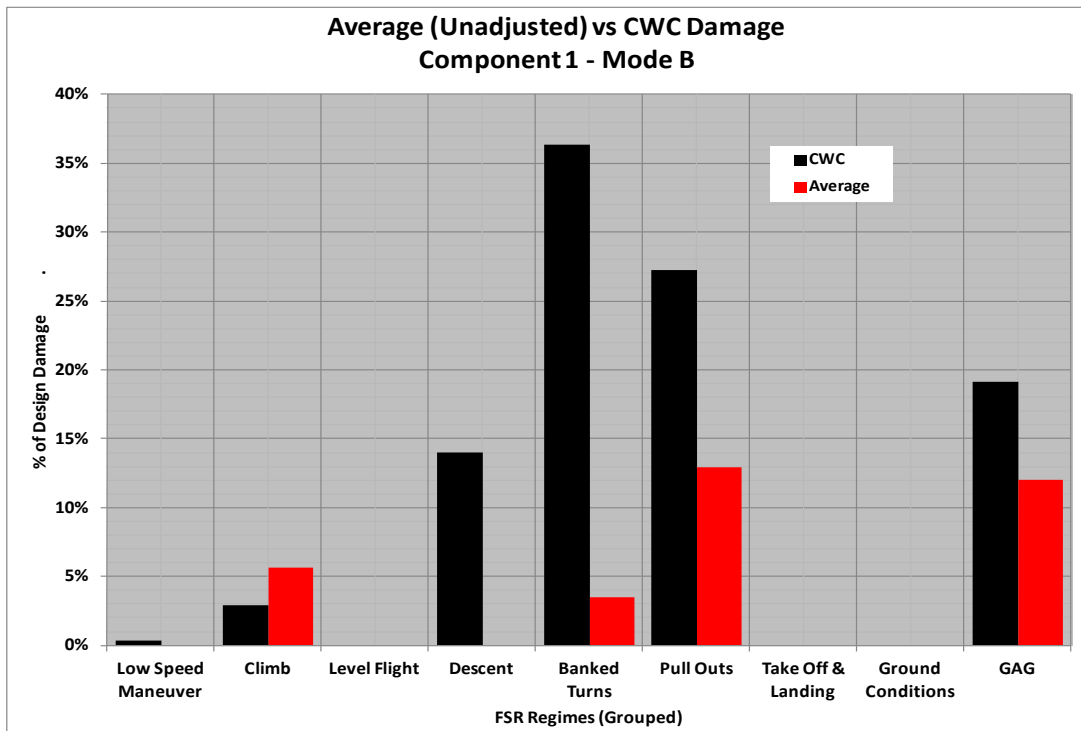


Figure 36. Average usage versus CWC damage—grouped regimes (component 1–mode B)

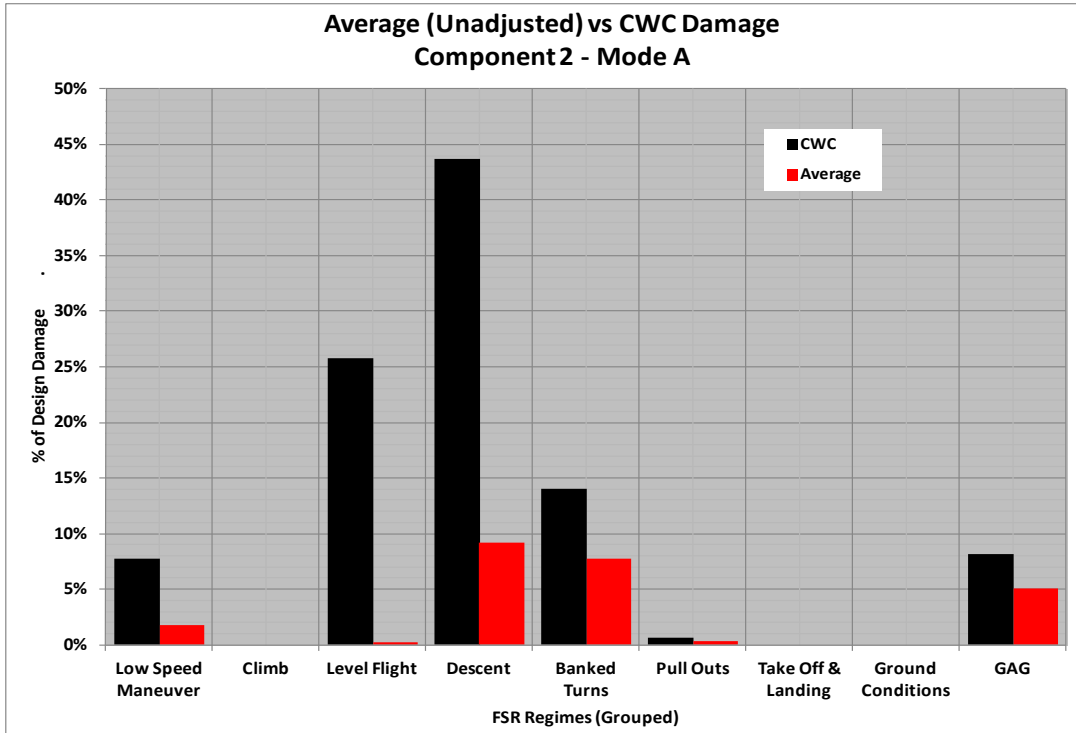


Figure 37. AVERAGE usage versus CWC damage—grouped regimes (component 2—mode A)

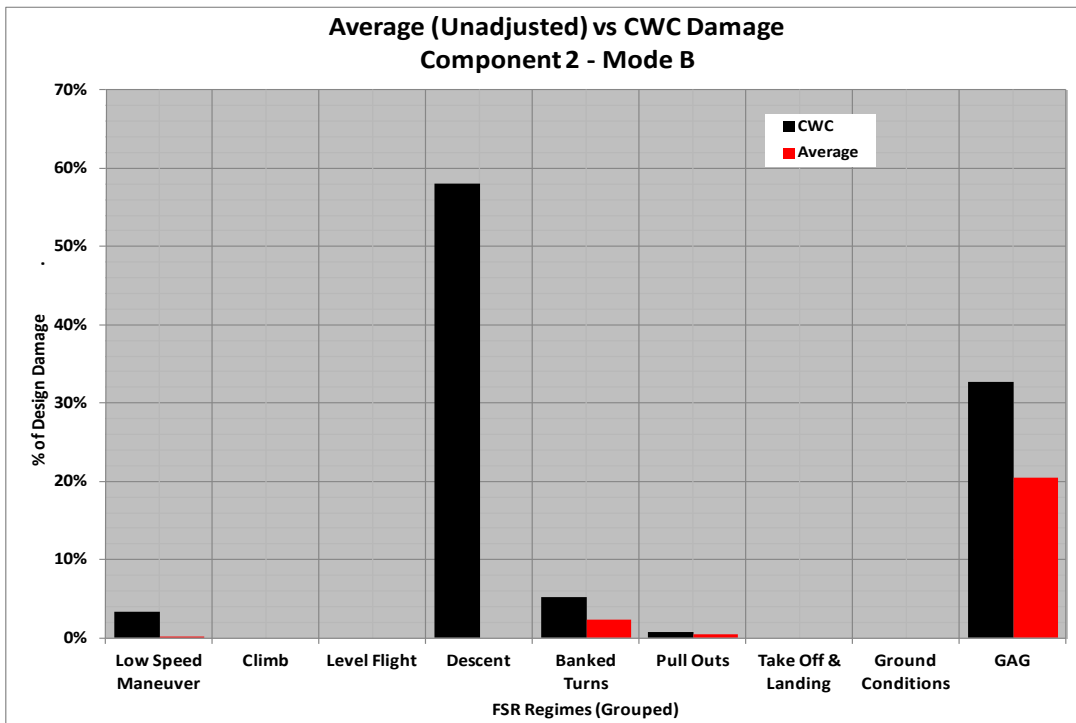


Figure 38. Average usage versus CWC usage—grouped regimes (component 2—mode B)

Figure 39 shows the build-up of normalized damage (i.e., damage produced by average usage divided by damage produced by CWC damage) for each of the component failure modes as a function of flight hours. It illustrates that the normalized damage for component 1 and component 2 failure modes essentially stabilize at approximately 300 and 200 flight hours, respectively. This gives an indication as to how many flight hours of usage data are required to produce a dependable average value.

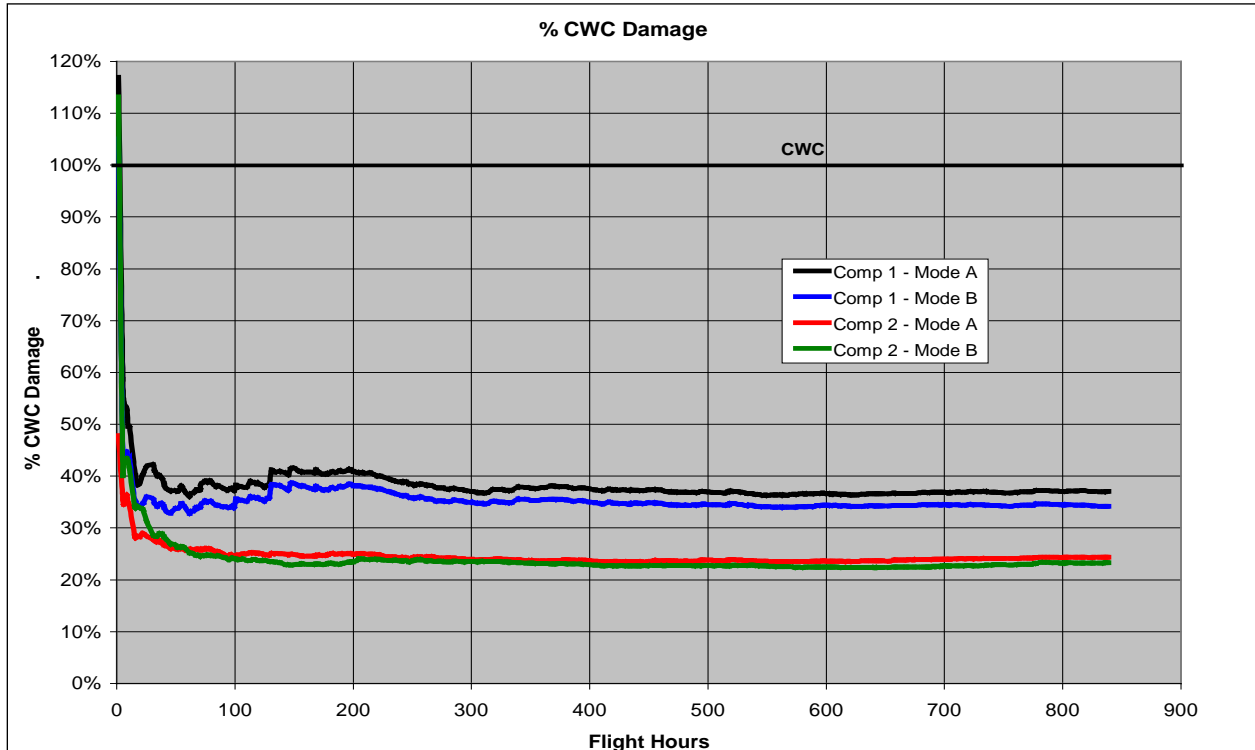


Figure 39. Component normalized damage versus flight hours

Figures 40 and 41 show comparisons of the component failure mode fatigue life that result from the following usages:

- Black bar: CWC usage
- Red bar: Average usage (unadjusted)
- Green bar: Average usage (adjusted per paragraph 6.4 of ADS-79C [7])

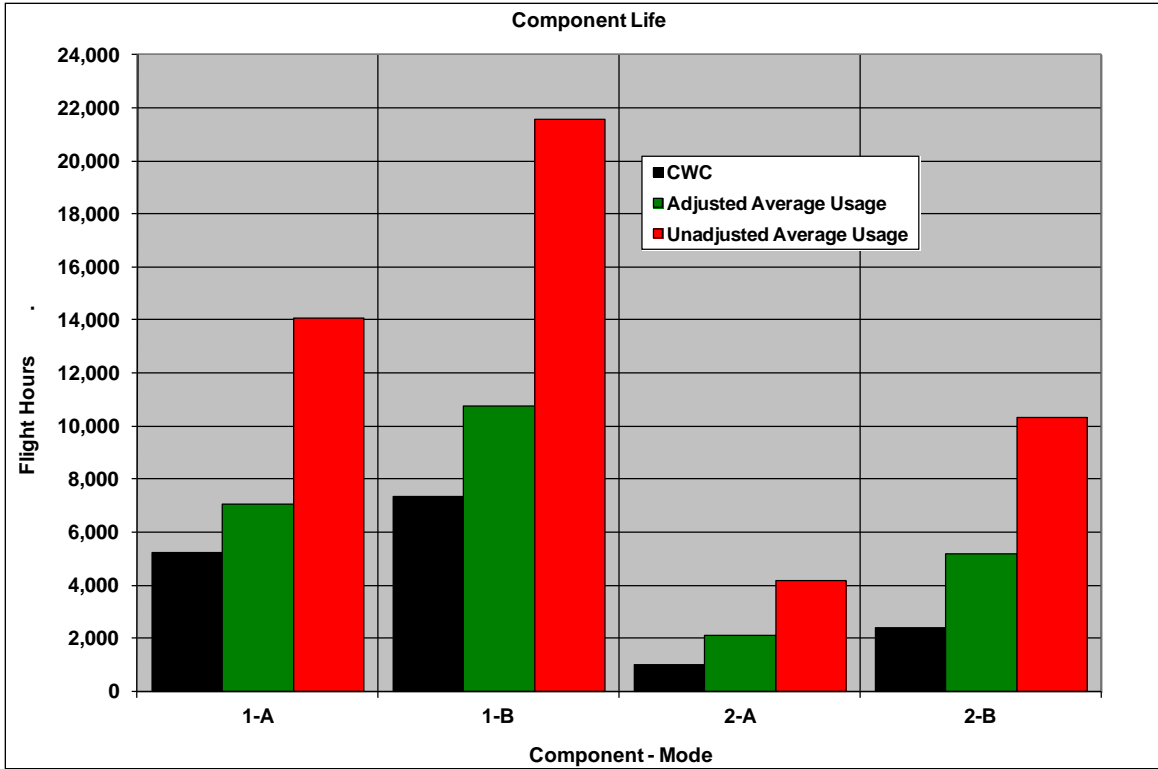


Figure 40. CWC, actual, and adjusted life in hours

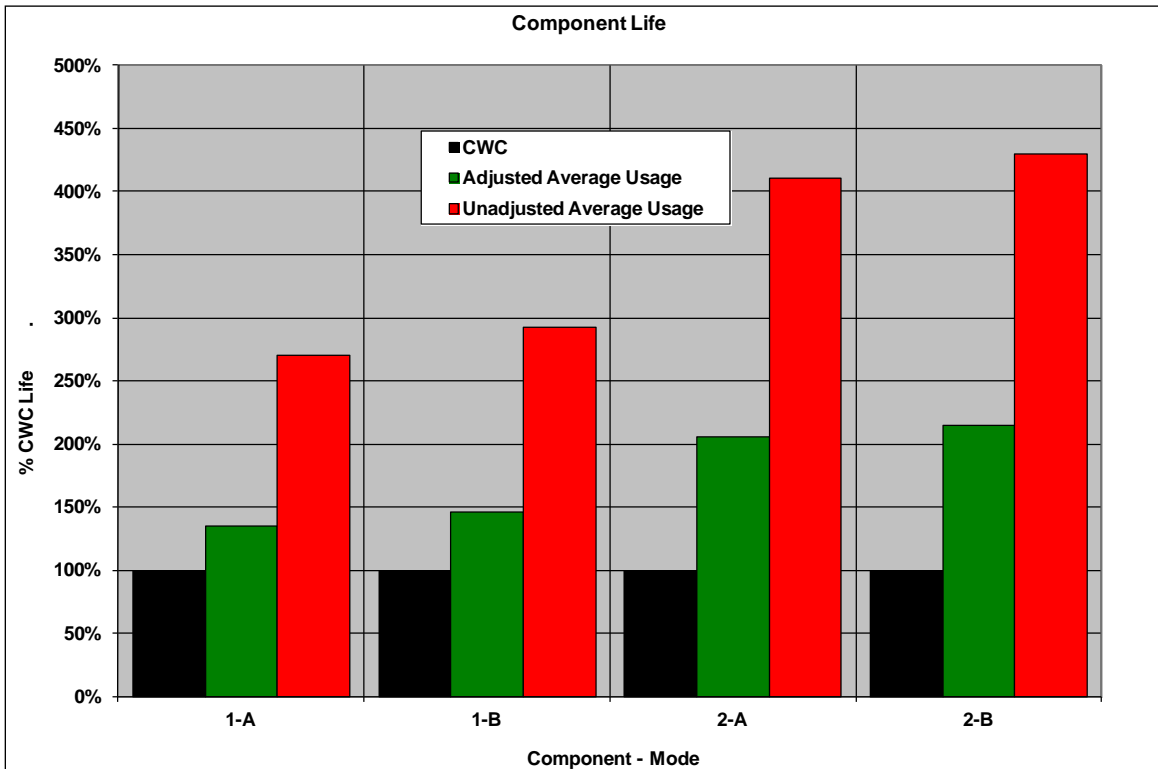


Figure 41. CWC, actual, and adjusted life normalized to CWC life

3.3.5 Develop Usage Credits

This section describes a method developed for applying usage credits based upon tracking individual aircraft and individual components by serial number. A damage index (DI) was developed to track accumulated fatigue damage in individual components that result from operational usage. The DI is the normalized value of operational usage accumulated damage as compared to the CWC damage at CRT.

A component must be replaced at, or prior to, a DI equal to 1.0.

$$DI = (\text{Actual Damage})/(\text{CWC Damage at CRT})$$

DI is adjusted to comply with paragraph A.6.4 of ADS-79C [7], as follows:

$$DI = (\text{Actual Damage})/(\text{CWC Damage at CRT}) \times 0.5$$

Figures 42–45 show the DI build-up for each of the component failure modes based upon CWC, actual usage, and actual usage adjusted for reliability. For illustrative purposes, the 839 hours recorded during 474 flights on 14 operational aircraft was duplicated twice to compile a database to simulate a single aircraft with >2500 hours. Figure 46 shows how the DI can be extrapolated to identify the range of actual (adjusted) flight hours, at which time the component must be removed and replaced. There are two methods of extrapolation:

- The CWC extrapolation (dotted line) presumes there will be no future usage information. In that case, the default position is to assume those flights experience CWC usage.
- The average usage extrapolation (solid line) presumes future flight will be monitored and the aircraft will continue to experience the same average usage in the future as in the past.

It is recommended that both extrapolation methods be employed to provide both a conservative (CWC) and “expected” (average usage) view of projected future life. Note that as the DI approaches 1.0, the differences in the extrapolated CWC and extrapolated average usage values will decrease.

It is recommended that for the development of usage credits, all usage data be archived in a usage database. The creation of a usage database will allow further development and refinement of the methodology employed in determining usage credits. It will also allow an independent and objective third party to evaluate how the systems involved in the usage credit calculation are performing. Processing of the usage credits completely onboard the aircraft may hinder this further development and evaluation stage if the raw parametric data are lost.

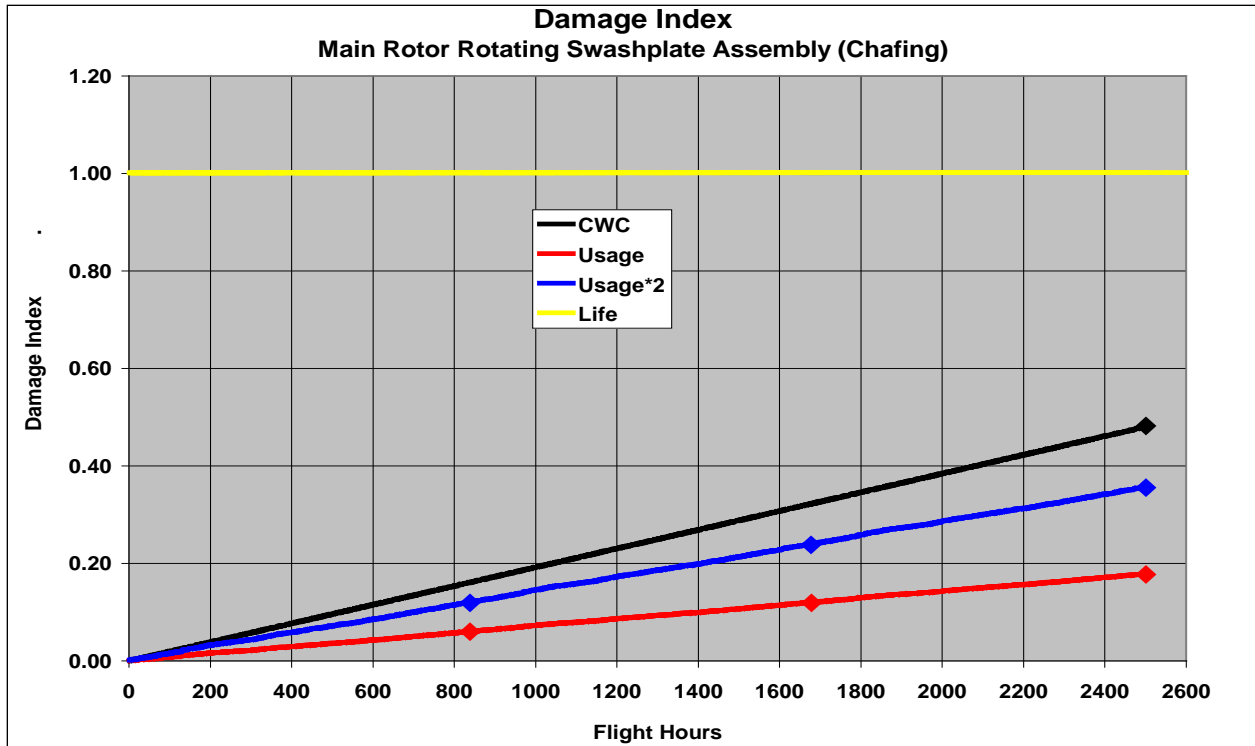


Figure 42. DI build-up for component 1—mode A

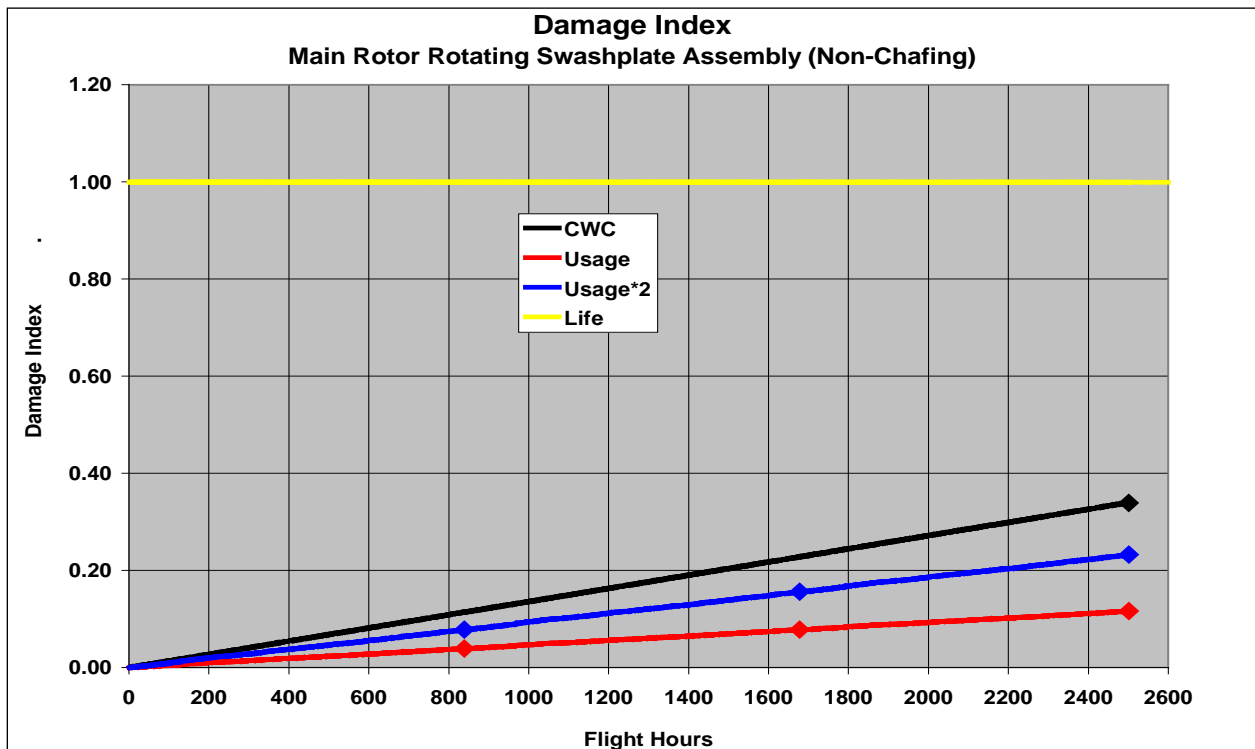


Figure 43. DI build-up for component 1—mode B

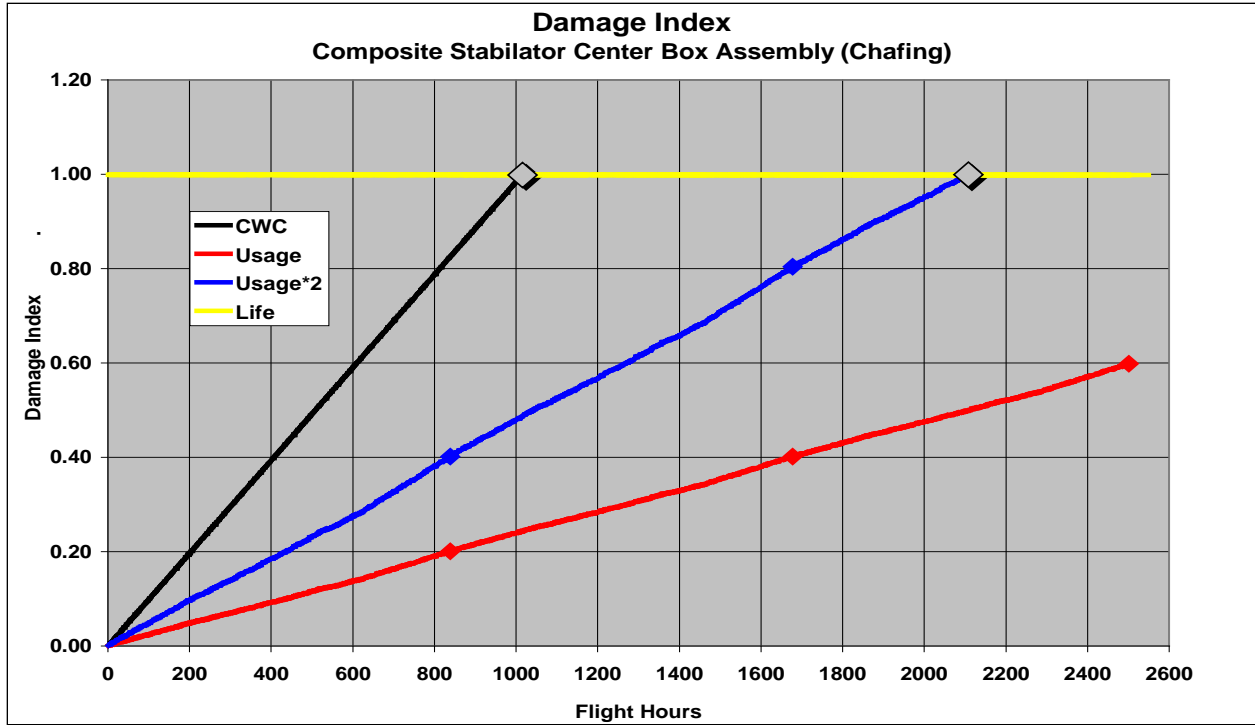


Figure 44. DI build-up for component 2—mode A

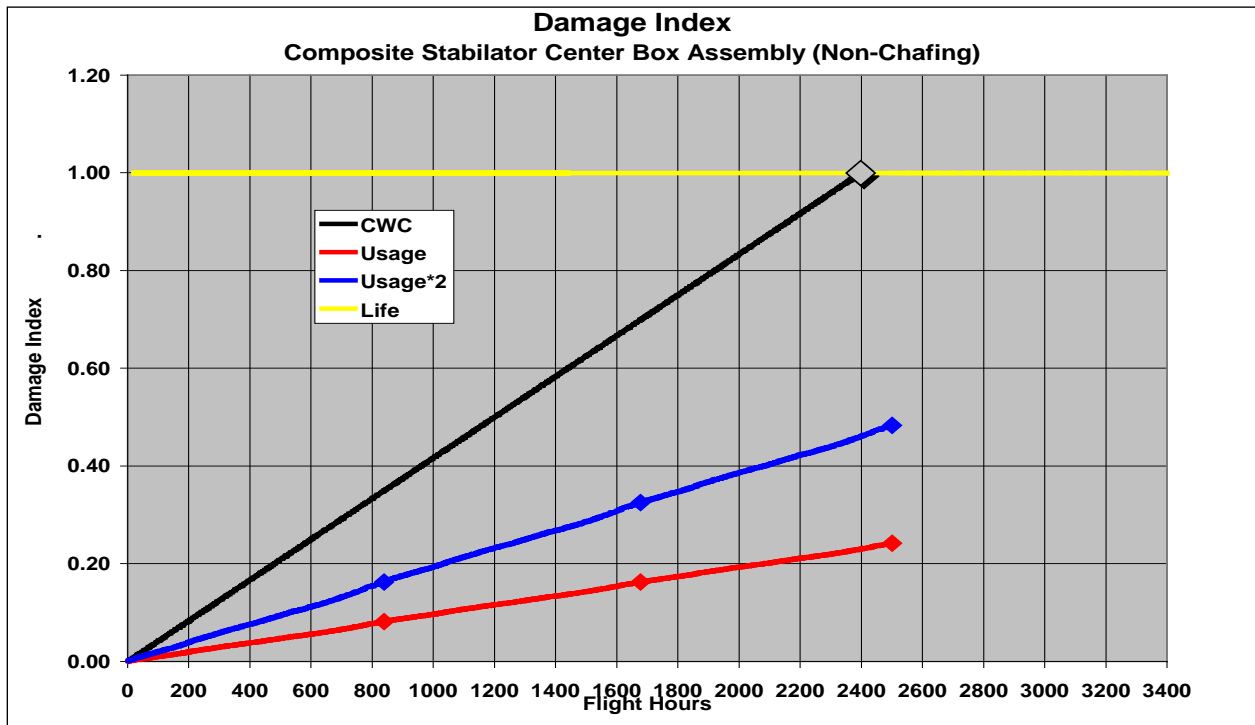


Figure 45. DI build-up for component 2—mode B

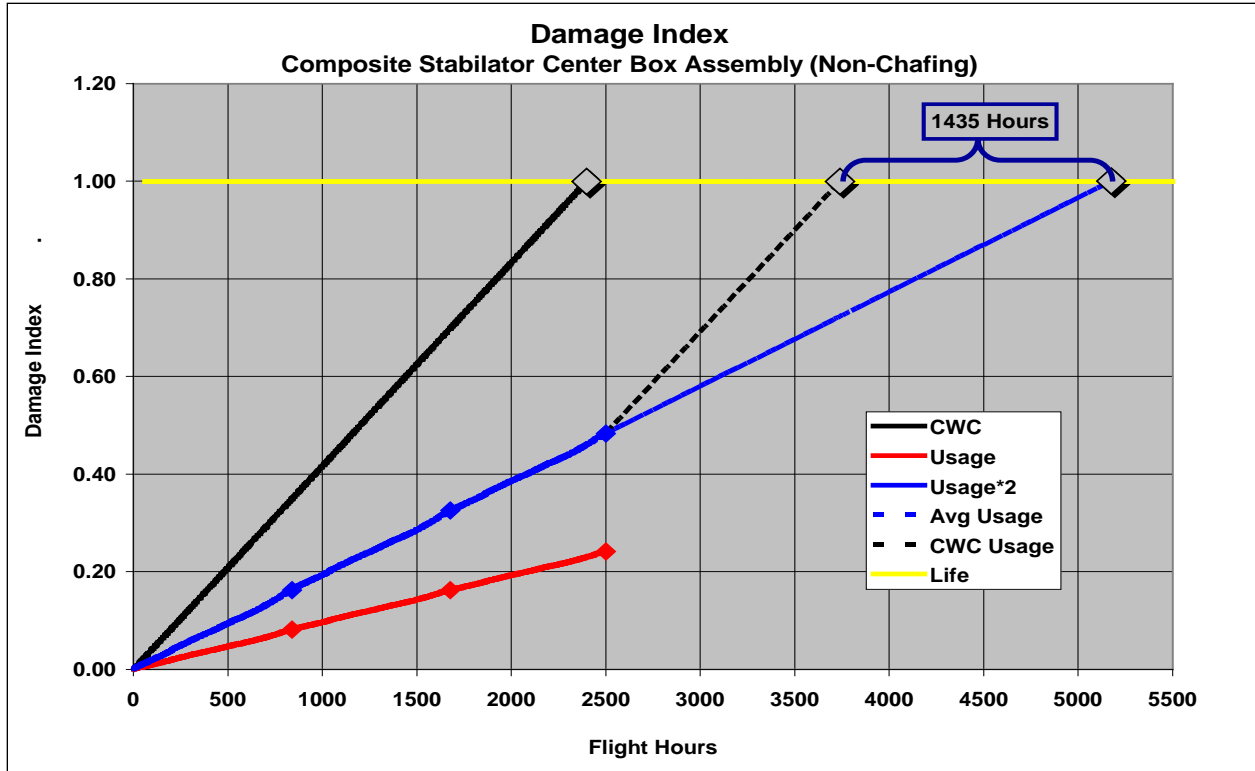


Figure 46. DI extrapolation for component 2—mode B

3.4 TASK 2 UPDATE— USAGE CREDIT METHOD

3.4.1 Analyze UH-60M Operational Usage

3.4.1.1 Analyze Regime Usage by Aircraft and Operational Environment

The revised spectrum is based on ADS-79C [7], paragraph A.6.5, which states:

“Evaluation of reliability for usage spectrum update. For the case of updating usage spectrums for legacy aircraft, statistical analysis of the usage data is used to determine a statistical approximation of an updated composite worst-case spectrum, as discussed in [7] section A.5.1. Consider use of a ‘mean plus two sigma’ spectrum to avoid the need for additional fatigue strength working curve reductions or probability analysis. As an alternative, a “mean plus sigma” spectrum may be applied with appropriate probability analysis. In this instance, σ is the sample standard deviation of the time (in seconds) per flight hour among the aircraft in the sample for a particular regime. Use of a mean spectrum is not appropriate.”

Therefore, the revised CWC Spectrum is the $\mu+2\sigma$ spectrum.

Note also that both the original and revised CWC spectra are truncated to 81 regimes, mainly because the RRA cannot recognize entry/recovery transients. However, since entry and recovery to a maneuver occur immediately before and after the recognized maneuver, the FSR CWC damage associated with entry and recovery were added to the basic maneuver.

Tables 10–18 show the revised CWC spectrum for both Continental United States (CONUS) and OCONUS at varying GW. The adjustment factor in the right column is used to reduce the spectrum time to 100% because biasing time in each regime will result in a total spectrum time greater than the actual. It is calculated by reducing the time in selected regimes until the spectrum time is back to 100%. Nominally, the selected regimes are those that are non-damaging for all parts. However, in the examples shown, it was generally applied to groups of regimes, which is not technically proper. Note the large difference in the percentage of time spent in taxi (regimes 38 and 77 for low-mid GW and mid-high GW, respectively). The percentage of time difference is because the criteria states that a mission starts with the initial rotation of the rotor blades.

Table 10. Revised CWC spectrum for CONUS training (low-mid GW)

	CONUS Training (Low-Mid GW)								Adjustment Factor = 0.494766
	Design Regimes		Legacy CWC Usage			Revised CWC “ $\mu+2\sigma$ ” Usage			
	Regime No.	Description	PCT Time	Occs/hr	Secs/Occ	PCT Time	Occs/hr	Secs/Occ	Adj Pct Time
Basic Mission UH-60M Usage Spectrum (E/R Events Removed and Reallocated to SS Complementary Event) Low GW	1	Hover	1.06			13.58			6.72
	2	Left Sideward Flight	0.45			0.76			0.38
	3	Right Sideward Flight	0.45			3.93			1.94
	4	Rearward Flight	0.45			4.14			2.05
	5	Climb	2.52			5.82			2.88
	6	Level Flight @ 0.1VH	1.38			0.00			0.00
	7	Level Flight @ 0.2VH	0.92			2.82			1.39
	8	Level Flight @ 0.4VH	1.84			1.82			0.90
	9	Level Flight @ 0.5VH	1.84			3.70			1.83
	10	Level Flight @ 0.6VH	2.53			9.58			4.74
	11	Level Flight @ 0.7VH	2.76			25.48			12.60
	12	Level Flight @ 0.8VH	9.19			23.26			11.51
	13	Level Flight @ 0.9VH	13.78			12.39			6.13
	14	Level Flight @ 1.0VH	6.89			3.65			1.81
	15	Sideslip	0.60			1.49			0.74
	16	Autorotation	0.86			0.00			0.00
	17	Partial Power Descent	1.50			4.95			2.45
	18	Dive	1.39			0.80			0.39
	19	Turn 30 Degrees Left	2.50			6.99			3.46
	20	Turn 30 Degrees Right	2.50			5.77			2.86
	21	Turn 45 Degrees Left	0.43			0.18			0.09
	22	Turn 45 Degrees Right	0.43			0.10			0.05
	23	Turn 60 Degrees Left	0.09			0.00			0.00
	24	Turn 60 Degrees Right	0.09			0.00			0.00
	25	Take Off	0.60	3.60	6	1.33	7.99	6	1.33
	26	Left Hover Turn	0.50	1.50	12	1.01	3.02	12	1.01
	27	Right Hover Turn	0.50	1.50	12	0.81	2.44	12	0.81
	35	Auto Turn Left	0.14	0.33	15	0.00	0.00	15	0.00
	36	Auto Turn Right	0.14	0.33	15	0.00	0.00	15	0.00
	37	Hover Approach	0.33	3.00	4	0.07	0.67	4	0.07
	38	Taxi	0.27			45.08			22.30
	39	Taxi Turn	0.33	4.80	2.5	1.13	16.30	2.5	1.13

Table 11. Revised CWC spectrum for CONUS training (mid-high GW)

	CONUS Training (Mid-High GW)							Adjustment Factor = 0.494766	
	Design Regimes		Legacy CWC Usage			Revised CWC “ $\mu+2\sigma$ ” Usage			
	Regime No.	Description	PCT Time	Occs/hr	Secs/Occ	PCT Time	Occs/hr	Secs/Occ	Adj Pct Time
Basic Mission UH-60M Usage Spectrum (E/R Events Removed and Reallocated to SS Complementary Event) Low GW	40	Hover	0.71			2.03			1.00
	41	Left Sideward Flight	0.30			0.07			0.04
	42	Right Sideward Flight	0.30			0.36			0.18
	43	Rearward Flight	0.30			0.46			0.23
	44	Climb	1.68			0.38			0.19
	45	Level Flight @ 0.1VH	0.92			0.00			0.00
	46	Level Flight @ 0.2VH	0.61			0.20			0.10
	47	Level Flight @ 0.4VH	1.22			0.12			0.06
	48	Level Flight @ 0.5VH	1.22			0.17			0.09
	49	Level Flight @ 0.6VH	1.68			0.36			0.18
	50	Level Flight @ 0.7VH	1.84			2.47			1.22
	51	Level Flight @ 0.8VH	6.13			1.26			0.62
	52	Level Flight @ 0.9VH	9.19			0.55			0.27
	53	Level Flight @ 1.0VH	4.59			0.23			0.11
	54	Sideslip	0.40			0.07			0.03
	55	Autorotation	0.58			0.00			0.00
	56	Partial Power Descent	1.00			0.27			0.13
	57	Dive	0.93			0.04			0.02
	58	Turn 30 Degrees Left	1.67			0.68			0.34
	59	Turn 30 Degrees Right	1.67			0.43			0.21
	60	Turn 45 Degrees Left	0.28			0.01			0.01
	61	Turn 45 Degrees Right	0.28			0.00			0.00
	62	Turn 60 Degrees Left	0.060			0.000			0.00
	63	Turn 60 Degrees Right	0.060			0.000			0.00
	64	Take Off	0.40	2.40	6	0.08	0.45	6	0.08
	65	Left Hover Turn	0.33	1.00	12	0.05	0.16	12	0.05
	66	Right Hover Turn	0.33	1.00	12	0.05	0.15	12	0.05
	74	Auto Turn Left	0.06	0.22	15	0.00	0.00	15	0.00
75	Auto Turn Right	0.06	0.22	15	0.00	0.00	15	0.00	
76	Hover Approach	0.22	2.00	4	0.01	0.07	4	0.01	
77	Taxi	0.18			3.82			1.89	
78	Taxi Turn	0.22	3.20	2.5	0.07	1.05	2.5	0.07	

Table 12. Revised CWC spectrum for CONUS training (any GW)

	CONUS Training (Any GW)								Adjustment Factor = 0.494766
	Design Regimes		Legacy CWC Usage			Revised CWC “ $\mu+2\sigma$ ” Usage			
	Regime No.	Description	PCT Time	Occs /hr	Secs /Occ	PCT Time	Occs /hr	Secs /Occ	Adj Pct Time
Basic Mission UH-60M Usage Spectrum (E/R Events Removed and Reallocated to SS Complementary Event) Low GW	79	Normal Landing	0.46	5.50	3	1.22	17.54	2.5	0.60
	80	Run-on Landing	0.10	0.50	7	0.00	0.00	2.5	0.00
	81	Hover Rudder Reversal	0.05		1.5	0.00	0.00	1.5	0.00
	82	Level Flight Rudder Reversal	0.12		1.5	0.00	0.00	1.5	0.00
	83	Hover Longitudinal Reversal	0.05		1.5	0.05	1.14	1.5	0.02
	84	Level Flight Longitudinal Reversal	0.12		1.5	0.01	0.20	1.5	0.00
	85	Hover Lateral Reversal	0.05		1.5	0.21	4.95	1.5	0.10
	86	Level Flight Lateral Reversal	0.12		1.5	0.02	0.58	1.5	0.01
	87	Moderate Pullout	0.22	0.80	10	1.02	3.66	10	0.50
	88	Severe Pullout	0.06	0.40	5	0.00	0.01	5	0.00
	97	Droop Stop Pounding	0.00	5.00	1	0.00	0.00	1	0.00
	98	Extreme Maneuver	0.00	0.00	5	0.01	0.07	5	0.00
	99	3.3G Pullout (Structural Design)	0.00	0.02	5	0.00	0.00	5	0.00
	100	Single Engine Failure in Hover		0.50					
	101	Single Engine Failure at Altitude		1.00					
102	GAG/Flight		6.00			6.76			
103	Min-Max (a.k.a. Full-Stop Landing)		2.00			1.48			

Table 13. Revised CWC spectrum for OCONUS 1 (low-mid GW)

	OCONUS 1 (Low-Mid GW)								Adjustment Factor = 0.385698
	Design Regimes		Legacy CWC Usage			Revised CWC “ $\mu+2\sigma$ ” Usage			
	Regime No.	Description	PCT Time	Occs/hr	Secs/Occ	PCT Time	Occs/hr	Secs/Occ	Adj Pct Time
Basic Mission UH-60M Usage Spectrum (E/R Events Removed and Reallocated to SS Complementary Event) Low GW	1	Hover	1.06			1.51			
	2	Left Sideward Flight	0.45			0.24			
	3	Right Sideward Flight	0.45			0.78			
	4	Rearward Flight	0.45			1.05			
	5	Climb	2.52			1.99			
	6	Level Flight @ 0.1VH	1.38			0.00			
	7	Level Flight @ 0.2VH	0.92			0.67			
	8	Level Flight @ 0.4VH	1.84			0.88			
	9	Level Flight @ 0.5VH	1.84			0.90			
	10	Level Flight @ 0.6VH	2.53			1.51			
	11	Level Flight @ 0.7VH	2.76			5.57			
	12	Level Flight @ 0.8VH	9.19			22.02			
	13	Level Flight @ 0.9VH	13.78			16.39			
	14	Level Flight @ 1.0VH	6.89			1.16			
	15	Sideslip	0.60			0.69			
	16	Autorotation	0.86			0.00			
	17	Partial Power Descent	1.50			1.51			
	18	Dive	1.39			0.23			
	19	Turn 30 Degrees Left	2.50			1.83			
	20	Turn 30 Degrees Right	2.50			2.18			
	21	Turn 45 Degrees Left	0.43			0.03			
	22	Turn 45 Degrees Right	0.43			0.01			
	23	Turn 60 Degrees Left	0.09			0.00			
	24	Turn 60 Degrees Right	0.09			0.00			
	25	Take Off	0.60	3.60	6	0.47	2.84	6.00	
	26	Left Hover Turn	0.50	1.50	12	0.11	0.34	12.00	
	27	Right Hover Turn	0.50	1.50	12	0.06	0.18	12.00	
	35	Auto Turn Left	0.14	0.33	15	0.00	0.00	15.00	
	36	Auto Turn Right	0.14	0.33	15	0.00	0.00	15.00	
	37	Hover Approach	0.33	3.00	4	0.03	0.23	4.00	
	38	Taxi	0.27			39.36	0.00		
	39	Taxi Turn	0.33	4.80	2.5	0.98	14.04	2.50	

Table 14. Revised CWC spectrum for OCONUS 1 (mid-high GW)

	OCONUS Training 1 (Mid-High GW)								Adjustment Factor = 0.0385698
	Design Regimes		Legacy CWC Usage			Revised CWC “ $\mu+2\sigma$ ” Usage			
	Regime No.	Description	PCT Time	Occs/hr	Secs/Occ	PCT Time	Occs/hr	Secs/Occ	Adj Pct Time
Basic Mission UH-60M Usage Spectrum (E/R Events Removed and Reallocated to SS Complementary Event) Low GW	40	Hover	0.71			2.85			1.10
	41	Left Sideward Flight	0.30			0.38			0.15
	42	Right Sideward Flight	0.30			1.48			0.57
	43	Rearward Flight	0.30			1.07			0.41
	44	Climb	1.68			2.18			0.84
	45	Level Flight @ 0.1VH	0.92			0.00			0.00
	46	Level Flight @ 0.2VH	0.61			0.90			0.35
	47	Level Flight @ 0.4VH	1.22			0.94			0.36
	48	Level Flight @ 0.5VH	1.22			0.95			0.37
	49	Level Flight @ 0.6VH	1.68			1.36			0.53
	50	Level Flight @ 0.7VH	1.84			3.87			1.49
	51	Level Flight @ 0.8VH	6.13			18.12			6.99
	52	Level Flight @ 0.9VH	9.19			44.09			17.00
	53	Level Flight @ 1.0VH	4.59			11.27			4.35
	54	Sideslip	0.40			1.60			0.62
	55	Autorotation	0.58			0.00			0.00
	56	Partial Power Descent	1.00			1.55			0.60
	57	Dive	0.93			0.61			0.23
	58	Turn 30 Degrees Left	1.67			1.94			0.75
	59	Turn 30 Degrees Right	1.67			1.70			0.65
	60	Turn 45 Degrees Left	0.28			0.07			0.03
	61	Turn 45 Degrees Right	0.28			0.06			0.02
	62	Turn 60 Degrees Left	0.060			0.010			0.00
	63	Turn 60 Degrees Right	0.060			0.005			0.00
	64	Take Off	0.40	2.40	6	0.60	3.63	6.00	0.60
	65	Left Hover Turn	0.33	1.00	12	0.21	0.62	12.00	0.21
	66	Right Hover Turn	0.33	1.00	12	0.19	0.58	12.00	0.19
	74	Auto Turn Left	0.06	0.22	15	0.00	0.00	15.00	0.00
75	Auto Turn Right	0.06	0.22	15	0.00	0.00	15.00	0.00	
76	Hover Approach	0.22	2.00	4	0.02	0.18	4.00	0.02	
77	Taxi	0.18			48.54			18.72	
78	Taxi Turn	0.22	3.20	2.5	1.81	26.06	2.50	1.81	

Table 15. Revised CWC spectrum for OCONUS 1 (any GW)

	OCONUS 1 Training (Any GW)								Adjustment Factor = 0.385698
	Design Regimes		Legacy CWC Usage			Revised CWC “ $\mu+2\sigma$ ” Usage			
	Regime No.	Description	PCT Time	Occs /hr	Secs /Occ	PCT Time	Occs /hr	Secs /Occ	Adj Pct Time
Basic Mission UH-60M Usage Spectrum (E/R Events Removed and Reallocated to SS Complementary Event) Low GW	79	Normal Landing	0.46	5.50	3	0.57	8.16	2.5	0.22
	80	Run-on Landing	0.10	0.50	7	0.00	0.00	2.5	0.00
	81	Hover Rudder Reversal	0.05		1.5	0.00	0.01	1.5	0.00
	82	Level Flight Rudder Reversal	0.12		1.5	0.00	0.00	1.5	0.00
	83	Hover Longitudinal Reversal	0.05		1.5	0.00	0.11	1.5	0.00
	84	Level Flight Longitudinal Reversal	0.12		1.5	0.00	0.06	1.5	0.00
	85	Hover Lateral Reversal	0.05		1.5	0.02	0.39	1.5	0.01
	86	Level Flight Lateral Reversal	0.12		1.5	0.00	0.05	1.5	0.00
	87	Moderate Pullout	0.22	0.80	10	0.63	2.28	10	0.24
	88	Severe Pullout	0.06	0.40	5	0.00	0.00	5	0.00
	97	Droop Stop Pounding	0.00	5.00	1	0.00	0.00	1	0.00
	98	Extreme Maneuver	0.00	0.00	5	0.00	0.03	5	0.00
	99	3.3G Pullout (Structural Design)	0.00	0.02	5	0.00	0.00	5	0.00
	100	Single Engine Failure in Hover		0.50					
	101	Single Engine Failure at Altitude		1.00					
102	GAG/Flight		6.00			2.34			
103	Min-Max (a.k.a. Full-Stop Landing)		2.00			0.12			

Table 16. Revised CWC spectrum for OCONUS 2 (low-mid GW)

	OCONUS 2 (Low-Mid GW)								Adjustment Factor = 0.617055
	Design Regimes		Legacy CWC Usage			Revised CWC “ $\mu+2\sigma$ ” Usage			
	Regime No.	Description	PCT Time	Occs/hr	Secs/Occ	PCT Time	Occs/hr	Secs/Occ	Adj Pct Time
Basic Mission UH-60M Usage Spectrum (E/R Events Removed and Reallocated to SS Complementary Event) Low GW	1	Hover	1.06			1.00			0.61
	2	Left Sideward Flight	0.45			0.05			0.03
	3	Right Sideward Flight	0.45			0.27			0.16
	4	Rearward Flight	0.45			0.19			0.12
	5	Climb	2.52			0.33			0.21
	6	Level Flight @ 0.1VH	1.38			0.00			0.00
	7	Level Flight @ 0.2VH	0.92			0.23			0.14
	8	Level Flight @ 0.4VH	1.84			0.24			0.15
	9	Level Flight @ 0.5VH	1.84			0.30			0.18
	10	Level Flight @ 0.6VH	2.53			0.51			0.31
	11	Level Flight @ 0.7VH	2.76			0.80			0.49
	12	Level Flight @ 0.8VH	9.19			0.52			0.32
	13	Level Flight @ 0.9VH	13.78			0.20			0.12
	14	Level Flight @ 1.0VH	6.89			0.01			0.00
	15	Sideslip	0.60			0.09			0.06
	16	Autorotation	0.86			0.00			0.00
	17	Partial Power Descent	1.50			0.22			0.13
	18	Dive	1.39			0.04			0.02
	19	Turn 30 Degrees Left	2.50			0.61			0.38
	20	Turn 30 Degrees Right	2.50			0.26			0.16
	21	Turn 45 Degrees Left	0.43			0.04			0.02
	22	Turn 45 Degrees Right	0.43			0.02			0.01
	23	Turn 60 Degrees Left	0.09			0.00			0.00
	24	Turn 60 Degrees Right	0.09			0.00			0.00
	25	Take Off	0.60	3.60	6	0.11	7.99	6	0.11
	26	Left Hover Turn	0.50	1.50	12	0.07	3.02	12	0.07
	27	Right Hover Turn	0.50	1.50	12	0.07	2.44	12	0.07
	35	Auto Turn Left	0.14	0.33	15	0.00	0.00	15	0.00
	36	Auto Turn Right	0.14	0.33	15	0.00	0.00	15	0.00
	37	Hover Approach	0.33	3.00	4	0.01	0.67	4	0.01
	38	Taxi	0.27			6.25			3.86
	39	Taxi Turn	0.33	4.80	2.5	0.11	16.30	2.5	0.11

Table 17. Revised CWC spectrum for OCONUS 2 (mid-high GW)

		OCONUS Training 1 (Mid-High GW)							Adjustment Factor = 0.617055
		Design Regimes		Legacy CWC Usage			Revised CWC “ $\mu+2\sigma$ ” Usage		
		Regime No.	Description	PCT Time	Occs/hr	Secs/Occ	PCT Time	Occs/hr	Secs/Occ
Basic Mission UH-60M Usage Spectrum (E/R Events Removed and Reallocated to SS Complementary Event) Low GW	40	Hover	0.71			4.46			2.75
	41	Left Sideward Flight	0.30			0.88			0.55
	42	Right Sideward Flight	0.30			2.13			1.32
	43	Rearward Flight	0.30			2.00			1.23
	44	Climb	1.68			5.06			3.12
	45	Level Flight @ 0.1VH	0.92			0.00			0.00
	46	Level Flight @ 0.2VH	0.61			1.90			1.17
	47	Level Flight @ 0.4VH	1.22			2.53			1.56
	48	Level Flight @ 0.5VH	1.22			4.63			2.86
	49	Level Flight @ 0.6VH	1.68			6.55			4.04
	50	Level Flight @ 0.7VH	1.84			13.19			8.14
	51	Level Flight @ 0.8VH	6.13			29.28			18.07
	52	Level Flight @ 0.9VH	9.19			8.77			5.41
	53	Level Flight @ 1.0VH	4.59			1.07			0.66
	54	Sideslip	0.40			3.10			1.91
	55	Autorotation	0.58			0.00			0.00
	56	Partial Power Descent	1.00			5.03			3.10
	57	Dive	0.93			0.76			0.47
	58	Turn 30 Degrees Left	1.67			4.50			2.78
	59	Turn 30 Degrees Right	1.67			5.41			3.34
	60	Turn 45 Degrees Left	0.28			0.23			0.14
	61	Turn 45 Degrees Right	0.28			0.15			0.09
	62	Turn 60 Degrees Left	0.060			0.027			0.02
	63	Turn 60 Degrees Right	0.060			0.014			0.01
	64	Takeoff	0.40	2.40	6	0.93	0.45	6	0.93
	65	Left Hover Turn	0.33	1.00	12	0.38	0.16	12	0.38
	66	Right Hover Turn	0.33	1.00	12	0.27	0.15	12	0.27
	74	Auto Turn Left	0.06	0.22	15	0.00	0.00	15	0.00
75	Auto Turn Right	0.06	0.22	15	0.00	0.00	15	0.00	
76	Hover Approach	0.22	2.00	4	0.04	0.07	4	0.04	
77	Taxi	0.18			40.05			24.71	
78	Taxi Turn	0.22	3.20	2.5	1.81	1.05	2.5	1.81	

Table 18. Revised CWC spectrum for OCONUS 2 (any GW)

	OCONUS 2 Training (Any GW)								Adjustment Factor = 0.617055
	Design Regimes		Legacy CWC Usage			Revised CWC “ $\mu+2\sigma$ ” Usage			
	Regime No.	Description	PCT Time	Occs /hr	Secs /Occ	PCT Time	Occs /hr	Secs /Occ	Adj Pct Time
Basic Mission UH-60M Usage Spectrum (E/R Events Removed and Reallocated to SS Complementary Event) Low GW	79	Normal Landing	0.46	5.50	3	0.85	12.26	2.5	0.53
	80	Run-on Landing	0.10	0.50	7	0.00	0.00	2.5	0.00
	81	Hover Rudder Reversal	0.05		1.5	0.00	0.00	1.5	0.00
	82	Level Flight Rudder Reversal	0.12		1.5	0.00	0.00	1.5	0.00
	83	Hover Longitudinal Reversal	0.05		1.5	0.04	0.85	1.5	0.02
	84	Level Flight Longitudinal Reversal	0.12		1.5	0.01	0.18	1.5	0.00
	85	Hover Lateral Reversal	0.05		1.5	0.04	0.92	1.5	0.02
	86	Level Flight Lateral Reversal	0.12		1.5	0.00	0.11	1.5	0.00
	87	Moderate Pullout	0.22	0.80	10	0.93	3.36	10	0.58
	88	Severe Pullout	0.06	0.40	5	0.00	0.01	5	0.00
	97	Droop Stop Pounding	0.00	5.00	1	0.00	0.00	1	0.00
	98	Extreme Maneuver	0.00	0.00	5	0.01	0.04	5	0.00
	99	3.3G Pullout (Structural Design)	0.00	0.02	5	0.00	0.00	5	0.00
	100	Single Engine Failure in Hover		0.50					
	101	Single Engine Failure at Altitude		1.00					
102	GAG/Flight		6.00			4.71			
103	Min-Max (a.k.a. Full-Stop Landing)		2.00			1.16			

3.4.1.2 Compare Operational Usage Spectra With Design CWC Spectrum

The revised CWC usage spectra for each of the three operational environments is based on the ADS-79C [7] paragraph A.6.5 “ $\mu+2\sigma$ ” option and described in section 3.4. The revised CWC usage is compared with the design CWC usage for each regime in figures 47–49. Note that all of the regimes from hover to taxi turn (inclusive) are repeated in the figures to distinguish between the low-mid GW and mid-high GW regimes and the unique damage rates associated with each GW range.

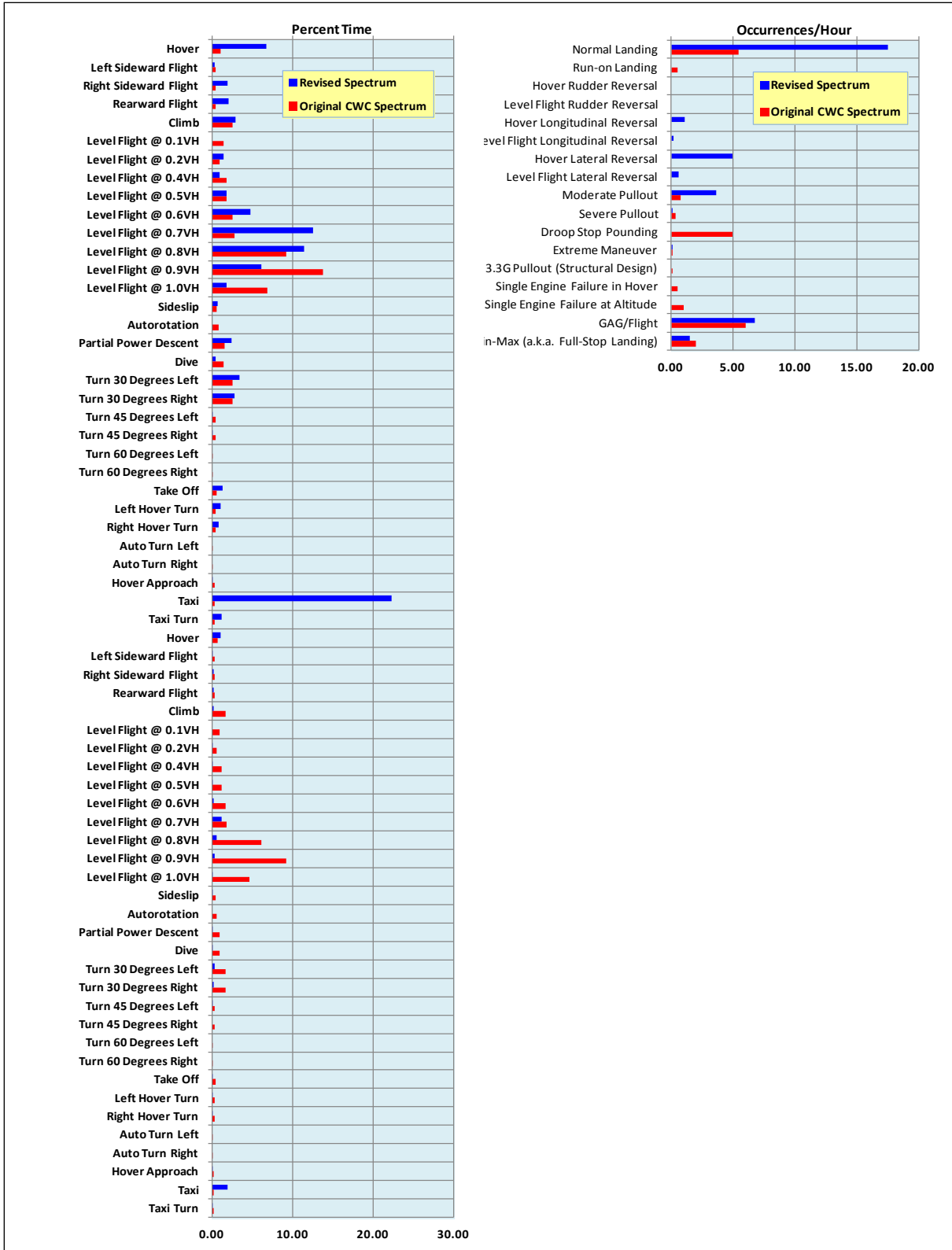


Figure 47. Comparison of revised CONUS training usage with CWC usage

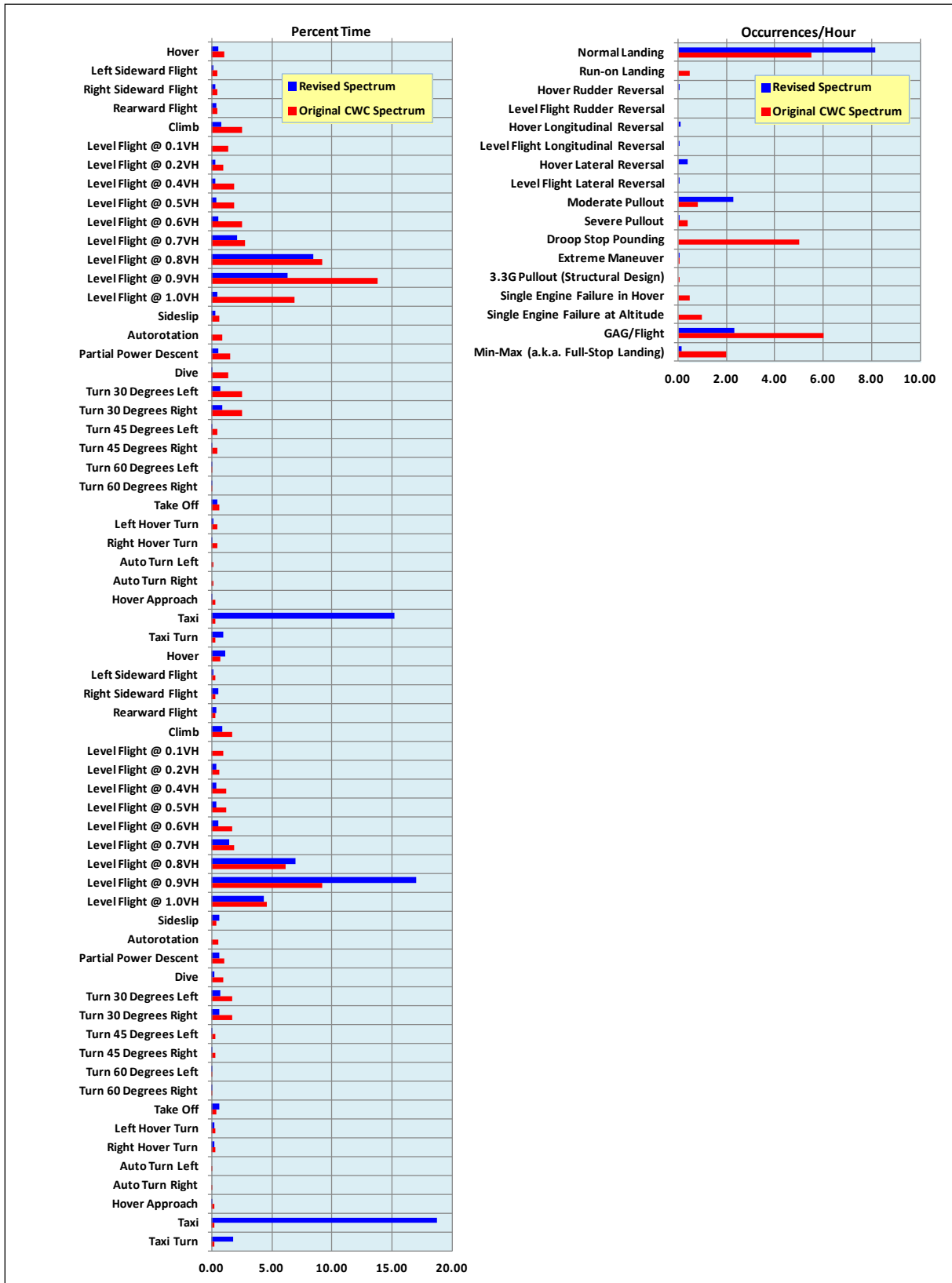


Figure 48. Comparison of revised OCONUS 1 usage with CWC usage

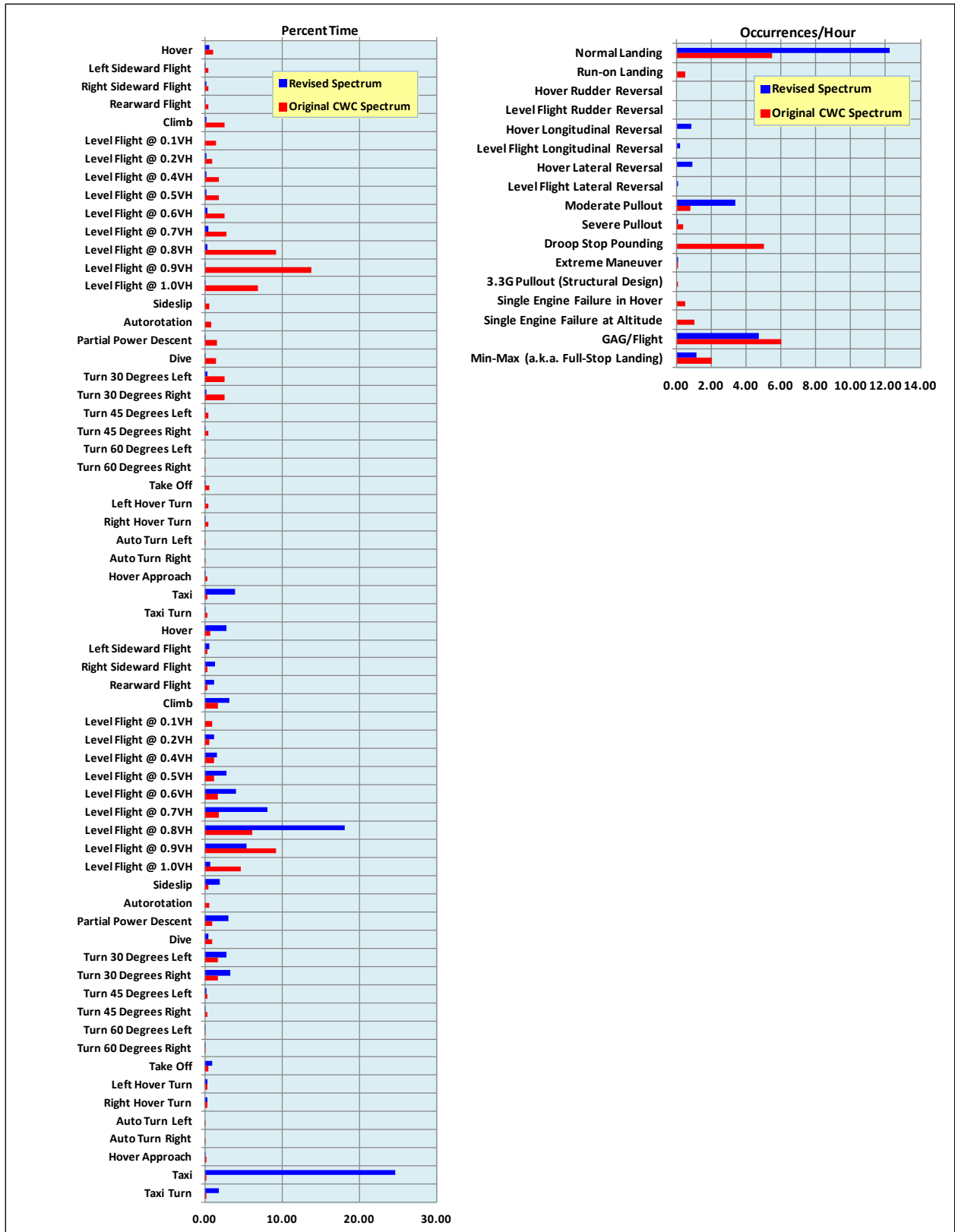


Figure 49. Comparison of revised OCONUS 2 usage with CWC usage

3.4.2 Evaluate Damage Accumulation and Demonstrate Usage Credit Process

3.4.2.1 Select Three Components

Criteria were developed for selecting three UH-60M components to be used for updating the process and benefits of usage monitoring. The criteria specified that each selected component have the following attributes:

- Be a major, high-value component
- Have a relatively short CRT
- Have sufficient reliability to safely benefit from usage-based life extension

The three components selected met these criteria and each had two failure modes. The selected components are identified and described in figure 50.

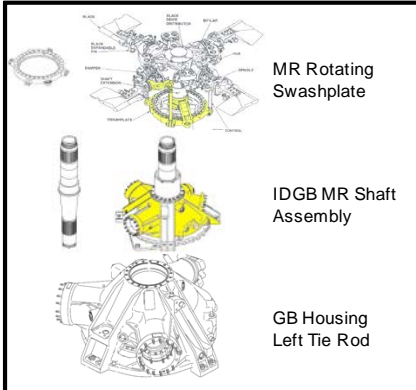
	COMPONENT	PART NO.	FAILURE MODE	STORE CONFIG.	CRT
 <p>MR Rotating Swashplate</p> <p>IDGB MR Shaft Assembly</p> <p>GB Housing Left Tie Rod</p>	MR ROTATING SWASHPLATE	70104-08001-044, -045, -050	PUSHROD ATTACHMENT MODE (CHAFING)	NO STORES	5,000
	IDGB MR SHAFT	70351-38131-042	CHAFING UNDER UPPER BEARING	WITH STORES	7,800
	LEFT TIE ROD	70400-08115-046	CHAFING ALUMINUM MODE	NO STORES	4,600

Figure 50. Selected components

3.4.2.2 Determine Operational Usage Damage Accumulation

Using ADS-79C [7] paragraph A.6.4 for operational damage, three theaters of operation were evaluated that included CONUS training, OCONUS 1, and OCONUS 2. The three theaters considered three dynamic failure modes:

- Main rotor rotating swashplate/pushrod attachment chafing (no stores)
- Increased durability gearbox (IDGB) MR shaft/chafing under upper bearing (with stores)
- Left tie rod/main gearbox housing attachment hole chafing (no stores)

All aircraft monitored in each operational environment were considered for inclusion in the evaluation of operational damage with the following results:

- CONUS training: One aircraft contained only a small fraction of an hour and was creating an outlier in the seconds per flight hour. It was therefore removed from the sample.
- OCONUS 1: All aircraft were included in the operational damage.
- OCONUS 2: All aircraft were included in the operational damage.

3.4.2.2.1 Introduction/Background

Revised spectrum alternatives versus CWC were evaluated using ADS-79C [7], paragraph A.6.5. This included:

- “ $\mu+1\sigma$ ” SUMS spectrum (with $\mu-3\sigma$ working curve)
- “ $\mu+2\sigma$ ” SUMS spectrum (with $\mu-3\sigma$ working curve)
- SUMS average spectrum (with $\mu-3.64\sigma$ working curve)
- Using $\mu-3.64\sigma$ recovers one 9 of reliability given assumption of five 9s of implicit reliability from TOS load bias and $\mu-3\sigma$ EL

The mathematical basics when estimating spectrum time of occurrence follow:

Law of large numbers (law of averages) applies:

- $$P(|\bar{X}_n - \mu| > \varepsilon) = P(|\bar{X}_n - E[\bar{X}_n]| > \varepsilon) \leq \frac{1}{\varepsilon^2} \text{Var}(\bar{X}_n) = \frac{\sigma^2}{n\varepsilon^2}$$
- *where: $P(|\bar{X}_n - \mu| = \text{Absolute Value of Sample Mean} - \text{True Mean}$*
- *where: $\frac{1}{\varepsilon^2} \text{Var}(\bar{X}_n) = \frac{\sigma^2}{n\varepsilon^2}$;*
 $\text{Var}(\bar{X}_n)$ is Variance when Estimating the Sample Mean;
 σ is the True Variance

- Simply put: As n gets larger, the standard error of the estimate, ϵ , approaches zero and the cumulative average approaches true average, while the variance in the sample mean approaches the true variance.

The mathematical basics when estimating spectrum time of occurrence follow:

Consider a 1-hour average spectrum:

For SS regimes, use SUMS average secs/hr:

$$\text{Secs} / \text{hr} = \frac{\sum_{i=1}^N t_i}{\sum_{i=1}^N T_i} ; t = \text{regime time (secs)}; T = \text{flight time (hrs)}; N = \text{total number of flights}$$

For Transient (SS) regimes, use SUMS average occurrences/hr:

$$\text{Occs} / \text{hr} = \frac{\sum_{i=1}^N n_i}{\sum_{i=1}^N T_i} ; n = \text{regime occurrences}; T = \text{flight time (hrs)}; N = \text{total number of flights}$$

Consider “ $\mu+1\sigma$ ” and “ $\mu+2\sigma$ ” spectra:

Use \bar{X}_N as best Estimate for μ ;

Use $\sqrt{N} \times \epsilon$ as best Estimate for σ

- Most regimes are time-based (SS) except for control reversals, GAG, and max-min.
- An overall time correction will be needed to ensure that supplemental spectra (“ μ ”, “ $\mu+1\sigma$,” and “ $\mu+2\sigma$ ”) fit in a 1-hour block:
 - Multiply benign SS regimes to expand or contract spectra to get standard 1-hour block

Ground rules are suggested for spectrum development versus the research data. The basic ground rules for composite (average) usage development are covered in “Composite Usage Spectrum Development,” presented September 9–11, 2009 by Dr. Robert Benton [18], which calls for:

Goal: Collect a total of 5000 hours of SUMS data, with 2000 hours from each operational environment.

- Research results: Collected slightly more than 6000 total hours, with 741 hours of CONUS Training, 3367 hours of OCONUS 1, and 1923 hours of OCONUS 2.

Goal: Collect data from a minimum of 20 aircraft with at least 10 per operational environment.

- Research results: Collected data from 29–31 aircraft in each operational environment.

Goal: Collect a minimum of 250 hours per aircraft.

- Research results: Although few aircraft came close to this objective, censoring one CONUS training aircraft generated generally homogeneous results; hours/aircraft ranged from 5.6–232.4 with an average of 67.0.

Goal: Collect at least 12 calendar months of data per aircraft.

- Research results: Most aircraft reached this threshold.

Goal: Collect data from three to four operational environments.

- Research results: Collected data from three different operational environments.

3.4.2.2.2 Deterministic Assessment of SUMS Average Spectrum

Figure 51 illustrates the method to ensure that spectrum reliability meets or exceeds one 9 by replacing CWC reliability with one 9 from EL, as described in paragraph A.6.4 of ADS-79C [7]. The figure 51 flowchart is explained in the following paragraph.

The large disparity between the SUMS average and CWC spectra in regime composition alone does not provide any direct mechanism for quantifying the reliability inherent in the CWC spectrum. To do this, one must determine which of the regimes in the two spectra cause damage. As such, the flowchart in figure 51 is proposed as a direct method for ensuring that one 9 (0.9) of reliability will be present in a revised spectrum (i.e., factored applied cycles of damage applied to SUMS average spectrum) and also for assimilating reliability inherent in the CWC spectrum. The first step in the flowchart is to locate the FSR from the OEM for component failure mode of interest. This fatigue calculation must then be converted into the form of a spreadsheet. Once the spreadsheet is able to produce the life in the FSR, it can be replicated and the SUMS average spectrum of usage substituted for the CWC spectrum of usage. Now replicate this spreadsheet and substitute the $\mu-3.64\sigma$ for the $\mu-3\sigma$ EL. If the life is higher than the one published in the FSR, the reliability of the CWC spectrum exceeds one 9; whereas, if the life is lower than the published FSR life, the reliability of the CWC spectrum is less than one 9. The actual life computed from the SUMS average spectrum and $\mu-3.64\sigma$ EL ensures that the one additional 9 is added to offset the reliability lost from the reduction in bias present in the FSR.

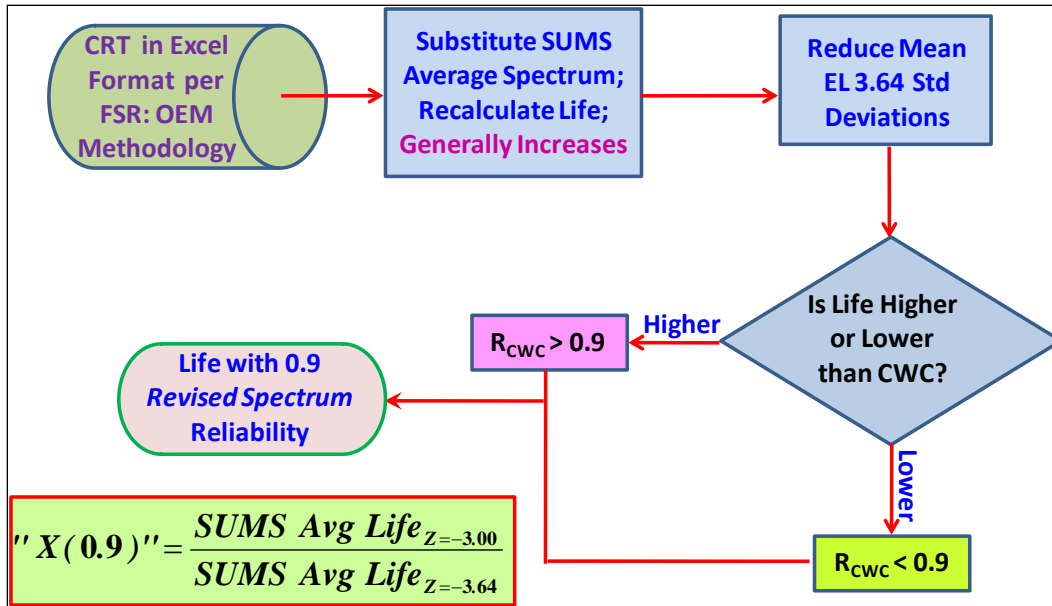


Figure 51. Method to ensure that spectrum reliability meets or exceeds one 9

3.4.2.2.3 Assessment of Three Critical Components in Three Operational Environments

Figures 52–69 examine the effect of the three operational environments (i.e., CONUS training, OCONUS 1, and OCONUS 2) on three fatigue-critical components (i.e., MR rotating swashplate, IDGB MR shaft, left tie rod) for individually tracked tail numbers. Each operational environment/fatigue-critical component combination is depicted graphically on one page according to the following protocol. In the upper LH corner is a table listing flight hours, damage/100 hours, and life by tail number. The small table titled “Box Plot Statistics” lists the minimum, 25th percentile, median, 75th percentile, and maximum life among all tail numbers. Adjacent to the box plot statistics is the actual constructed box plot. A box plot is nothing more than a method of illustrating the characteristics of the data in terms of range, spread, and skewness. Below the box plot is the “Best-Fit Probability Distribution” of predicted life (damage fraction = 1) based on recorded usage by tail number in terms of least squares estimation (LSE). The R^2 -value provides a measure of how well the model explains the data; it is the ratio of the regression (i.e., least-squares fit) sum-of-squares to the total sum-of-squares, or, more specifically, how well the regression line fits the data. Also provided on the best-fit probability distribution plot is the maximum likelihood estimation (MLE) line. The column chart at the bottom of the page provides an additional means of visualizing the scatter in the data.

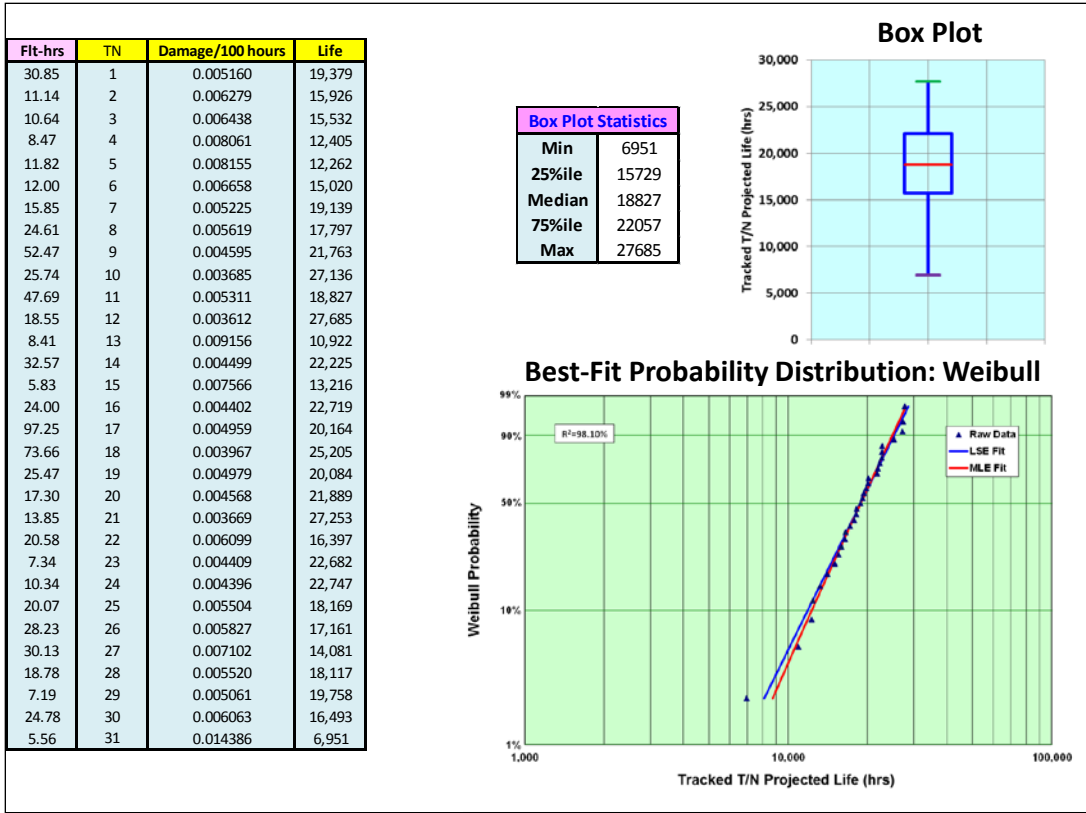


Figure 52. Effects of usage on MR rotating swashplate (CONUS training)

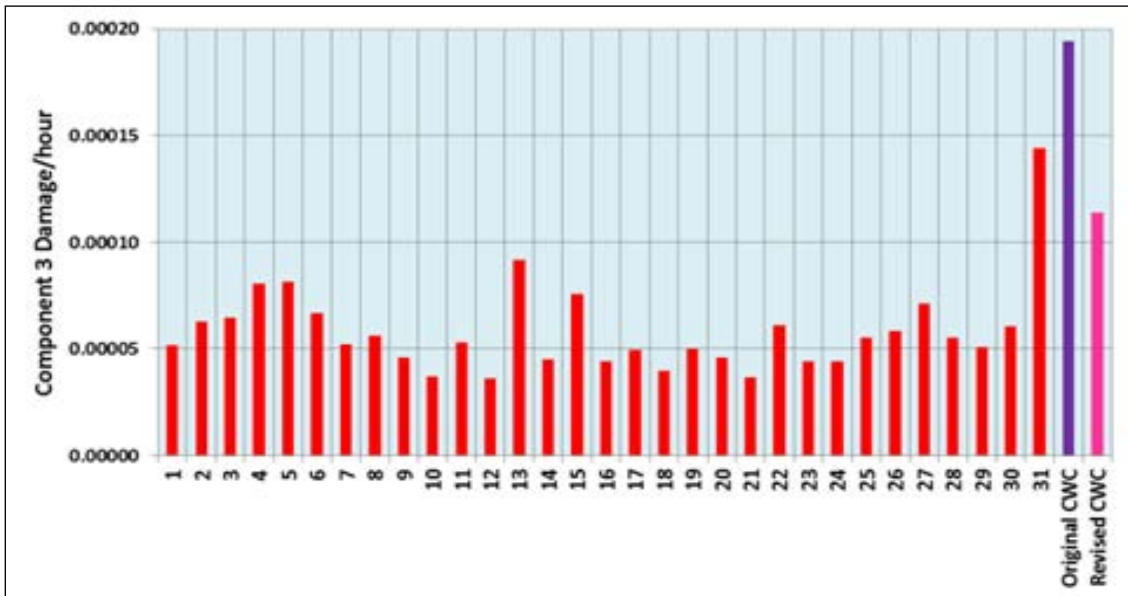


Figure 53. Usage data scatter for MR rotating swashplate (CONUS training)

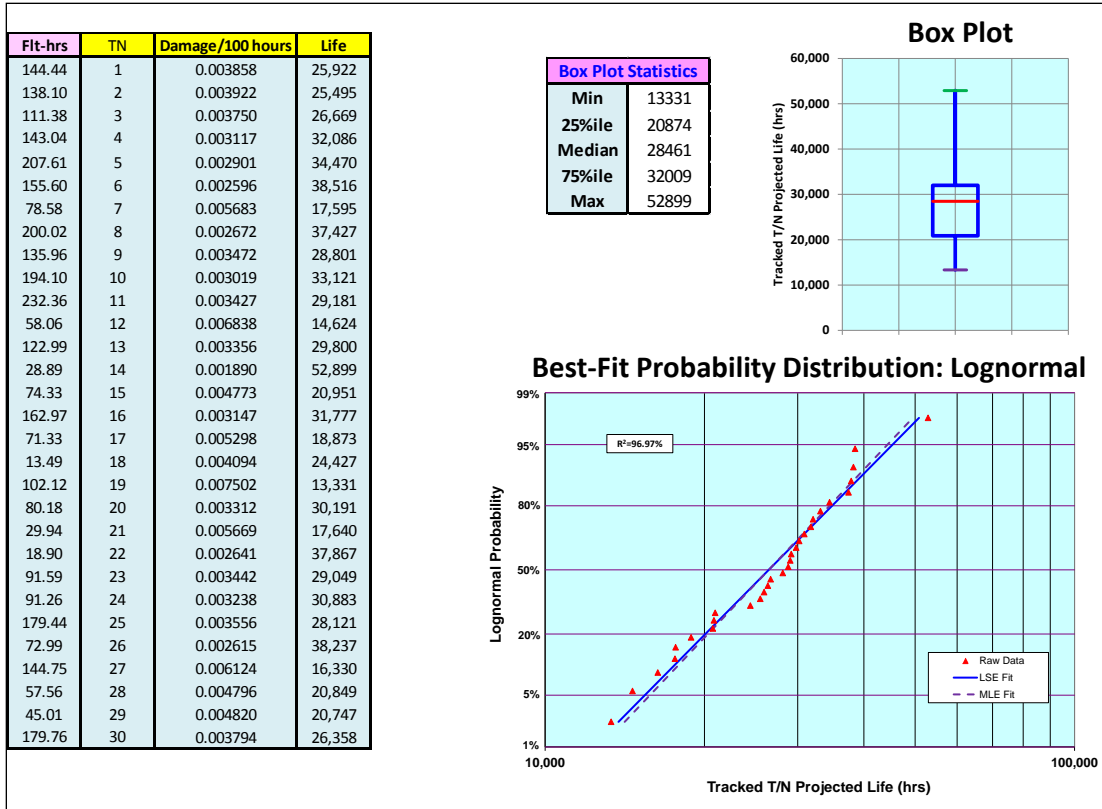


Figure 54. Effects of usage on MR rotating washplate (OCONUS 1)

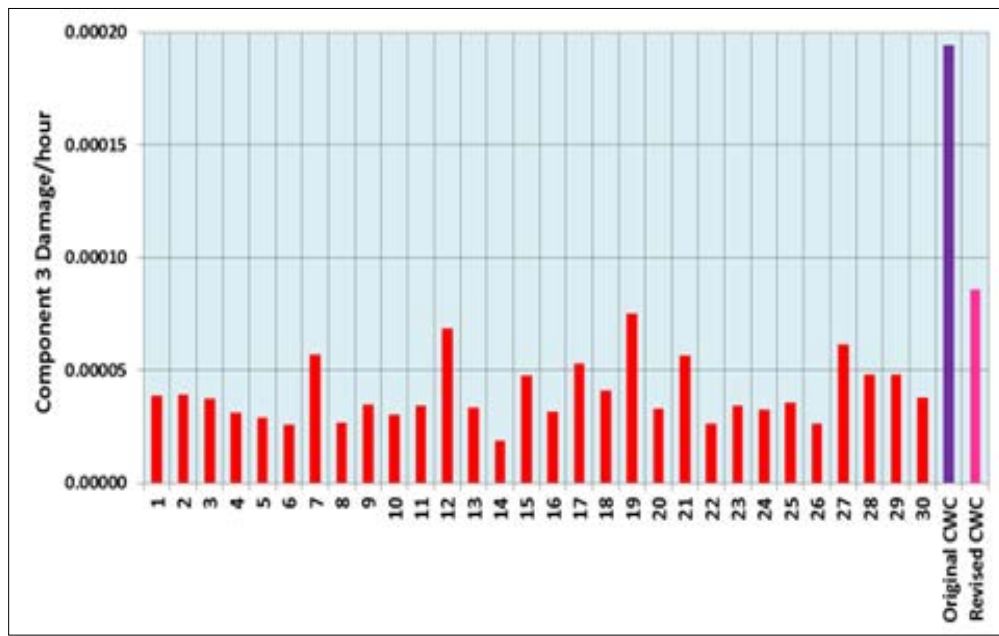


Figure 55. Usage data scatter for MR rotating washplate (OCONUS 1)

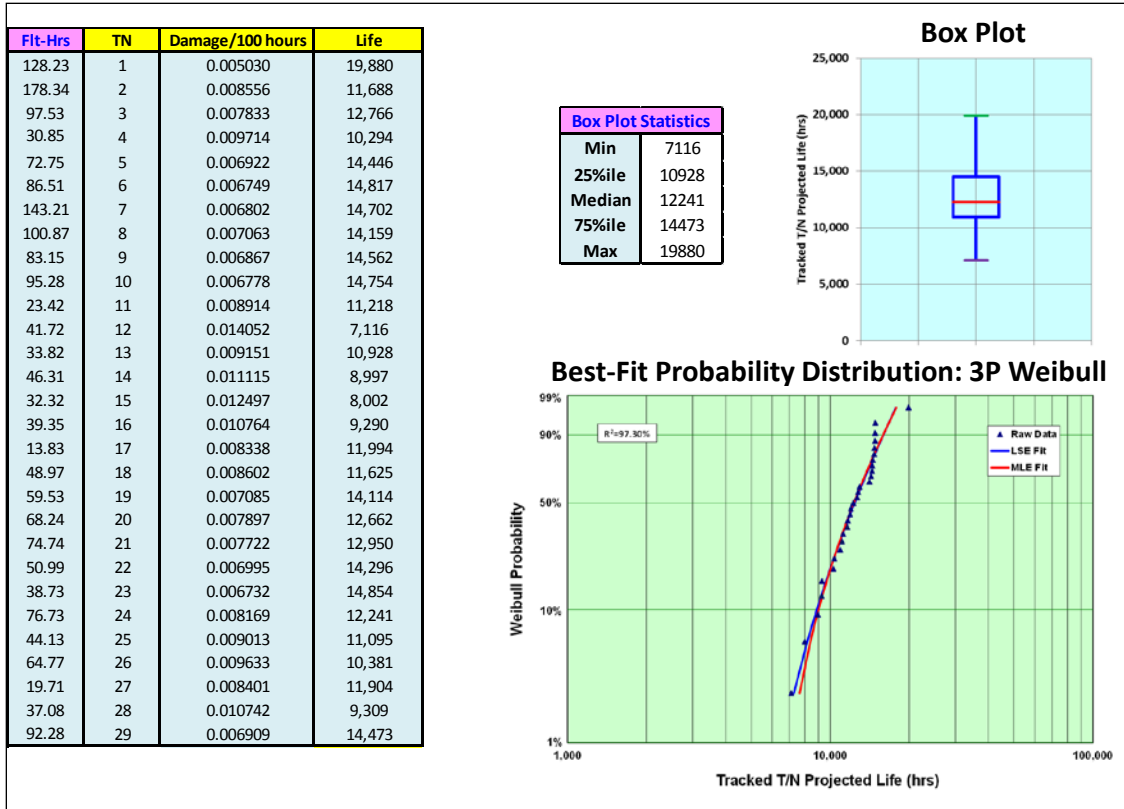


Figure 56. Effects of usage on MR rotating washplate (OCONUS 2)

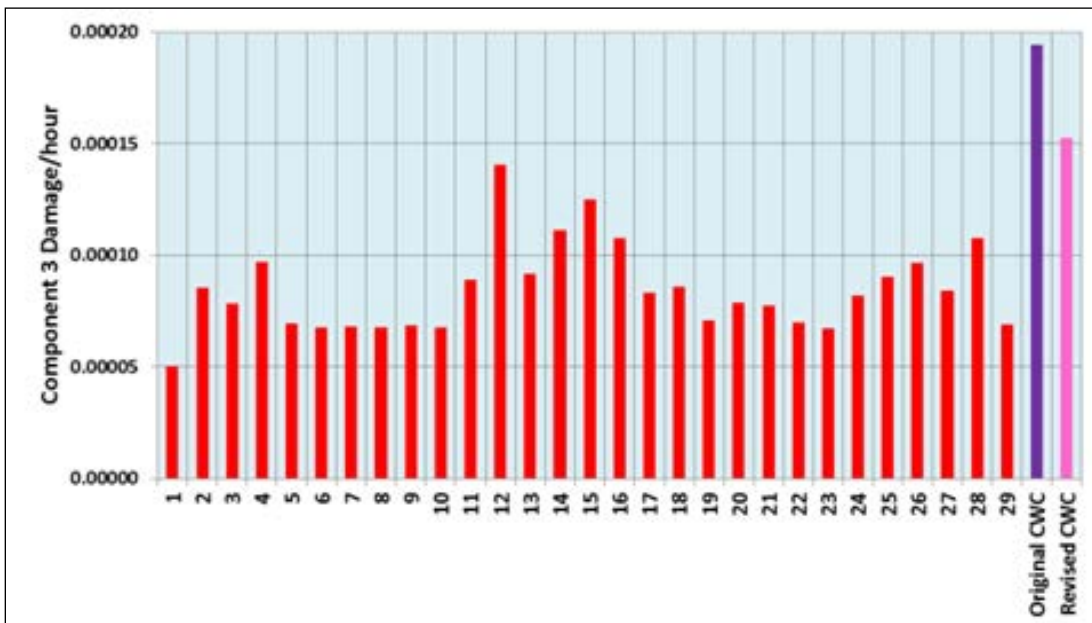


Figure 57. Usage data scatter for MR rotating washplate (OCONUS 2)

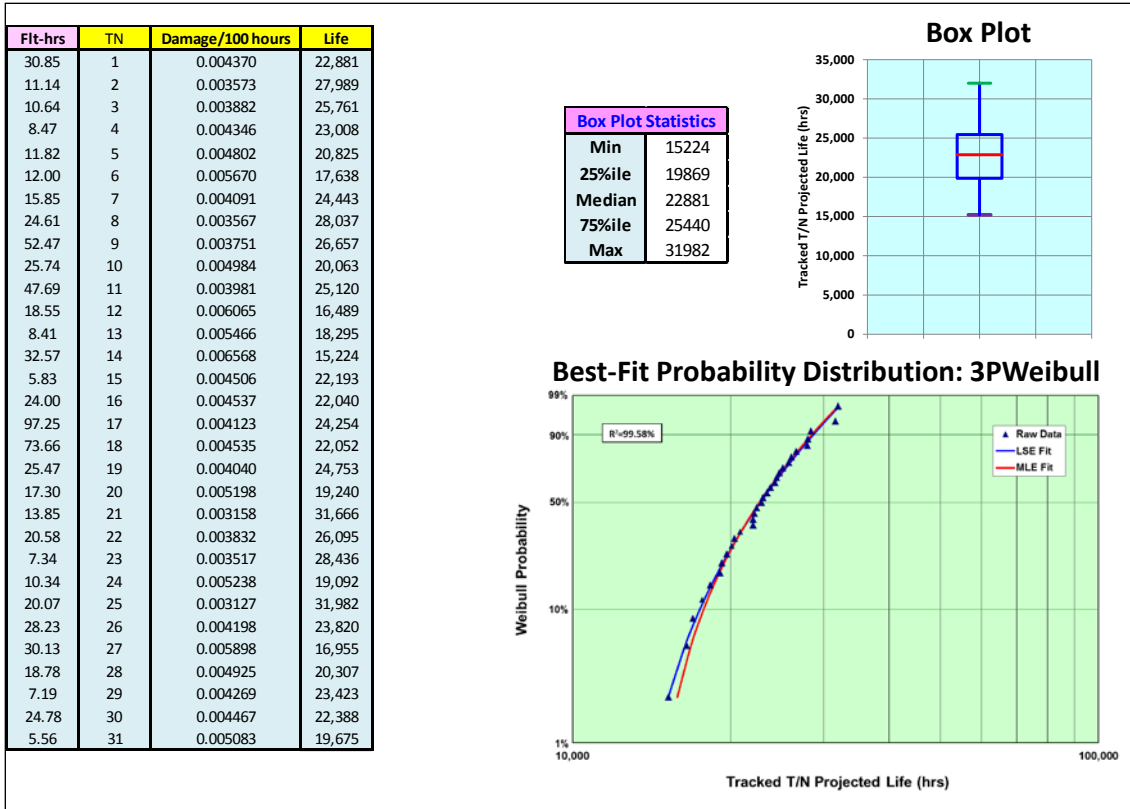


Figure 58. Effects of usage on IDGB MR shaft (CONUS training)

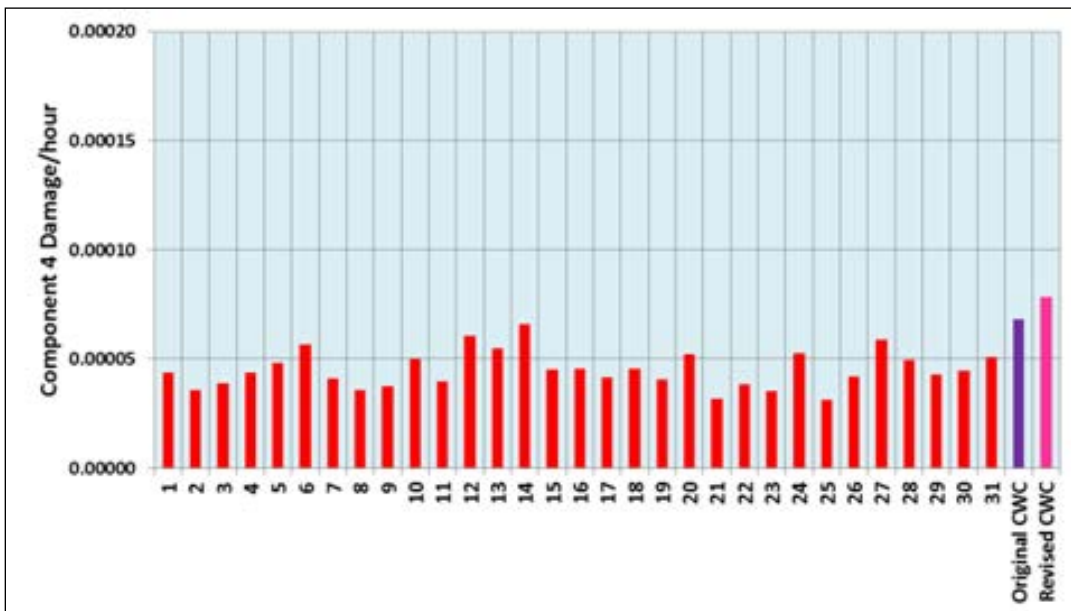


Figure 59. Usage data scatter for IDGB MR shaft (CONUS training)

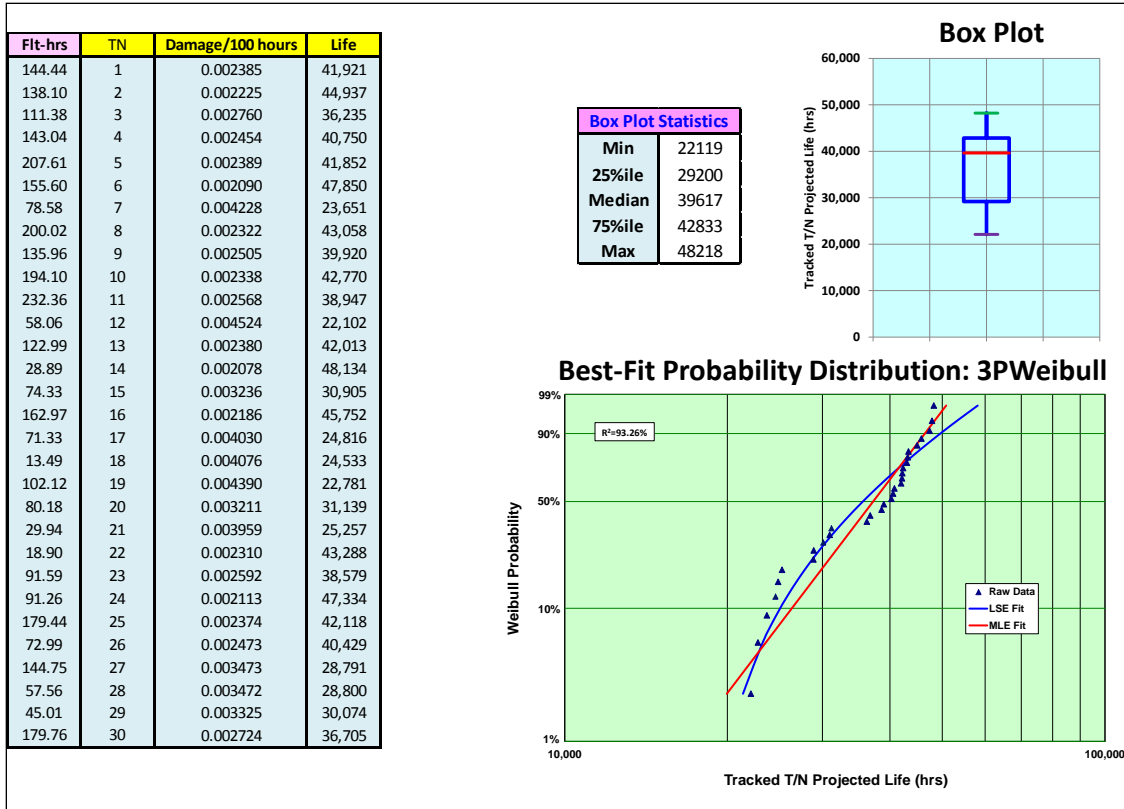


Figure 60. Effects of usage on IDGB MR shaft (OCONUS 1)

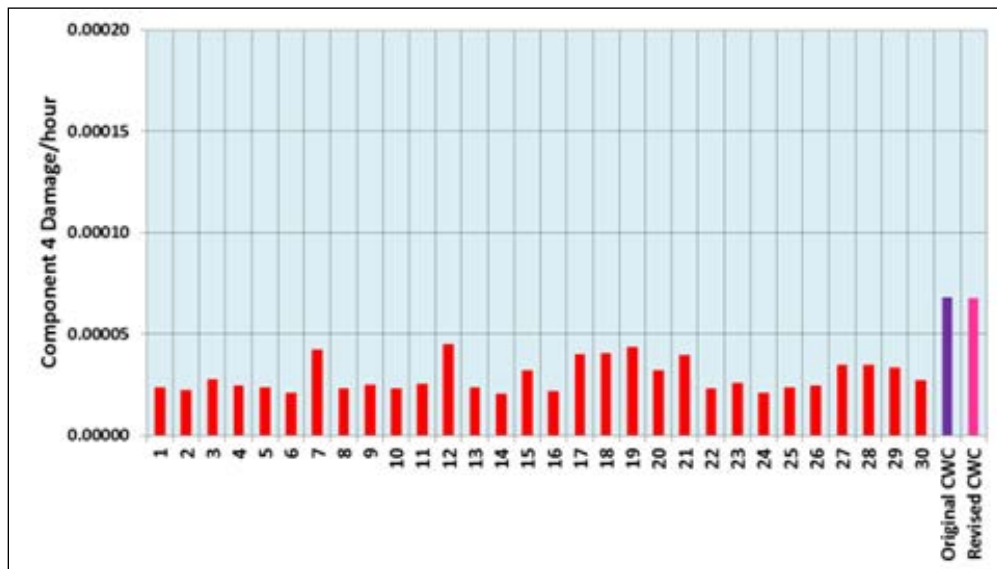


Figure 61. Usage data scatter for IDGB MR shaft (OCONUS 1)

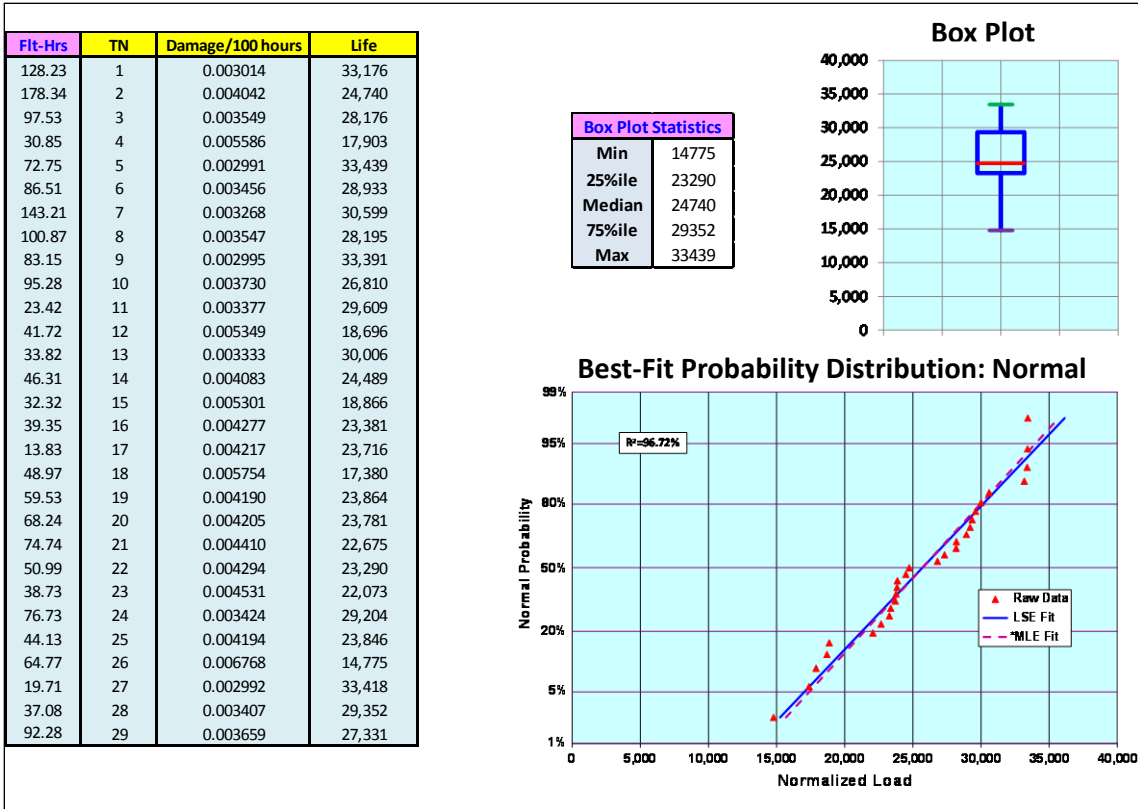


Figure 62. Effects of usage on IDGB MR shaft (OCONUS 2)

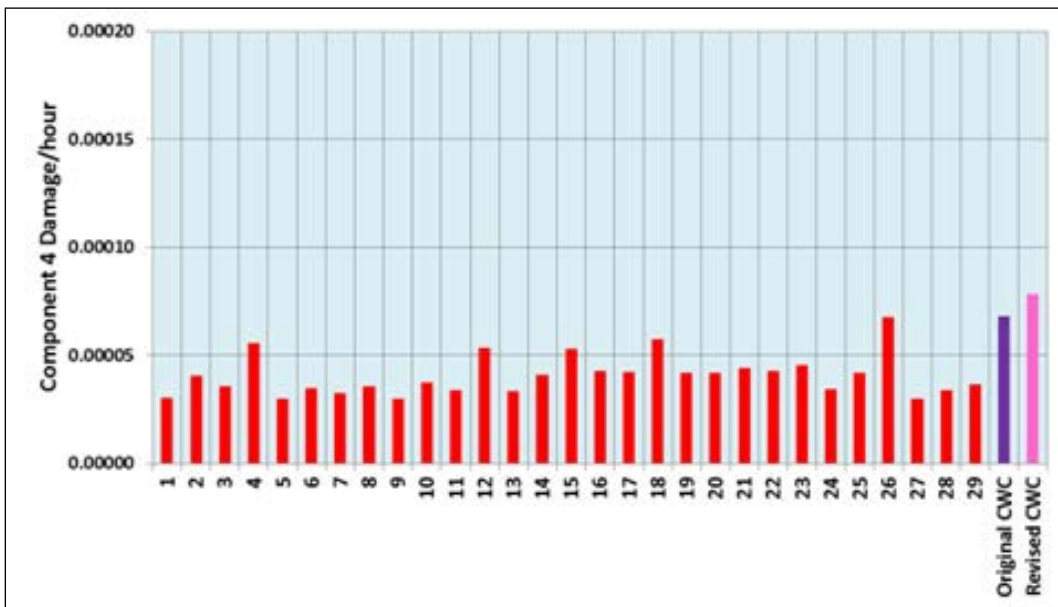


Figure 63. Usage data scatter for IDGB MR shaft (OCONUS 2)

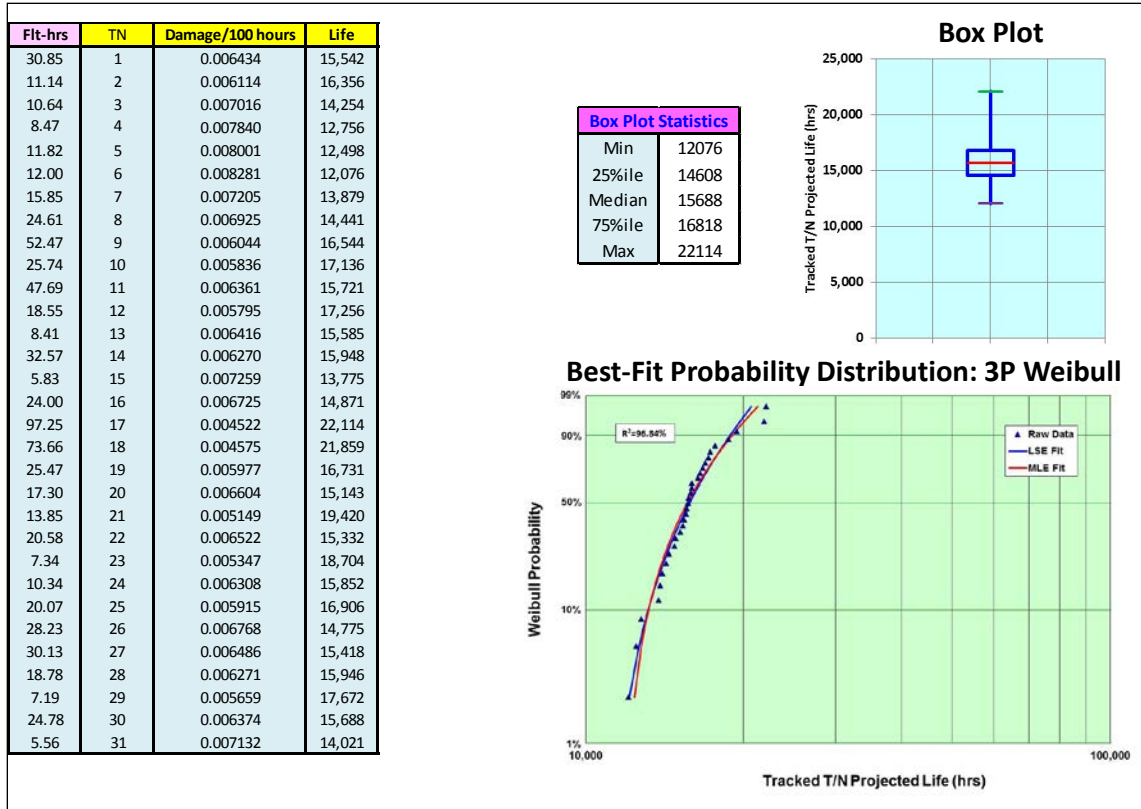


Figure 64. Effects of usage on left tie rod (CONUS training)

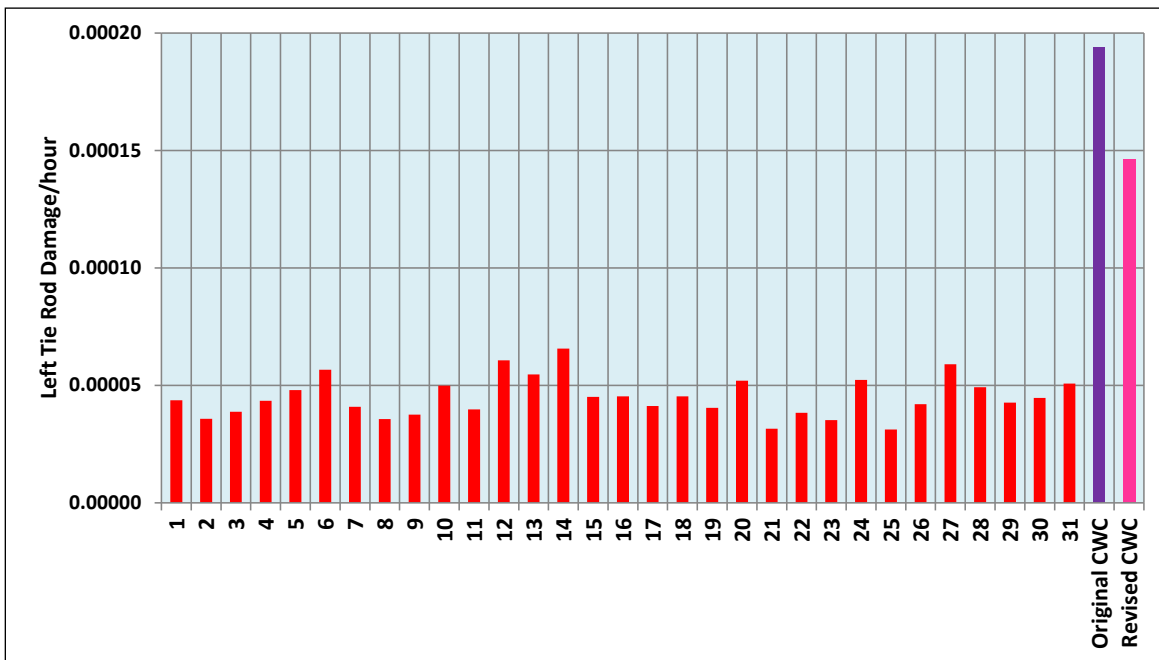


Figure 65. Usage data scatter for left tie rod (CONUS training)

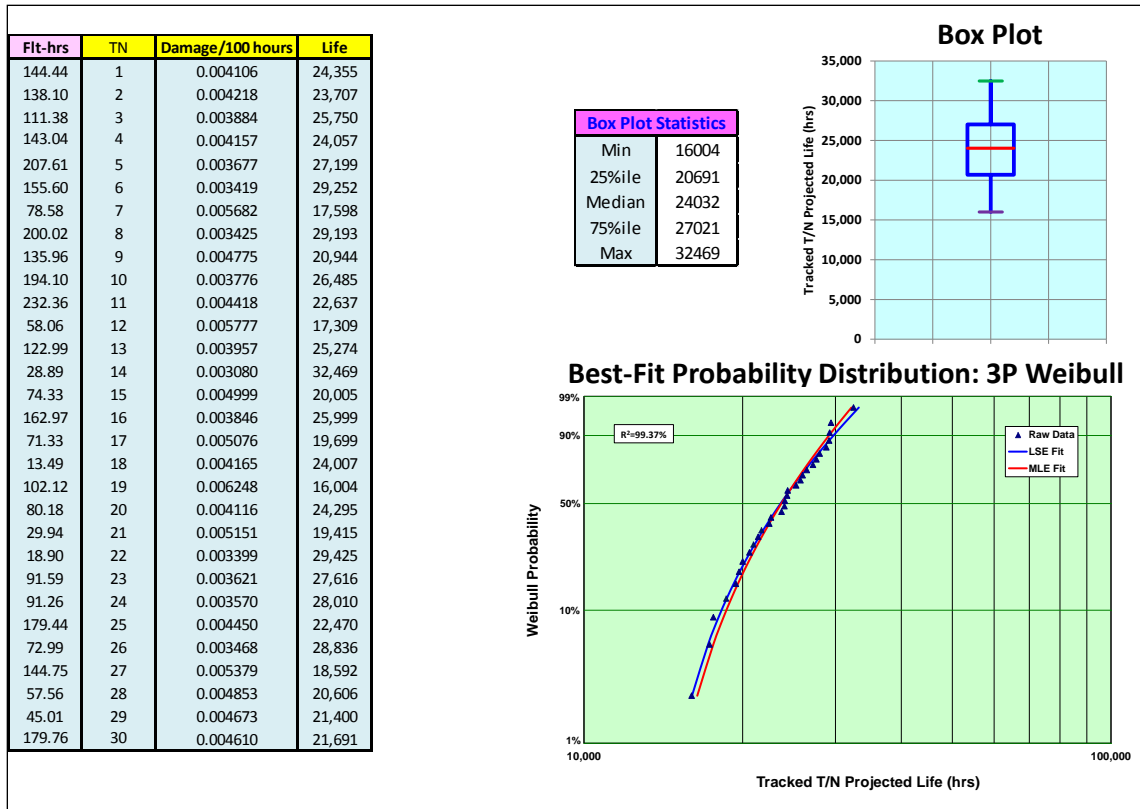


Figure 66. Effects of usage on left tie rod (OCONUS 1)

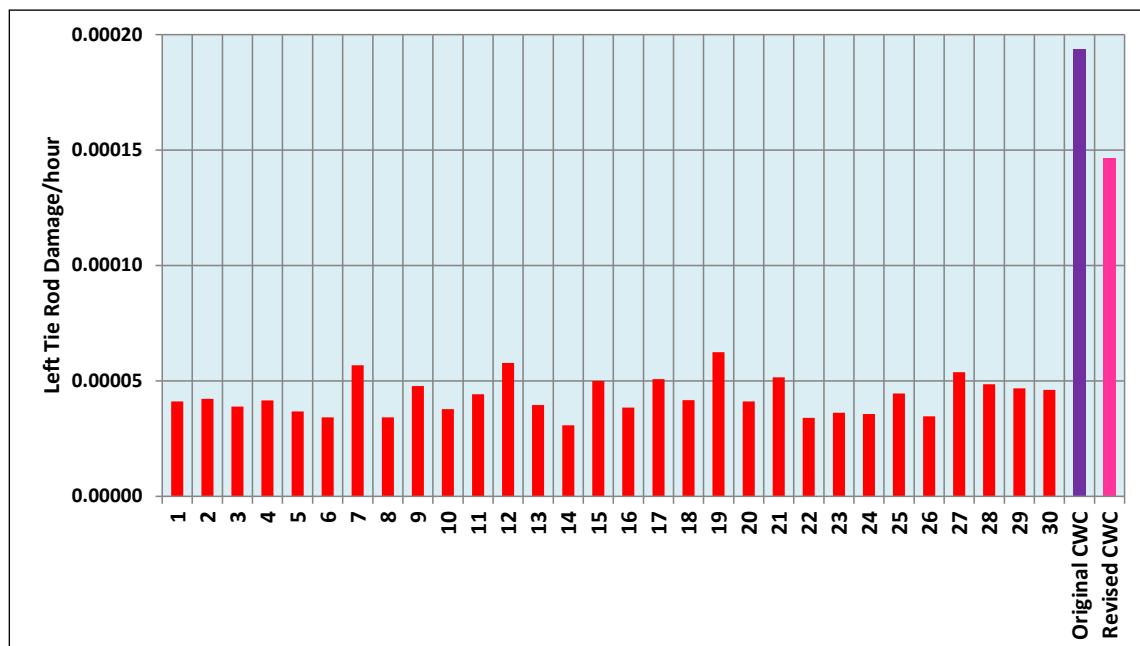


Figure 67. Usage data scatter for left tie rod (OCONUS 1)

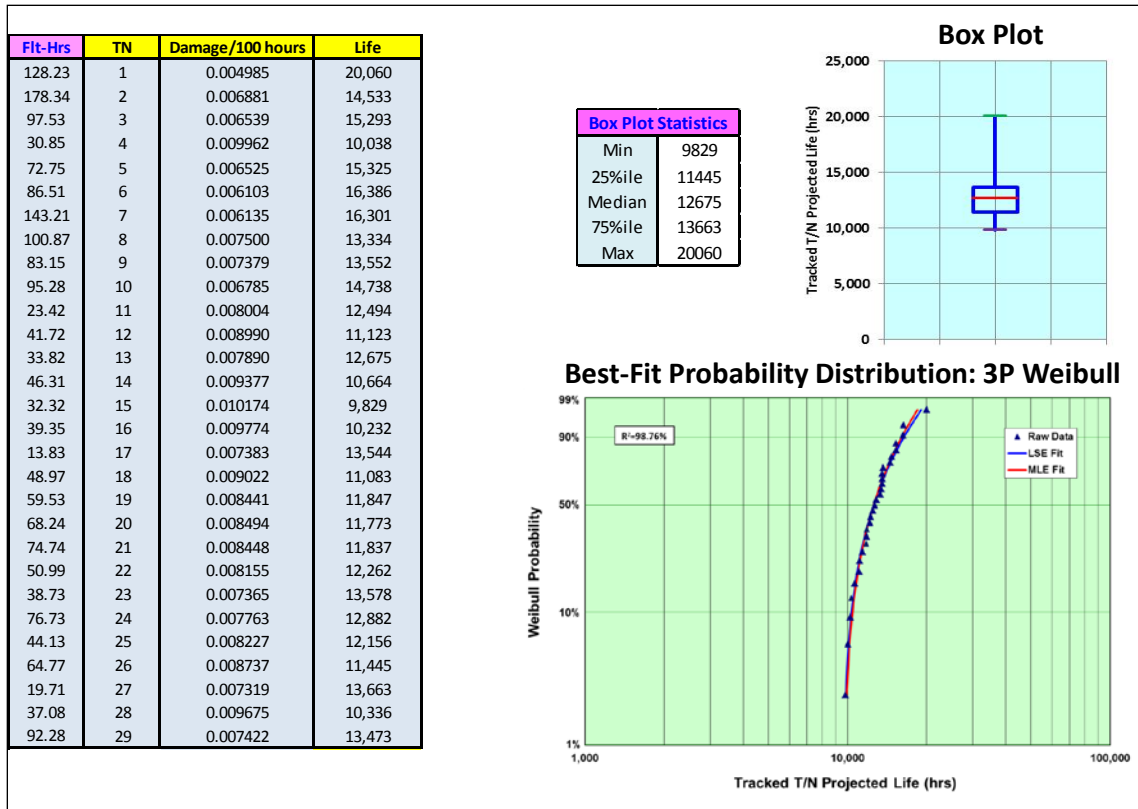


Figure 68. Effects of usage on left tie rod (OCONUS 2)

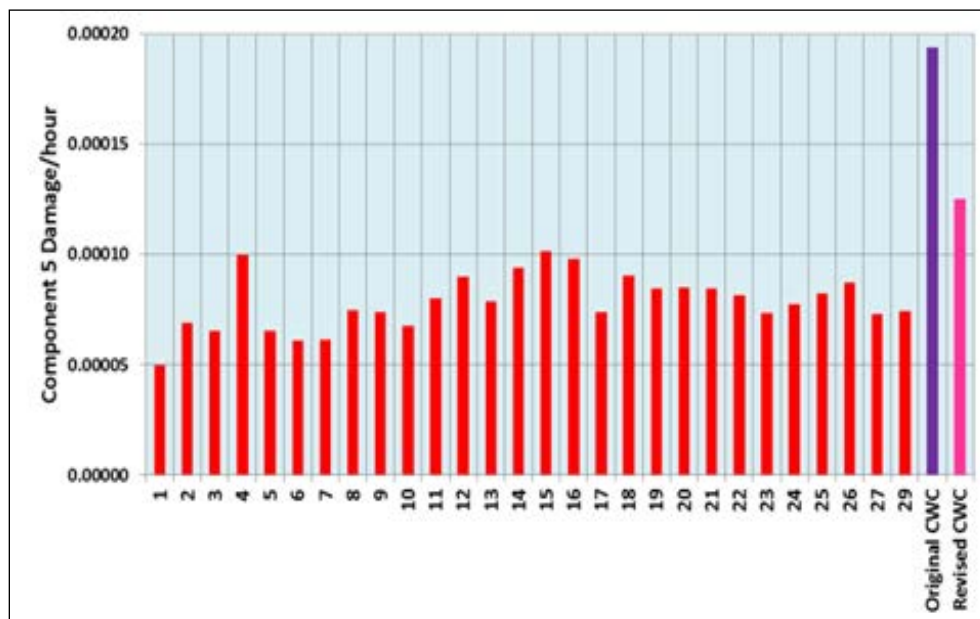


Figure 69. Usage data scatter for left tie rod (OCONUS 2)

3.4.2.2.4 Results of Operational Usage by Tail Number

Operational usage by tail number was evaluated using ADS-79C [7], paragraph A.6.4. Three missions were considered: CONUS training, OCONUS 1, and OCONUS 2.

Probability distribution plots and box plots were developed. Fits ranged from a low coefficient of determination (R^2) of 92.58% to a high of 99.58%. In the vast majority of cases, individual aircraft accrue damage more slowly than by either the original or revised CWC usage. The most significant damage accrued on a low-flight-hour aircraft (see figure 53). The recorded data per aircraft are relatively low, with an overall median of only 25 hours. The results would be expected to move closer to the average, with more flight hours per aircraft.

3.4.2.3 Evaluate ADS-79C-HDBK [7] Options for Ensuring Reliability

3.4.2.3.1 Introduction/Background

ADS-79C [7], paragraph A.6.5, revised spectrum alternatives were evaluated versus CWC and included:

- “ $\mu+1\sigma$ ” SUMS spectrum (with $\mu-3\sigma$ working curve)
- “ $\mu+2\sigma$ ” SUMS spectrum (with $\mu-3\sigma$ working curve)
- SUMS average spectrum with $\mu-3.64\sigma$ working curve, which recovers one 9 of reliability given the assumption of five 9s of implicit reliability from TOS load bias and $\mu-3\sigma$ EL

SUMS from CONUS Training, OCONUS 1, and OCONUS 2 were evaluated with respect to three dynamic component failure modes, which included the MR rotating washplate, IDGB MR shaft, and left tie rod.

Figures 70–78 show the average usage lives that result from the ADS-79C [7], paragraph A6.5 options. The results are summarized in table 19.

The X-factor plotted in figures 70–78 is defined as the ratio of the life whose spectrum is deliberately biased to maintain a certain level of reliability to the life based on the SUMS average spectrum and a baseline $\mu-3\sigma$ EL.

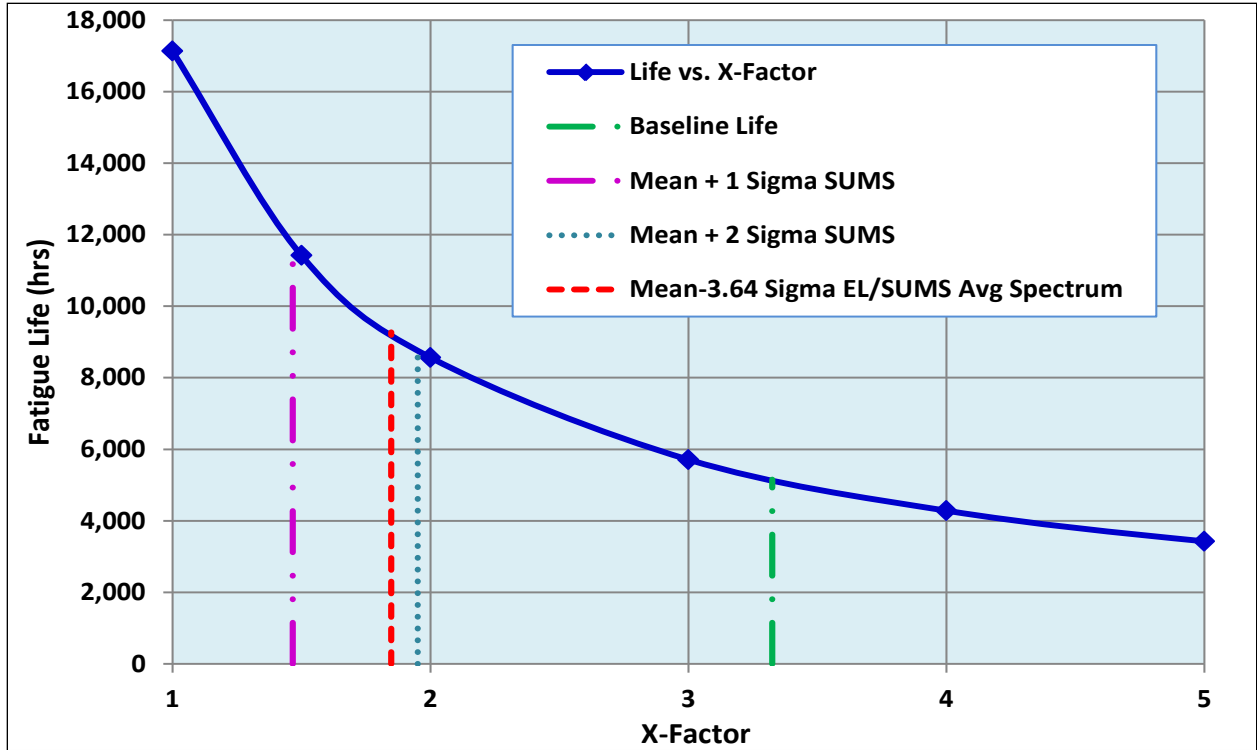


Figure 70. SUMS comparison for MR rotating swashplate (CONUS training)

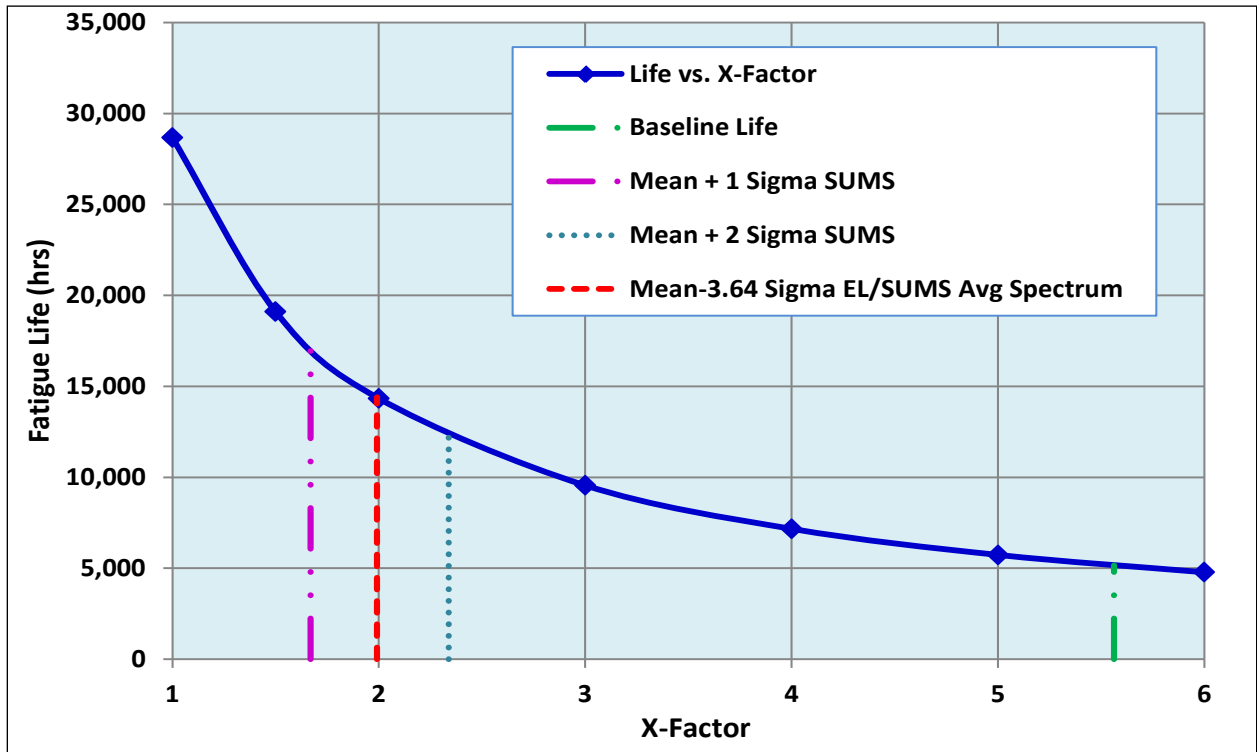


Figure 71. SUMS comparison for MR rotating swashplate (OCONUS 1)

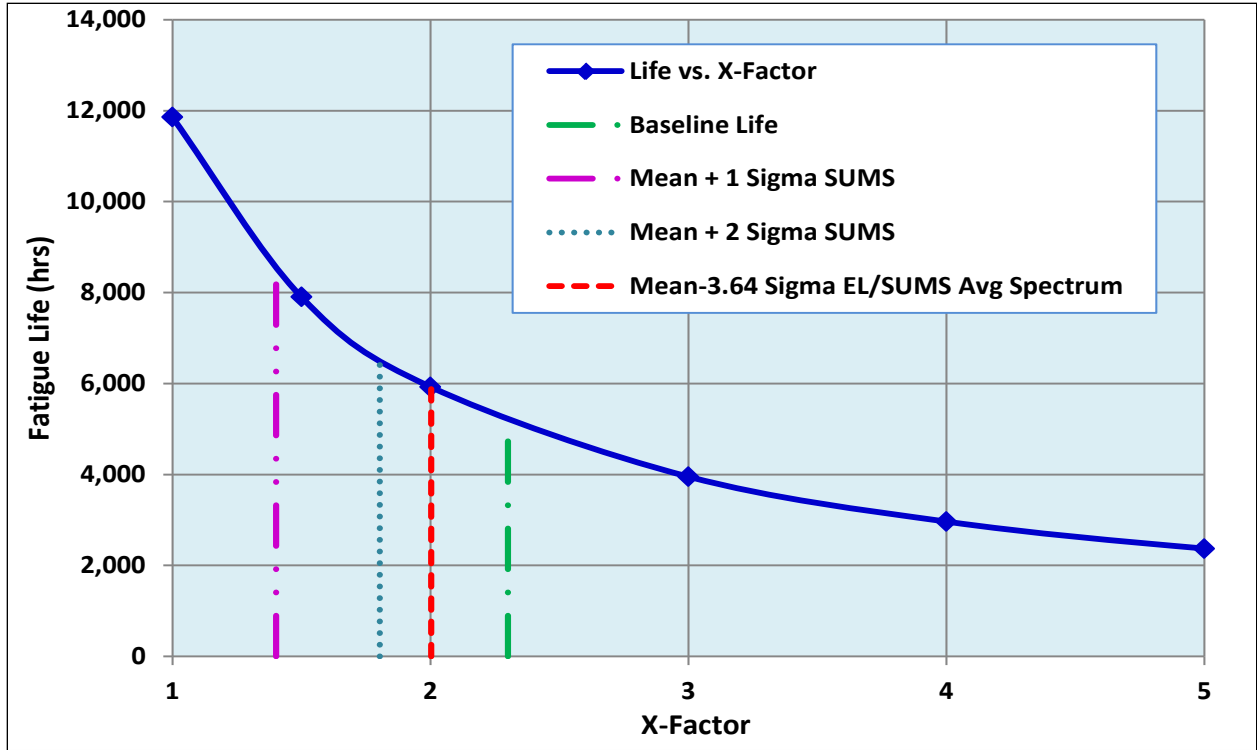


Figure 72. SUMS comparison for MR rotating swashplate (OCONUS 2)

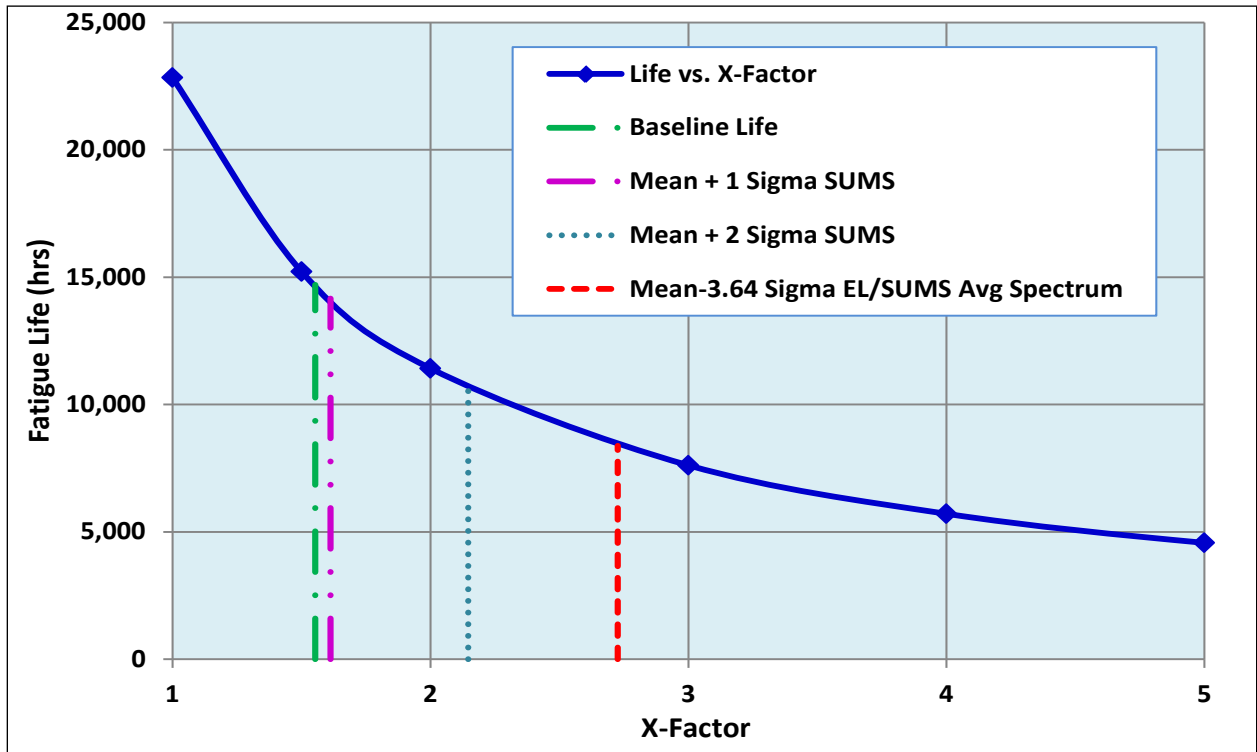


Figure 73. SUMS comparison for IDGB MR shaft (CONUS training)

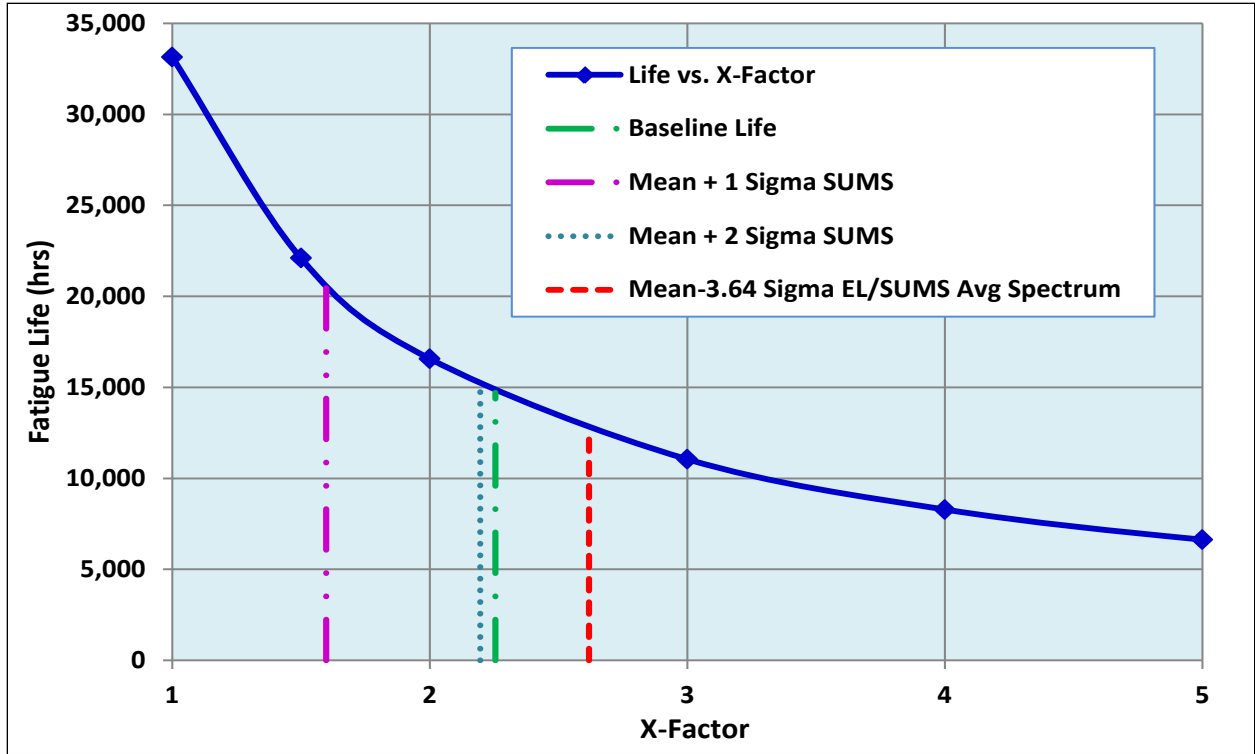


Figure 74. SUMS comparison for IDGB MR shaft (OCONUS 1)

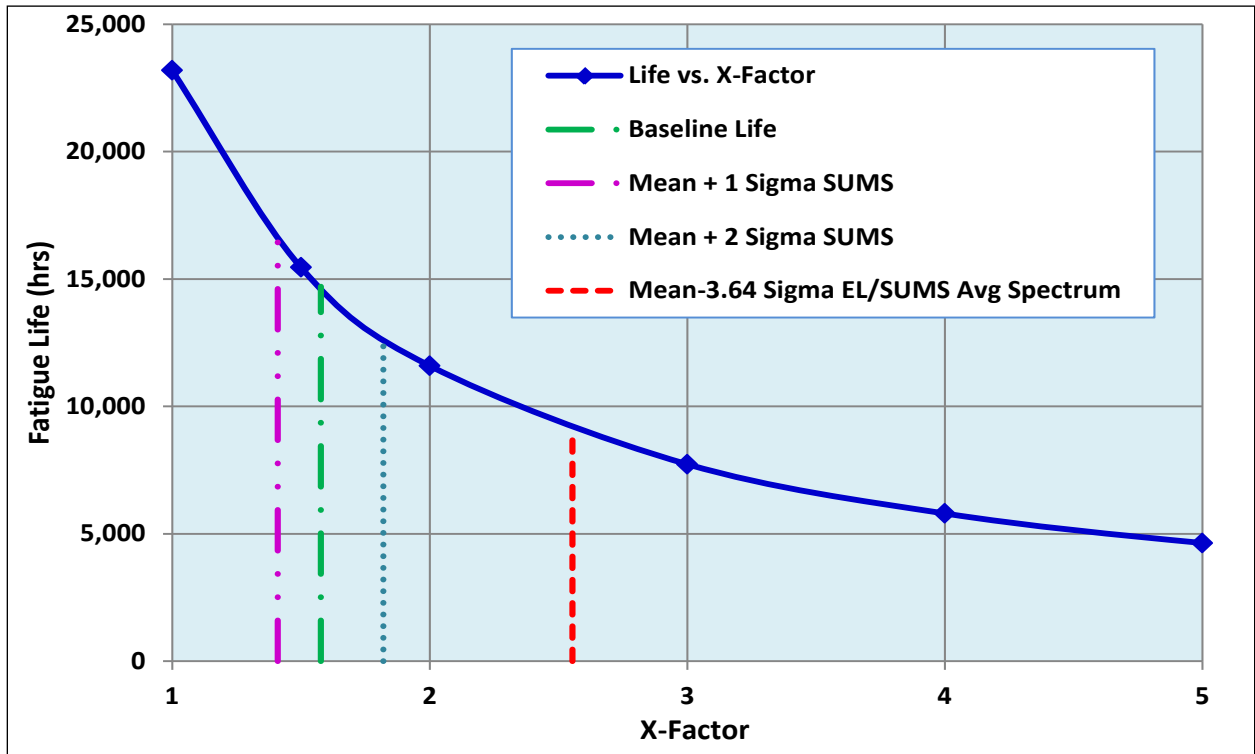


Figure 75. SUMS comparison for IDGB MR shaft (OCONUS 2)

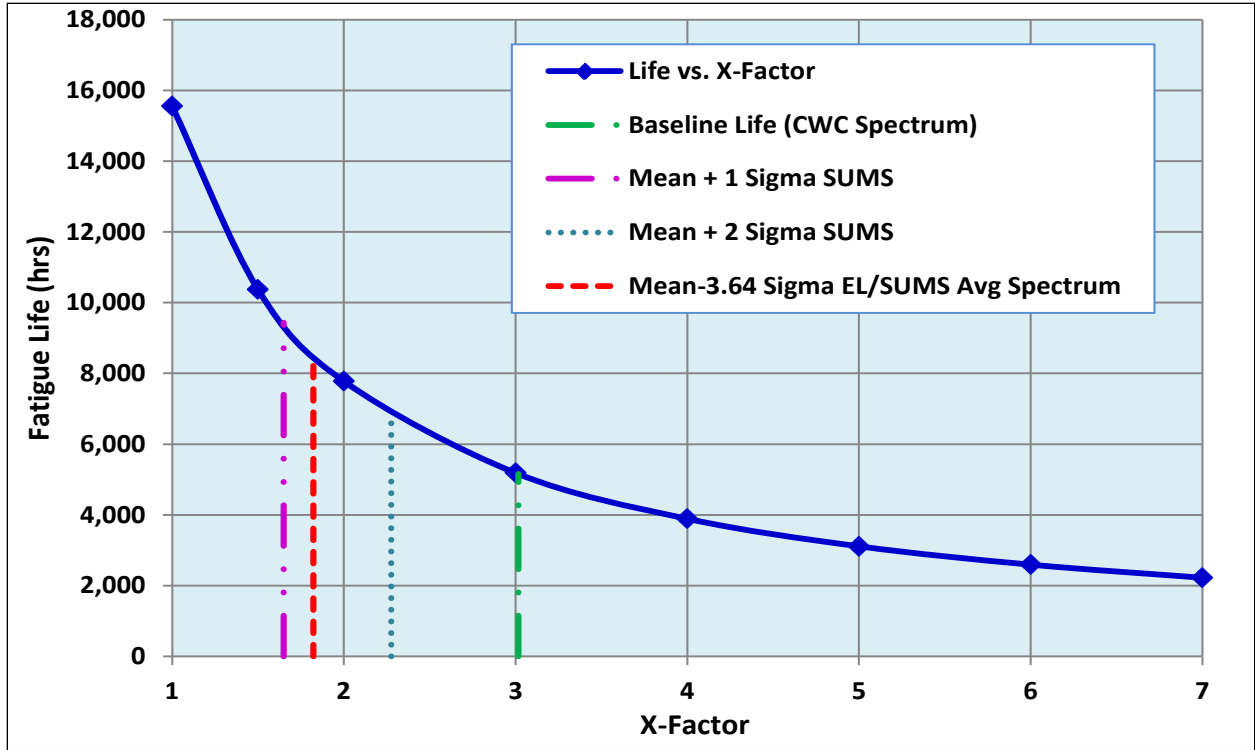


Figure 76. SUMS comparison for left tie rod (CONUS training)

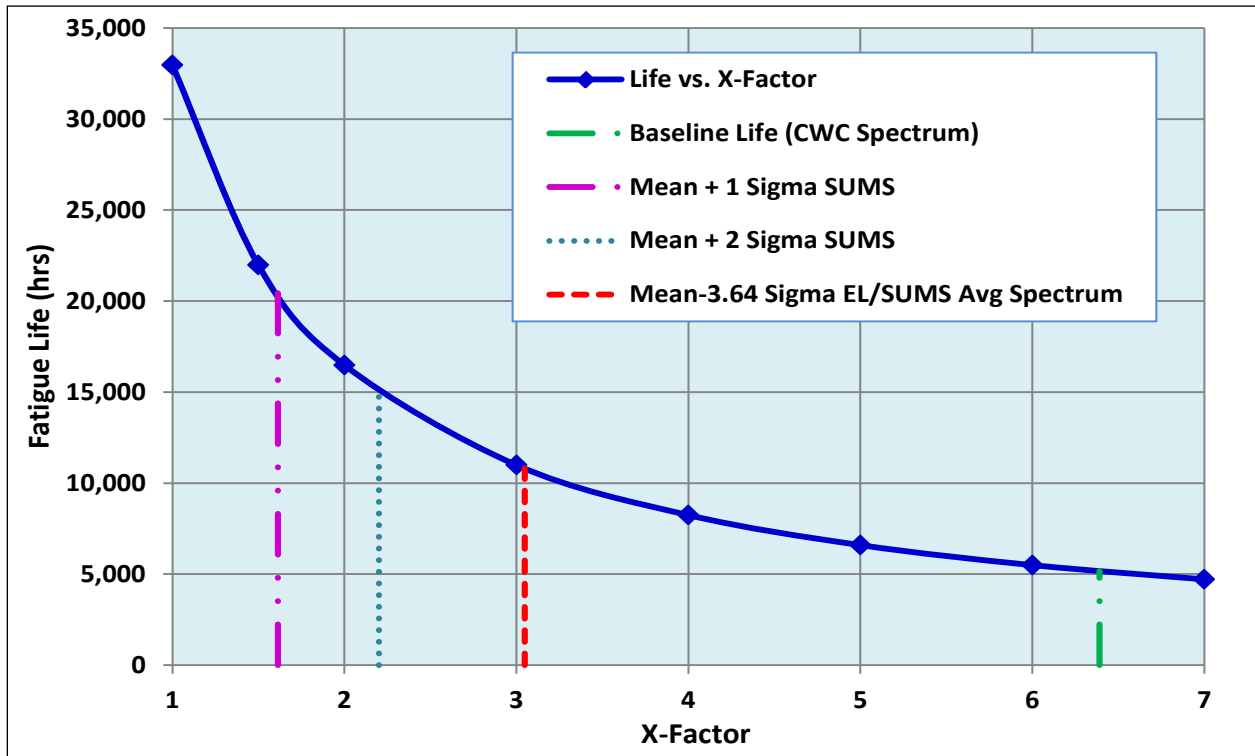


Figure 77. SUMS comparison for left tie rod (OCONUS 1)

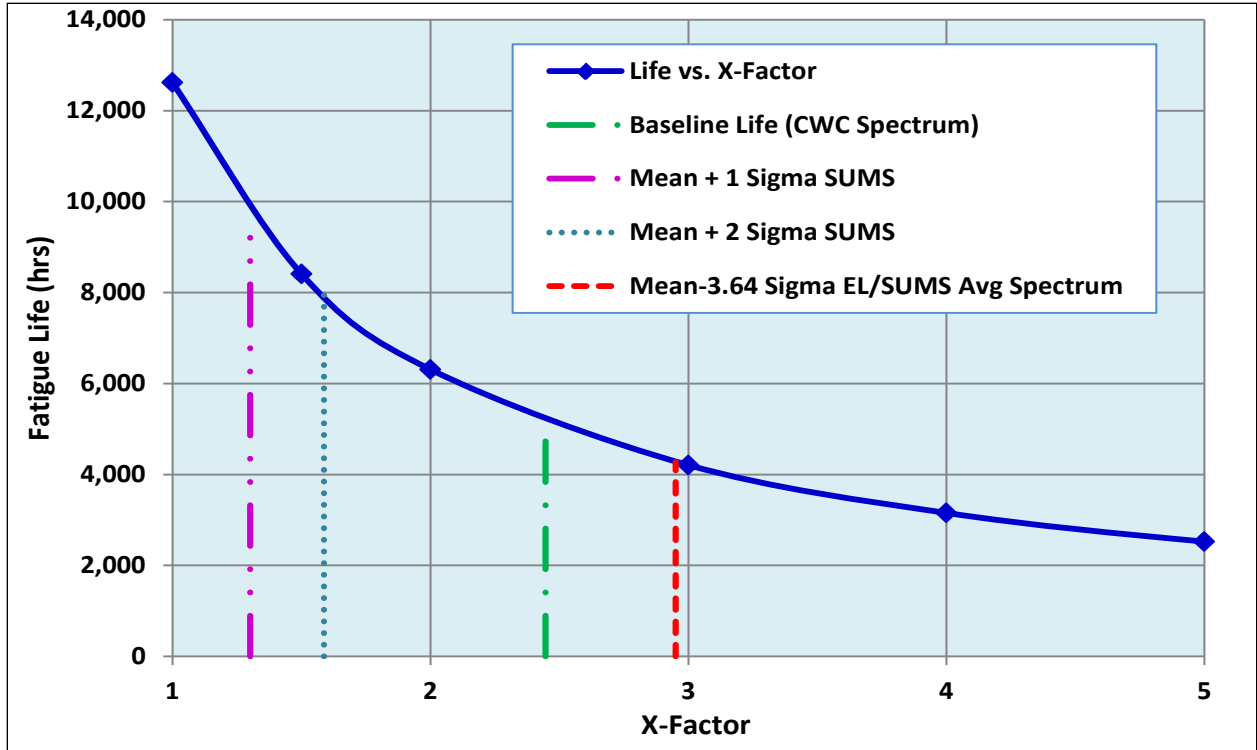


Figure 78. SUMS comparison for left tie rod (OCONUS 2)

3.4.2.3.2 Summary of Results

The X-Factor = 1.0 when the SUMS average spectrum is used with baseline damage rates (assuming five 9s reliability). For example, X=1.59 for the MR rotating swashplate at a CONUS training life of 10,869 hours.

Table 19. Component life and X-factor for operational environments

		MR Rotating Swashplate		IDGB MR Shaft Assembly		(Gearbox Housing) Left Tie Rod	
		Life	X-Factor	Life	X-Factor	Life	X-Factor
CONUS Training	CWC Spectrum	5153	3.36	14699	1.55	5158	3.02
	SUMS $\mu+1\sigma$ Spectrum	11684	1.47	14159	1.61	9433	1.65
	SUMS $\mu+2\sigma$ Spectrum	8782	1.95	10638	2.15	6836	2.28
	SUMS Average/ $\mu-3.64\sigma$ EL	9271	1.85	8377	2.73	8538	1.82
OCONUS 1	CWC Spectrum	5153	4.88	14699	2.16	5158	4.47
	SUMS $\mu+1\sigma$ Spectrum	15243	1.65	20165	1.57	16183	1.43
	SUMS $\mu+2\sigma$ Spectrum	10937	2.30	14784	2.14	12592	1.83
	SUMS Average/ $\mu-3.64\sigma$ EL	13043	1.93	12325	2.57	9188	2.51
OCONUS 2	CWC Spectrum	5153	2.30	14699	1.58	5158	2.45
	SUMS $\mu+1\sigma$ Spectrum	8444	1.40	16443	1.41	9730	1.30
	SUMS $\mu+2\sigma$ Spectrum	6562	1.80	12739	1.82	7987	1.58
	SUMS Average/ $\mu-3.64\sigma$ EL	5909	2.00	8983	2.58	4282	2.95
Uses ADS-79C, Paragraph A.6.5 $\mu+2\sigma$ SUMS as Revised CWC Criteria for Usage Credit Viability							

MR rotating swashplate results show that usage credits are viable in all three operational environments.

The IDGB MR shaft results show that usage credits are viable in OCONUS 1 only. The adjusted ($\mu+2\sigma$) usage in CONUS training and the OCONUS 2 result in fatigue lives that are less than that of the original CWC spectrum.

Left tie rod results show that usage credits are viable in all three operational environments and that $\mu+2\sigma$ SUMS criteria are not always as conservative as SUMS average/ $\mu-3.64\sigma$ EL (which ensure one 9 of reliability).

3.4.2.4 Describe and Demonstrate Usage Credit Implementation

Section 3.3.5 describes and demonstrates a method for applying usage credits based on tracking individual aircraft and individual components by serial number. Section 3.4.2.3 describes and demonstrates the derivation of the adjusted ($\mu+2\sigma$) average CWC fatigue lives for the three selected fatigue life limited component failure modes at the three selected operational environments. The new CWC for each of the three operational environments would be applied to each aircraft and component in those environments.

Table 20 summarizes the adjusted fatigue life for three components in each of three operational environments using the $\mu+2\sigma$ option. When compared with the CWC spectrum, the black numbers indicate an increase in CRT, whereas the red numbers indicate a reduction in CRT.

Table 20. Component adjusted CRT for operational environments

Operational Environment	MR Rotating Swashplate		IDGB MR Shaft		Left Tie Rod	
	CWC Spectrum	$\mu+2\sigma$ Spectrum	CWC Spectrum	$\mu+2\sigma$ Spectrum	CWC Spectrum	$\mu+2\sigma$ Spectrum
CONUS Training	5153	7861	14699	10638	5158	6836
OCONUS 1		12255		15045		15073
OCONUS 2		6562		12739		7987

In summary, the three component replacement times for the three evaluated operational environments will be in accordance with table 20. An example of the implementation of this process is shown in figure 79. The fatigue life expenditure is shown for the original CWC usage and each of the adjusted ($\mu+2\sigma$) average CWCs for each of the operational environments. There is a mix of usage in each of the operational environments that illustrates the scenario of flying 2000 hours in CONUS training, followed by 4000 hours in OCONUS 1, with the remainder of the life flown in OCONUS 2.

Figure 79 presents an example for identifying and quantifying usage credits for a monitored MR swashplate. The swashplate CWC life for OCONUS 2 is 6560 hours. The example swashplate, by serial number, is evaluated at the 6000-hour point and has a monitored DI of 0.295. In accordance with ADS-79C A.6.4, the DI is doubled to 0.590. The CWC-based equivalent life therefore becomes $0.590 * 6560 = 3870$ hours. This produces a credit of 6560 (CWC life for OCONUS) – 3870 (equivalent life for monitored MR swashplate) = 2690 hours. The new life for the example MR swashplate becomes $6000 + 2690 = 8690$ hours.

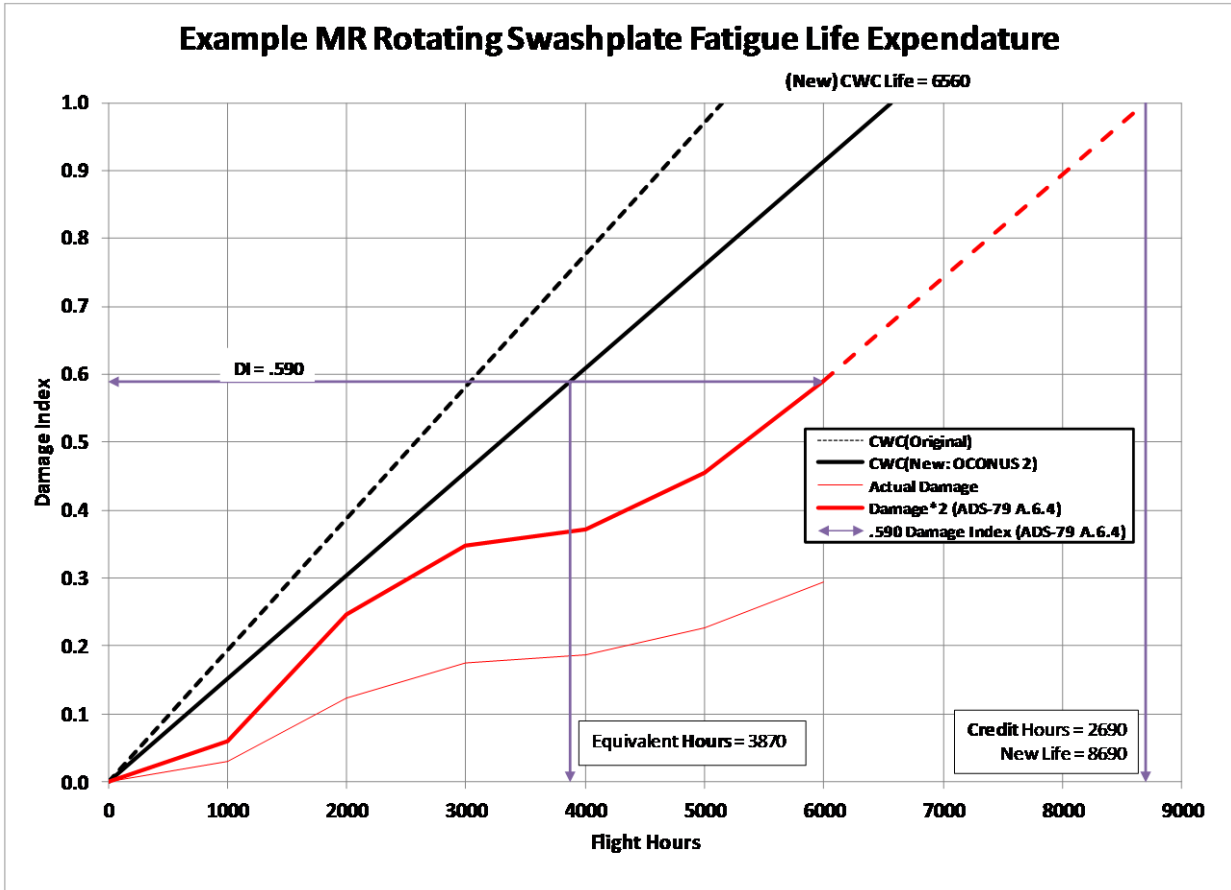


Figure 79. Example MR swashplate fatigue life expenditure

4. CONCLUSIONS

This report documents the consolidated results of four tasks that spanned a period of more than 2 years and included the performance of fleet HUMS data analysis, developing usage credits, updating the HUMS fleet data analysis, and developing a usage credit method. The processes developed, described, demonstrated, and documented in each of these four efforts have been presented in this report.

Overall, this research has demonstrated that usage monitoring typically provides significant benefits in terms of part lives. However, it should be noted that it is also possible that lives can be consumed more quickly.

This report has documented methods for analyzing and verifying HUMS data and applying them to the calculation of the RUL of life-limited parts. Based on these analyses and processes, the FAA will be able to make informed decisions regarding the application of CBM to civil rotorcraft.

4. REFERENCES

1. Federal Aviation Administration Advisory Circular 29-2C, "Certification of Transport Category Rotorcraft," U.S. Department of Transportation, April 25, 2006.
2. Vaughan, R.E., Chang, J.H., Rogers, M.H., "Obtaining Usage Credits From Monitoring of Helicopter Dynamic Components Without Impacting Safe Life Reliability," *American Helicopter Society Annual Forum*, Virginia Beach, Virginia, May 2007.
3. 3019555-CDD-0111, "CDD for Army UH-60L IMDS Usage," Goodrich Corporation, 2002.
4. S01122-CDDD0101, "CDD for the UH-60M IVHMS Operational Usage and Regime Processing," Goodrich Corporation, 2008.
5. SER-703333, Rev. 1, "UH-60M Dynamic Component Fatigue Substantiation Report," Sikorsky, 2005.
6. SER-704458 (Draft), "Draft Fatigue Life Management Interim Report," Sikorsky, 2010.
7. ADS-79C-HDBK, "Aeronautical Design Standard Handbook for Condition Based Maintenance Systems for U.S. Army Aircraft Systems," January 16, 2011.
8. "Metallic Materials Properties Development and Standardization," FAA Report DOT/FAA/AR-MMPDS-01, Washington, 2003.
9. Everett, R.A., Bartlett, F.D., and Elber, W., "Probabilistic Fatigue Methodology for Six Nines Reliability, NASA Technical Memorandum 102757, December 1990.
10. Thompson, A.E. and Adams, D.O., "A Computational Method for the Determination of Structural Reliability of Helicopter Dynamic Components," *American Helicopter Society Annual Forum*, Washington, D.C., May 1990.
11. Zion, H.L., "Safe Life Reliability: Evaluation of New Statistical Methods," *American Helicopter Society Annual Forum*, Phoenix, Arizona, May 1991.
12. SER-70100, "Methods of Structural Reliability Substantiation Based on Laboratory Fatigue and Flight Test Data," Sikorsky.
13. Shooman, M.L., "Probabilistic Reliability: An Engineering Approach," 2nd ed., Krieger Publishing, Malabar, FL, 1990, pp. 259, 507–508.
14. Press, W.H., Flannery, B.P., Teukolsky, S.A., and Vetterling, W.T., "Numerical Recipes in C: The Art of Scientific Computing," 2nd ed., Cambridge University Press, 1992, pp. 316–328.
15. Kapur, K.C. and Lamberson, L.R., "Reliability in Engineering Design," Wiley, New York, New York, 1977, pp. 126–139.

16. O'Connor, P.D.T., "Practical Reliability Engineering," 3rd ed. revised, Wiley, New York, New York, 1991, pp. 104–106,
17. Melchers, R.E., "Structural Reliability Analysis and Prediction," 2nd ed., Wiley, New York, New York, 1999, pp. 94–131,
18. Benton, R.E., "Composite Usage Spectrum Development," Apache Regime Recognition Review, Task 3 Exit, Task 4 Kickoff, 2009.

APPENDIX A—DETERMINISTIC EVALUATION OF INHERENT COMPOSITE WORST CASE (CWC) RELIABILITY

The process illustrated in this appendix is explained in section 3.3.3.3.2.

A.1 COMPONENT 1, FAILURE MODE 1

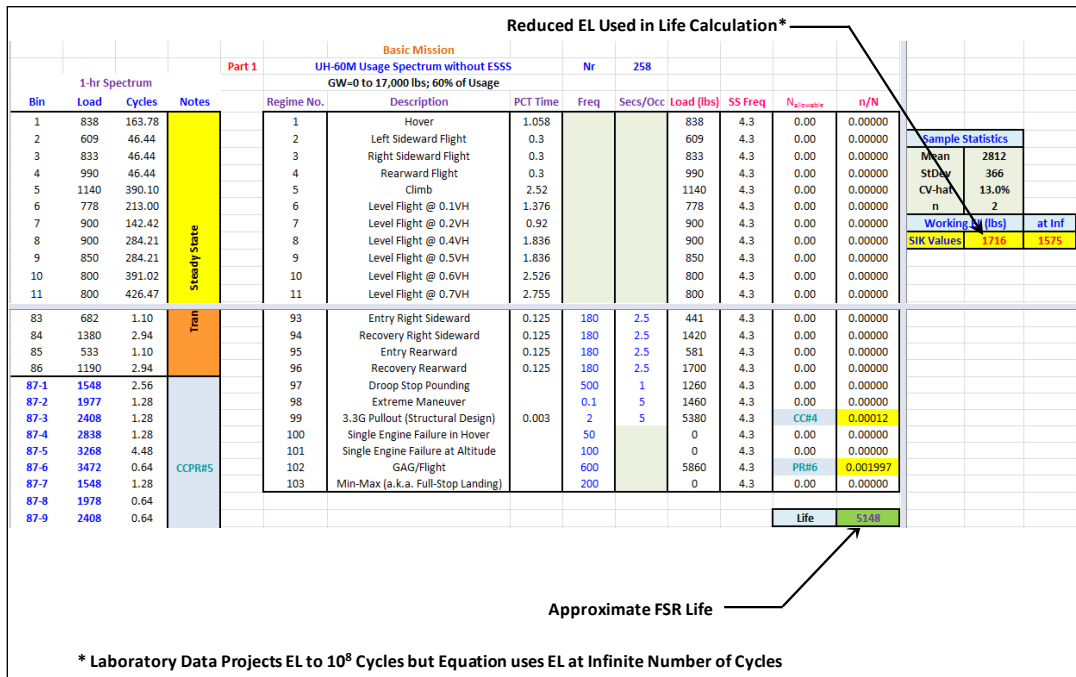


Figure A-1. Step 1: Reproduce the FSR component/failure mode life

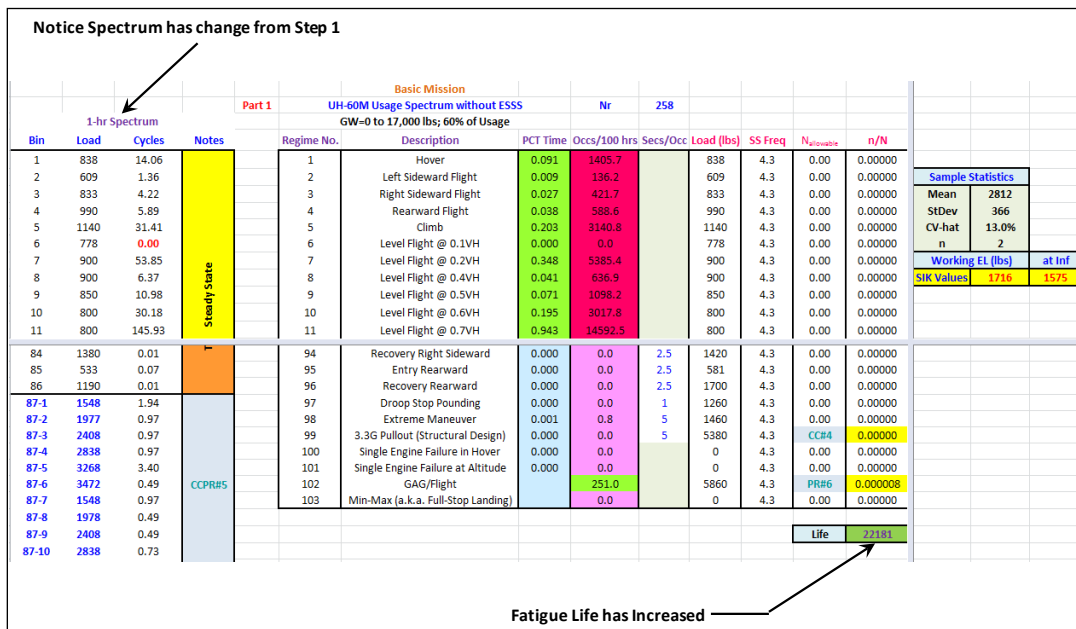


Figure A-2. Step 2: Replace CWC with RR average spectrum

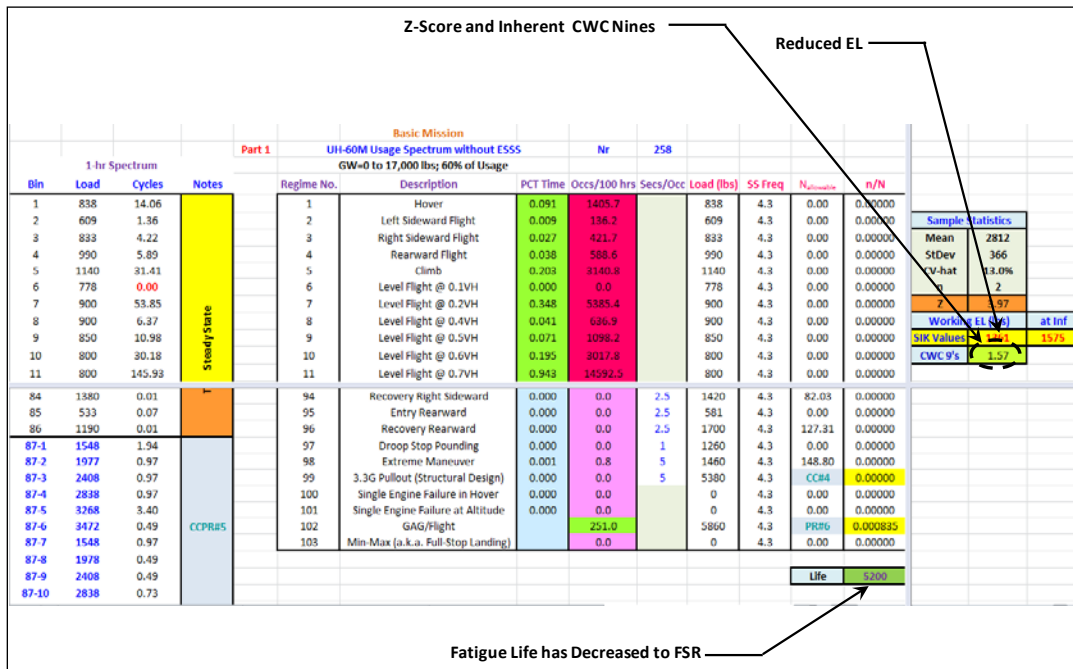


Figure A-3. Step 3: Reduce the $\mu-3\sigma$ EL from Step 2 until fatigue life matches FSR life

APPENDIX B—PROBABILISTIC EVALUATION OF INHERENT COMPOSITE WORST CASE (CWC) RELIABILITY

The process illustrated in this appendix is explained in section 3.3.3.3.2.

B.1 COMPONENT 1, FAILURE MODE 1

Bin	Cycles	Load	Normally Distributed Endurance Load						Mean	2812	StDev	366			
			Assume:		Load Sev (α)		984.2	1075.6	1167.0	1258.4	1349.8	1441.2	1532.5	1623.9	1715.2
			Fit Sev CoV:	8.00%	Mean	0.80	3.953E-07	1.329E-06	4.199E-06	1.247E-05	3.478E-05	9.117E-05	2.246E-04	5.199E-04	1.132E-03
1	163.78	838													
2	46.44	609													
3	46.44	833													
4	46.44	990													
5	390.10	1140													
6	213.00	778													
7	142.42	900													
8	284.21	900													
9	284.21	850													
10	391.02	800													
23	3.87	2670													
24	3.87	2500													
25	3.60	950													
26	1.50	517													
27	1.50	589													
28	7.20	942													
29	9.00	1010													
30	9.00	1550													
31	2.04	1340													
32	2.04	1500													
33-1	2.76	1548													
33-2	3.68	1978													
33-3	3.68	2350													
34-1	3.68	1978													
34-2	6.44	2350													
35	0.33	1390													

Figure B-1. Step 1: Evaluate the reliability of FSR fatigue life

Bin	Cycles	Load	Normally Distributed Endurance Load						Mean	2812	StDev	366				
			Assume:		Load Sev (α)		892.8	984.2	1075.6	1167.0	1258.4	1349.8	1441.2	1532.5	1623.9	1715.2
			Fit Sev CoV:	8.00%	Mean	0.80	3.953E-07	1.329E-06	4.199E-06	1.247E-05	3.478E-05	9.117E-05	2.246E-04	5.199E-04	1.132E-03	
1	14.06	838														
2	1.36	609														
3	4.22	833														
4	5.89	990														
5	31.41	1140														
6	0.00	778														
7	53.85	900														
8	6.37	900														
9	10.98	850														
10	30.18	800														
11	145.93	800														
12	211.33	800														
21	0.40	1590														
22	0.57	1680														
23	0.00	2670														
24	0.00	2500														
25	0.03	950														
26	0.02	517														
27	0.01	589														
28	0.00	942														
29	0.57	1010														
30	0.60	1550														
31	0.02	1340														
32	0.02	1500														
33-1	0.03	1548														
33-2	0.04	1978														
33-3	0.04	2350														
34-1	0.04	1978														

Figure B-2. Step 2: Replace CWC with RR average spectrum

